AD A124 626 SOIL LIQUEFACTION POTENTIAL AT THE NAVAL WEAPONS CENTER CHINA LAKE CALIFORNIA(U) NAVAL WEAPONS CENTER CHINA LAKE CA E W BANKS SEP 82 NWC-TP-6302 1/2

UNCLASSIFIED F/G 8/13 NL

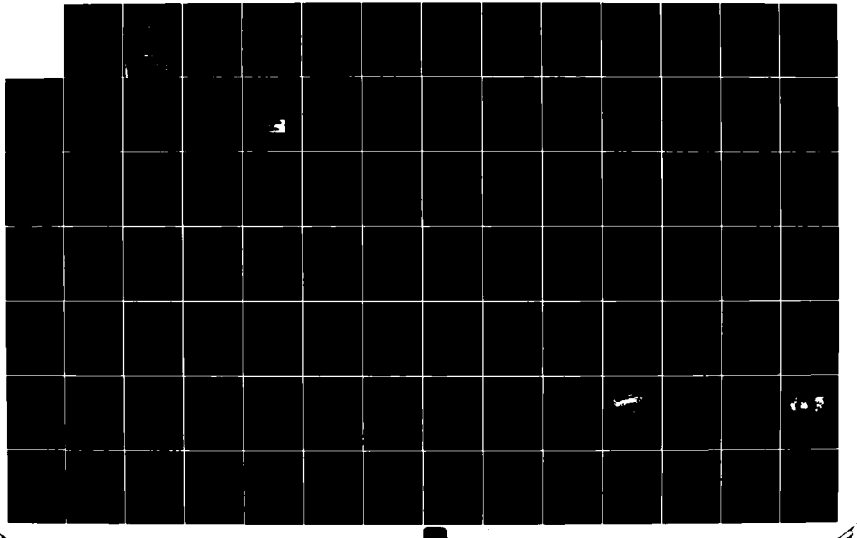

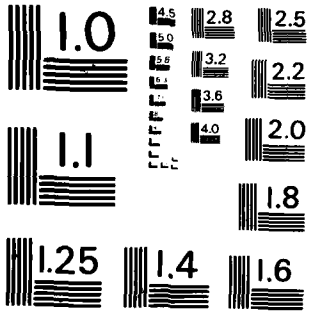

NWC TP 6392

12

Soil Liquefaction Potential at the Naval Weapons Center China Lake, California

by
Eric W. Banks
University of Nevada, Reno

SEPTEMBER 1982

NAVAL WEAPONS CENTER
CHINA LAKE, CALIFORNIA 93555

Naval Weapons Center

AN ACTIVITY OF THE NAVAL MATERIAL COMMAND

FOREWORD

The work described in this report was authorized by the Laboratory Director under Naval Weapons Center (NWC) General and Administrative funding as a Management Support Item. The study was conducted by an NWC summer employee during 1979 and 1980 and submitted as a master's thesis to the University of Nevada at Reno in May 1982. To save cost and publication time, a facsimile of the original dissertation is included herein. The dissertation has not been edited to NWC format except to add an NWC cover, foreword, DD form 1473, and distribution list.

The study is an investigation of the liquefaction potential of sediments in the Indian Wells Valley and identifies and characterizes the possibility of seismically induced liquefaction of sediments beneath the foundations of important structures located at NWC. This information could provide solutions to the problem of minor deformations that occur in concrete foundations and other structures located in Area "R" at NWC. The siting of new structures should include a detailed liquefaction study where indicated by this work.

This report was reviewed for technical accuracy by Dr. Glenn R. Roquemore, NWC Research Department, and by Professors Burton Slemmons and Robert Watters, University of Nevada, Reno.

Approved by
E. B. ROYCE, *Head*
Research Department
23 September 1982

Under authority of
J. J. LAHR
Capt., U.S. Navy
Commander

Released for publication by
B. W. HAYS
Technical Director

NWC Technical Publication 6392

Published by ..... *Technical Information Department*
Collation ..... Cover, 56 leaves
First printing ..... 250 unnumbered copies

UNCLASSIFIED

SECURITY CLASSIFICATION OF THIS PAGE *(When Data Entered)*

REPORT DOCUMENTATION PAGE		READ INSTRUCTIONS BEFORE COMPLETING FORM
1. REPORT NUMBER NWC TP 6392	2. GOVT ACCESSION NO. AD-A124 626	3. RECIPIENT'S CATALOG NUMBER
4. TITLE *(and Subtitle)* SOIL LIQUEFACTION POTENTIAL AT THE NAVAL WEAPONS CENTER, CHINA LAKE, CALIFORNIA		5. TYPE OF REPORT & PERIOD COVERED Thesis for degree of Master of Science; 1979-1980
		6. PERFORMING ORG. REPORT NUMBER
7. AUTHOR(s) Eric W. Banks		8. CONTRACT OR GRANT NUMBER(s)
9. PERFORMING ORGANIZATION NAME AND ADDRESS Naval Weapons Center China Lake, CA 93555		10. PROGRAM ELEMENT, PROJECT, TASK AREA & WORK UNIT NUMBERS Management Support Item (G&A funding)
11. CONTROLLING OFFICE NAME AND ADDRESS Naval Weapons Center China Lake, CA 93555		12. REPORT DATE September 1982
		13. NUMBER OF PAGES 106
14. MONITORING AGENCY NAME & ADDRESS*(if different from Controlling Office)*		15. SECURITY CLASS. *(of this report)* UNCLASSIFIED
		15a. DECLASSIFICATION/DOWNGRADING SCHEDULE

16. DISTRIBUTION STATEMENT *(of this Report)*

Approved for public release; distribution unlimited.

17. DISTRIBUTION STATEMENT *(of the abstract entered in Block 20, if different from Report)*

18. SUPPLEMENTARY NOTES

19. KEY WORDS *(Continue on reverse side if necessary and identify by block number)*

Ground surface acceleration
Seismicity
Soil liquefaction

20. ABSTRACT *(Continue on reverse side if necessary and identify by block number)*

See back of form.

DD FORM 1 JAN 73 1473 EDITION OF 1 NOV 65 IS OBSOLETE
S/N 0102-LF-014-6601

UNCLASSIFIED

SECURITY CLASSIFICATION OF THIS PAGE *(When Data Entered)*

(U) *Soil Liquefaction Potential at the Naval Weapons Center, China Lake, California*, by Eric W. Banks, University of Nevada, Reno. China Lake, Calif., Naval Weapons Center, September 1982, 104 pp. (NWC TP 6392, publication UNCLASSIFIED.)

(U) In the past, billions of dollars and numerous lives have been lost to catastrophies caused by seismically induced soil liquefaction. During the last 10-15 years this natural phenomenon has become increasingly understood; first in a qualitative, then in a more quantitative manner. High groundwater levels, post-Pleistocene soil deposits, and an area of intense seismicity suggests a high liquefaction potential for the United States Naval Weapons Center at China Lake, California. This potential is analyzed, first employing a qualitative method described by Youd (1977), and then a more quantitative procedure described in part by Dobry (1980). The end result is a relative liquefaction potential map utilizing a liquefaction potential ratio, i.e., a 100-year design peak ground surface acceleration, a_p, divided by a threshold peak ground surface acceleration, $(a_p)_t$. A probabilistic computer program, EQRISK (McGuire, 1975), is used to determine the design acceleration at each grid point on 1/2-mile centers. The threshold acceleration is calculated in-situ and is described as the acceleration required for the generation of excess pore pressure at a depth of 30 feet in the profile. Results suggest the strong likelihood of liquefaction occurring over a large part of the study area during the 100-year design interval.

University of Nevada

Reno

LIQUEFACTION POTENTIAL AT THE NAVAL WEAPONS CENTER, CHINA LAKE, CALIFORNIA

A thesis submitted in partial fulfillment of the requirements for the degree of Master of Science in Geological Engineering.

by

Eric W. Banks

MAY 1982

ACKNOWLEDGEMENTS

I gratefully acknowledge the assistance received at the Naval Weapons Center, China Lake, California for financial and technical support in the preparation of this thesis. Hans Lindblom of the NWC Computer Science Division provided relentless effort and expertise in solving the problems encountered with the computer graphics. Patricia O'Dell's drafting talents are greatly appreciated, as are the editing and typing efforts of Emilie Boguchwal, both of the Naval Weapons Center. Other field and computer assistance was donated by NWC's Dr. to be Eugene "Buddy" Schweig, Patrick Smith, and Marian Ash. A most important acknowledgement is made to NWC's research geologist, Dr. Glenn Roquemore, who provided necessary assistance in every form, from personal encouragement to professional management.

In addition, I would like to thank Dr. Robert Watters, Associate Professor of Geological Engineering at the University of Nevada, Reno, for both his comments in proofreading this manuscript as well as his continued technical support throughout my collegiate career. Dr. Gary Norris, Assistant Professor of Civil Engineering at UNR, is also recognized as initiating the interest for this study through his classroom lectures.

TABLE OF CONTENTS

Chapter 1
INTRODUCTION

STATEMENT OF THE PROBLEM

GENERAL

Historically, geotechnical failures caused by earthquakes have been a serious problem which is not fully understood. Stories of liquefied soil bubbling out of the ground, both during and after ground motion has ceased, have been noted in numerous accounts of historic earthquakes. Because of the extensive loss of life and tremendous amounts of damage that these earthquakes and related ground failures have caused during this century, many investigators have now started studying these natural phenomena. In the last 10-15 years the level of understanding the mechanisms of liquefaction have moved from an initial qualitative stage, to recently a much more detailed qualitative and now a quantitative level. The ultimate goal of every r ırcher in the field is the hope of being able to predict, and even prevent conditions of liquefaction both accurately and cost effectively. There are still, unfortunately, many questions pertaining to our present level of knowledge that must be addressed before we may eliminate the damage potential of this phenomenon.

The basic concepts of liquefaction were first illustrated by Casegrande (1936) in his studies on slope stability. Casegrande's work dealt mainly with volume change, and the corresponding pore pressure changes during the application of a static shearing stress. In recent years cyclic stress, like those created by earthquakes have been found to cause similar volume changes with resulting pore pressure phenomenon. This study deals with the potential for increased pore pressure, and the subsequent threat of liquefaction, created by cyclic stresses from earthquake generated ground motion in a soil profile.

DEFINITION OF LIQUEFACTION

The term liquefaction has been used and defined by different investigators over the years. There is also much controversy over how the term should be used to describe different phenomena. The term liquefaction, as it is used in this study, will refer to the changing of a soil from a solid state to a liquefied state due to the build-up of excess hydrostatic pore pressure. This change of state is further defined as a result of a loss of shear strength due to cyclic loading involving the reversal of shear stresses during dynamic loading, such as an earthquake. When a saturated fine-to-medium grained cohesionless soil mass is subjected to ground vibration, it tends to compact and decrease in volume. If drainage of the pore spaces is unable to occur, the tendency to decrease in volume is met with hydrostatic resistance and the result is an increase in pore-water pressure. When this excess pore-water pressure builds to the point at which it is equal to the overburden pressure, the effective stress becomes zero, the material looses its shear strength, and the resulting state is one of a dense fluid. At this point the material is said to have experienced initial liquefaction. Seed (1976) describes the build-up of excess pore pressure as the trade off between a tendency for a volume decrease, due to cyclic loading, and a rebound of the soil structure due to the load being transferred from the soil structure to the pore water. The difference between soil structure rebound and the tendency for the volume of the soil mass to compact results in the excess pore pressure.

This description of liquefaction appears in equation form as follows:

$$\tau_{ff} = \sigma'_{ff} \tan \phi = (\sigma_{ff} - \mu) \tan \phi$$

where

ϕ = angle of internal friction

τ_{ff} = shear stress on the failure plane at failure

σ_{ff} = normal stress on the failure plane at failure

μ = pore-water pressure

μ refers to μ static + μ excess build-up.

Then as μ approaches σ_{ff} due to dynamic loading,

τ_{ff} approaches 0, which responds as a fluid.

CASE HISTORIES

The sudden interest in expanding our knowledge of the liquefaction phenomenon can be credited to a select few major earthquakes occurring in the last 15-20 years. The most dramatic of these events occurred on June 16, 1964. On this day Niigata, Japan, was hit by a shock which registered 7.3 on the Richter scale with its epicenter located 35 miles north of the city (Seed and Idriss, 1967). During the event, the extensive liquefaction of the sand deposits resulted in major damage to buildings, bridges, highways, utilities, dock areas, oil refineries, and railroads. The most dramatic case of settlement and tilting was undoubtedly that experienced during a major bearing capacity failure by apartment buildings that tilted up to 80° from vertical. The occupants of the complexes were then able to walk down the face of the structure to safety (Seed, 1969). During the same event a sewage treatment tank floated to the surface because the buoyant forces lifting the tank were not resisted by the soil which had liquefied. In another part of the city a flowing spring 3-feet high developed in an urbanized area as a result of liquefaction and a release of the excess pore-water pressures to the surface.

Another illustrative example of extensive damage created by liquefaction is the 1964 Alaskan earthquake. This large magnitude earthquake (8.4) struck South Central Alaska, disrupting many highways and utilities and severely damaging structures. Youd (1978) estimates that ground failure caused 60% of the estimated $300 million (1964 value) total damage. Five major landslides caused about $50 million of the $85 million damage to nonmilitary facilities in the city of Anchorage. Lateral spread failures damaged highway and railway grades and bridges, requiring about $50 million in repairs, and severely disrupting these lifelines. Flow failures in three Alaskan coastal communities carried away ports, adjacent warehouses, and transportation facilities that cost approximately $15 million. In each of these ground failure modes the probable cause can be traced to liquefaction. Ross, Seed and Migliaccio (1969) also reviewed a number of highway bridge facilities and indicated that liquefaction of the support soils during and shortly after the earthquake caused the failures. Turnagain Heights, an upper-middle class residential area in Anchorage, slid into the sea as a

result of the liquefaction of thin (2-3 inches) sand and silt lenses within the sensitive Bootlegger Cove clay.

In 1971 an earthquake (M = 6.6) struck the San Fernando Valley of California causing millions of dollars of damage (Youd, 1971). A large portion of this damage was attributed to liquefaction. The near catastrophic failure of the lower San Fernando Dam has been attributed to liquefaction of the embankment soil (Seed, et al, 1975). The potential for a catastrophic loss of life was ever-present due to the dam's location above a large population center. Lew, Levendecker and Dikkers (1971) describe the extensive damage suffered by a juvenile hall due to ground cracking and ground spreading as a result of liquefaction in the foundation soils. The Joseph Jensen Filtration Plant also suffered structural damage due to slope failure, ground surface cracking, and differential building settlement (Dixon and Burke, 1973).

Youd and Hoose (1976) describe various ground failures that occurred during the 1906 San Francisco earthquake that have now been attributed to liquefaction of the soils. Estimates of 85% of the damage to San Francisco was caused by the fire that followed the earthquake. Much of the fire damage, however, could have been prevented if several main water lines into the city had not been severed by a liquefaction-induced ground failure.

TECHNOLOGICAL ADVANCES

As pointed out by the previous examples, liquefaction-induced ground failures have been directly or indirectly responsible for many expensive and/or fatal problems associated with earthquakes. As a result, renewed interest among noted investigators has been initiated in the field of liquefaction potential.

Laboratory testing procedures, such as the cyclic triaxial test, cyclic simple shear test, and the shaking table test have greatly enhanced the formulation of basic theories. Data from these tests, although sometimes ambiguous as to their interpretation, can enable investigators to determine the causes of liquefaction, the factors influencing the mechanism, and procedures of analysis and design for the control of the liquefaction problem.

As in any science, initial theories are proposed and tested against case histories and field observations. Further problems are identified and a back-analysis approach may be implemented to formulate empirical methods of analysis. A new source of data, which may prove very important in the future is the available information from the Chinese records on earthquakes. It is estimated that these records may extend further back in history than any other known earthquake records. The combination of these records with our present day earthquake records, and subsequent liquefaction observations creates a substantial collection of information which will be available for analysis and comparison.

Although much work has been done in the prediction of liquefaction potentials, it must be noted that a universally accepted method of analysis has not yet been developed. Any and all information that can be collected and used to find an acceptable approach to the problem would be a major contribution toward maintaining the integrity of structural foundations during earthquakes.

PURPOSE OF THIS STUDY

The purpose of this study is to develop a useful guide for evaluating the possibility of liquefaction and the subsequent potential for bearing capacity failures and/or differential settlement of dams, buildings, and other structures proposed by the United States Navy at their Weapons Research Center in China Lake, California. This study is meant to be a contribution to the work already being undertaken by the Geological Sciences group in an effort to respond to "Project 2000;" a generalized site investigation of the base area outlining the Navy's potential for expansion through the year 2000. This potential map will be useful as a preliminary tool in identifying general areas of potential liquefaction and suggested design life criteria for the proposed structures in regards to dynamic stability of the soil. At the time of a site's proposal, depending on the project, a more detailed site investigation should be performed for any site where liquefaction is considered possible. Threshold accelerations, $(a_p)_t$, and a subsequent potential ratio $(a_p/(a_p)_t$, design acceleration divided by threshold

acceleration) are quantitative measures for comparison, and should not be considered finalized design values for major structures.

The Naval Weapons Center is located in a very seismically active area. The area has been classified as a Zone 4 region, the highest classification, by the 1976 Uniform Building Code's seismic zone classification map (Figure 1.1). This zone is outlined by the UBC as an area of major damage, capable of an Intensity VIII or greater on the modified Mercalic scale. In addition, this area is said to be capable of further danger potential due to its proximity to major fault systems. Roquemore (1981), staff research geologist at the Naval Weapons Center,

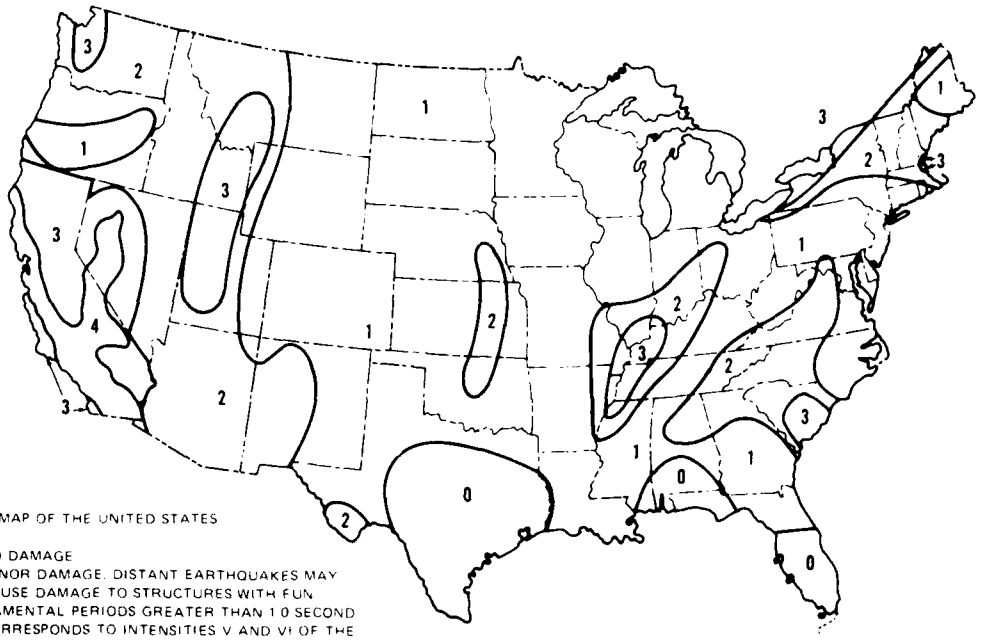

SEISMIC RISK MAP OF THE UNITED STATES

ZONE 0 NO DAMAGE
ZONE 1 MINOR DAMAGE. DISTANT EARTHQUAKES MAY CAUSE DAMAGE TO STRUCTURES WITH FUNDAMENTAL PERIODS GREATER THAN 1.0 SECOND CORRESPONDS TO INTENSITIES V AND VI OF THE M.M.* SCALE
ZONE 2 MODERATE DAMAGE. CORRESPONDS TO INTENSITY VII OF THE M.M.* SCALE
ZONE 3 MAJOR DAMAGE. CORRESPONDS TO INTENSITY VIII AND HIGHER OF THE M.M.* SCALE
ZONE 4 THOSE AREAS WITHIN ZONE NO. 3 DETERMINED BY THE PROXIMITY TO CERTAIN MAJOR FAULT SYSTEMS

*MODIFIED MERCALIC INTENSITY SCALE OF 1931

FIGURE 1.1. 1976 Uniform Building Code's Seismic Zone Classification Map.

is currently engaged in a detailed fault mapping program which will locate all major fault systems in the base vicinity and analyze their potential for activity. His on-going work will be a

constant source of updated input for the computer generated probabilistic peak accelerations to be used in the future prediction of liquefaction potential.

Numerous base facilities constructed in the last 10-15 years have been subjected to differential settlement resulting in cracked walls and undulating floors. It is realized that fluctuations in the already shallow water table may alter effective stresses causing consolidation and/or settlement. However, selected fault trenches analyzed by both Roquemore (1981) and St. Amand (1981) have illustrated sand blows or mud volcanoes at depth, indicating liquefaction and potential foundation instability. (See Figure 1.2.)

FIGURE 1.2. Mud Volcano in Little Lake Fault Trench Adjacent to Study Area.

Because of the high seismicity of the area, a high groundwater table, and the fact that many soils at China Lake are highly susceptible to liquefaction, it is very important that

potential locations for liquefaction be earmarked. Sudden and possibly catastrophic failures of structures, toxic waste settling ponds, and soil embankments could possibly be prevented if liquefaction susceptible areas are outlined. Given an understanding that potential sites could liquefy, more specific design parameters could be implemented to correct problems that exist at a site, or a problem site may be avoided completely.

The creation of "Project 2000" indicates the Navy's anticipated expansion of the facility at China Lake. It is the goal of this study to aid the planners and developers in both their site selections and the level of investigation and design that a specific site might require.

STUDY AREA

The Naval Weapons Center (NWC) at China Lake is a federal research facility employing approximately 3000 civilians under the Department of Defense. Significant projects in the past have included the development of the Sidewinder missile, numerous air-to-air, air-to-ground, and ground-to-ground guidance systems, and a very large collection of other weaponry research projects either too numerous to list or the publication of them would be classified for security reasons.

A survey of the structures currently on site encompases 3 very large multistoried laboratories, numerous warehouse facilities and operations and control buildings. Support facilities, including housing and special services were constructed for a capacity population of nearly 10,000. Armitage Air Field is the base for a moderately sized attack squadron as well as the host for numerous other military aircraft temporarily assigned to maneuvers and tests run in conjunction with NWC. Also located on site is the Supersonic Naval Ordnance Research Track (SNORT) which is a 5-mile track utilized for high speed rocket and sled launches, ballistic tests and many other sensitive operations requiring rigid test conditions and a dependable soil foundation for the track.

The base and range area is located approximately 100 miles due east of Bakersfield, California. The facility stretches some 1800 square miles across the high desert region at the

southern end of the Sierra Nevada mountain range. Due to only a locally high groundwater table, however, this study will be restricted to a 260 square mile region located at the southern end of the main facility area.

METHODOLOGY

The methodology utilized in this study is outlined by the flowchart illustrated in Figure 1.3. This method will combine concepts introduced by Youd and Perkins (1978) with those of Dobry and others (1979). In combining the two, an attempt will be made to utilize Youd and Perkins' ability to qualitatively and empirically predict ground failures due to liquefaction over a large area, and Dobry's quantitative approach to the prediction of liquefaction potential by the generation of excess pore pressure in the soil profile.

First, a detailed geologic map of the study area is used. Particular consideration is given to the composition of each unit, such as the soil type, method of deposition, age of the deposition, and any particular cementation noted. Other geotechnical factors affecting soil susceptibility to liquefaction are not considered at this stage. The result of this input will enable the deposit as a unit to be classified as to low, moderate, or high susceptibility.

Depths to the groundwater table were then collected from existing well sites on base. In areas lacking such information, a literature search was carried out to determine previous levels and current rates of table fluctuations. These depths and well locations were digitized for determination of precise latitudinal and longitudinal coordinates before being formatted for computer input. Two programs were utilized by the computer in the generation of a depth to groundwater contour map. The first program assembled all input data points and created a rectangular grid system with calculated depths at all intersections or grid corners. The original data points were then disregarded. The second program was a graphic tool that connected all grid points of equal depths with contour lines. The contour lines ranged from water levels located above ground surface to depths of 40 feet, at 2-foot intervals. The accuracy of these griding and contouring programs were then verified by the proximity of each original input

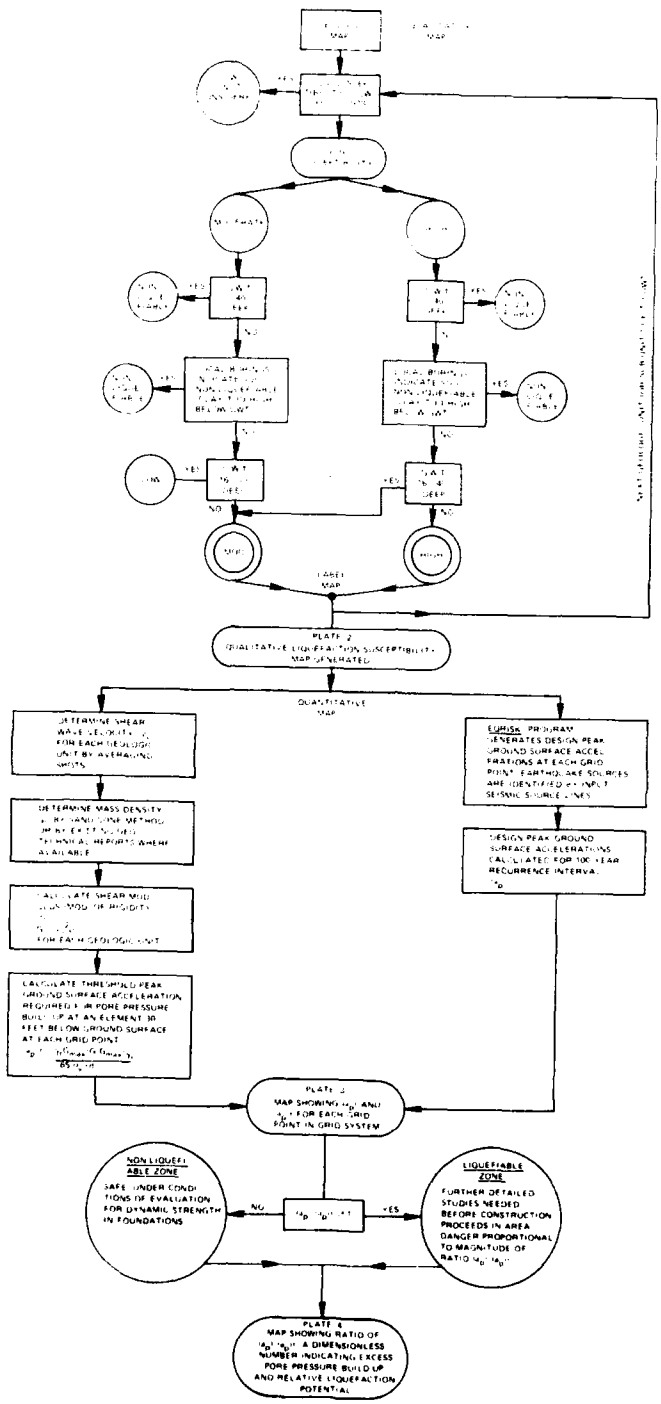

FIGURE 1.3. Methodology Utilized in the Study of Liquefaction.

data point with the nearest contour line. This graphic procedure was not accepted until each contour line accurately represented the originally known input data points.

All known boring logs were then collected and the down-hole profile was analyzed for potentially liquefiable soils. All borings revealing a lack of saturated sand or silt within the upper 40 feet enabled the locality to be classified as non-liquefiable.

The depth to groundwater contour map was then superimposed over the geologic map with the units classified as "high" and "moderate" highlighted. These 2 classifications, when falling in the range of depths to water less than or equal to 40 feet were then recorded as potentially prime liquefaction areas. It is these areas that were further analyzed in a more quantitative manner.

Dobry and others (1979) have proposed a profile stiffness method for liquefaction potential. This method utilizes the empirical and experimental findings of many authors to develop the threshold peak ground surface accelerations, $(a_p)_t$, at which the soil's cyclic strain is equal to $10^{-2}\%$; a strain level which has been found by many authors to be the level above which excess pore pressures develop. This will be discussed in detail in Chapter 4. Field data required for calculation of the threshold peak ground surface acceleration includes the shear wave velocity and the mass density of the soil. An ES-1200 twelve channel signal enhancement seismograph was utilized in the determination of the shear wave velocities from surface refraction. Available borings and/or a sand cone apparatus were utilized in the determination of the soil's mass density. Both of these values were averaged over the entire geologic unit, thereby defining the threshold acceleration for a single geologic unit as a function of only the depth to groundwater and the resultant total overburden stress. These threshold acceleration values were calculated at sites on half mile centers in a grid system set up over the entire study area.

A second grid system, identical to the first, was incorporated to analyze the seismicity of the study area. A computer program called EQRISK (McGuire, 1976) was then implemented to predict peak ground surface accelerations on this grid. EQRISK generates a probabilistic peak

ground surface acceleration knowing the fault characteristics in the area, their location, and the region's historic background seismicity.

Values of the calculated threshold peak ground surface accelerations, $(a_p)_t$, and the design peak ground surface accelerations, a_p, were compared for a 100 year return interval. The result was a regional map illustrating the potential and/or the relative ease of pore pressure increases and the possible liquefaction at any specific area.

Chapter 2
REVIEW OF THE LITERATURE

GENERAL

The realization that liquefaction is seismically induced is relatively new. In 1930 Casegrande introduced the term "liquefaction" as it related to slowly applied loads. The present concern over cyclic loading causing liquefaction only began in the early 1960's as a direct result of the case histories previously described. Since that time numerous investigators have supplied answers to many questions as to what liquefaction is, what causes it, what factors influence its development, and how to alleviate or design for the problem. In the past 10-15 years there has been much literature generated regarding laboratory studies, case histories, and methods of analysis of the liquefaction problem. The purpose of this chapter is not to review all the details of these studies, or even to attempt a complete list of what has been accomplished. This chapter will describe liquefaction and present various methods of analysis that are now being utilized, as well as introduce findings that have recently been developed.

DEFINITIONS OF LIQUEFACTION

Because of the numerous independent studies that have been performed on liquefaction, there have been some slight differences in definitions of terms. Youd (1975) observes two basic components to most definitions of liquefaction; a strength loss criteria and a flow deformation criteria. He indicates the attempt to combine these two distinct phenomena into a single universal definition has resulted in controversy. Some of the definitions that Youd uses to illustrate his point are:

"The sudden decrease of shearing resistance of a quicksand from its normal value to almost zero without the aid of seepage pressure." (Terzaghi and Peck, 1948)

"The sudden large decrease of shearing resistance of a cohesionless soil, caused by a collapse of the structure by shock or strain, and associated with a sudden but temporary increase of the pore fluid pressure [is liquefaction]. It involves a temporary transformation of the material into a fluid mass." (A.S.C.E., 1958) (American Geological Institute, 1972)

"The phenomenon of the loss of strength of saturated granular soils during earthquakes is generally referred to as liquefaction. The process of liquefaction transforms an element of soil from a state of saturated granular solid to a state of viscous fluid." (Ghaboussi and Wilson, 1973)

"A phenomenon in which a cohesionless soil loses strength during an earthquake and acquires a degree of mobility sufficient to permit movements from several feet to several thousand feet." (Seed and Idriss, 1971)

"Complete liquefaction — when a soil exhibits no resistance (or negligible resistance) to deformation over a wide strain range, say a double amplitude of 20%.
Partial liquefaction — when a soil first exhibits any degree of partial liquefaction during cyclic loading.
Initial liquefaction — when a soil first exhibits any degree of partial liquefaction during cyclic loading." (Lee and Seed, 1967)

"The conventional use of the term [liquefaction], as it will be used throughout the study, refers to the phenomenon which takes place in a mass of soil during flow slides. Liquefaction, or flow failures of a sand is caused by a substantial reduction of its shear strength." (Castro, 1969)

As is noted, the first five definitions refer to liquefaction as the loss of shear strength of the soil mass. The last definition by Castro refers to flow failures or deformations as liquefaction, which is caused by soil losing its shear strength.

The controversy in literature results when asked the question, how much deformation constitutes liquefaction? Seed and Idriss (1971) and Lee and Seed (1967) indicate that any flow deformation of the soil mass constitutes a liquefaction condition. However, Castro (1969) and Casegrande (1976) feel that the term "liquefaction" should refer to a condition of unlimited flow and that "cyclic mobility" should refer to a condition where the deformation is arrested by a pore pressure reduction. The pore pressure reduction is a result of soil dilatancy.

The differences, though only slight, do exist in the literature. Seed (1976), in his state-of-the-art address, notes these similarities and proposes the terms "initial liquefaction with limited strain potential" or "cyclic liquefaction" [cyclic mobility] to refer to the condition where limited strains, which may be caused by liquefaction of denser sands for instance, are exhibited in a soil mass. This suggestion would hopefully allow all concerned to understand the basic mechanism.

Further, Youd (1975) also attempts to answer the controversy with the following definition:

> "Liquefaction is defined as the transformation of a granular material from a solid state into a liquefied state as a consequence of increased pore-water pressures. Solidification is defined as the opposite process, that is, the transformation of a granular material from a liquefied state into a solid state. Once liquefied, a granular material is free to flow, until solidification occurs. If solidification occurs after a finite flow deformation, the condition is termed limited flow. If flow continues unbated under constant total stress, the condition is termed unlimited flow."

This definition by Youd seemingly accounts for both "liquefaction" and "initial liquefaction with limited strain potential" as does Seed's (1976).

DEFINITION FOR THIS STUDY

The definition used in this study is: the transformation of a soil mass from a solid state to a liquefied state. This transformation is a result of an increase in the pore pressure caused by the cyclic loading of an earthquake. While soils at depth may be said to "liquefy", "liquefaction" is further qualified by requiring the shear strength failure to reach the ground surface. The term "liquefaction potential" refers to a seismically induced pore pressure build-up at depth which is capable, but not necessarily showing evidence of a loss of shear strength at the ground surface. The factors qualifying "capable" in this definition, which are the variables potentially allowing shear strength failure to reach the surface, will be outlined further in Factors Affecting Liquefaction (Chapter 2).

MECHANISM OF LIQUEFACTION

The basic cause of liquefaction is fairly well understood and accepted. As an earthquake occurs it creates waves of energy (shock waves) in the bedrock that radiate away from the source in all directions. Seed and Peacock (1971) suggest at a particular site, when the bedrock is excited by these waves, the soil profile above the bedrock is set into motion. Shear waves propogate upwards from the bedrock to the ground surface. These shear waves cause cyclic shearing stresses to develop within the soil mass, which leads to liquefaction. The typical elements illustrated in Figure 2.1(a) show the stresses applied during earthquake loading. As noted in part b of the referenced figure, if a granular soil mass is subjected to these shear waves, under undrained conditions, a build-up of excess hydrostatic pore pressure develops.

In an effort to best illustrate the three basic ideas mentioned in the definitions of liquefaction, i.e., pore pressure build-up, loss of strength, and flow deformation, it is helpful to discuss Seed's (1976) model. Seed indicates that the build-up of pore pressure results from two interacting mechanisms. As the cohesionless soil mass is subjected to cyclic loading, there is a tendency for the structure of the soil to change and to decrease in volume. As the soil is trying to compact, the load is transferred to the pore fluid which results in a build-up in pore pressure under undrained conditions.

The other mechanism that is associated with the build-up of pore pressure is the soil-structure rebound. As the load is transferred to the pore fluid, the structure exhibits an elastic rebound due to the load release. The structure will rebound enough to maintain a constant volume within the soil system. The combination of the volume decrease, due to cyclic loading, and the soil rebound, due to load release, determines the amount of excess pressure that is generated.

Figure 2.2 is a diagram used by Seed (1976) to illustrate this point. Point A on the void ratio versus log pressure compression curve is the existing effective pressure on the soil element. As the soil element is subjected to a cyclic shearing stress, the soil tends to compact to point B.

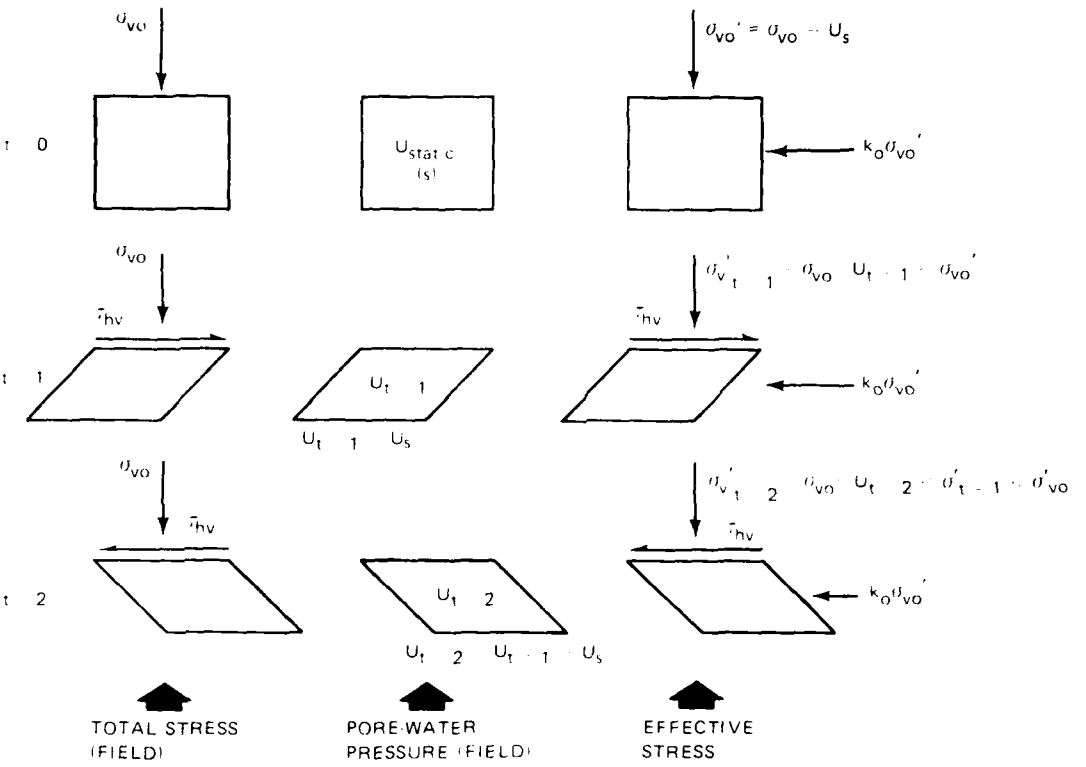

(a) Stress conditions involved in liquefaction.

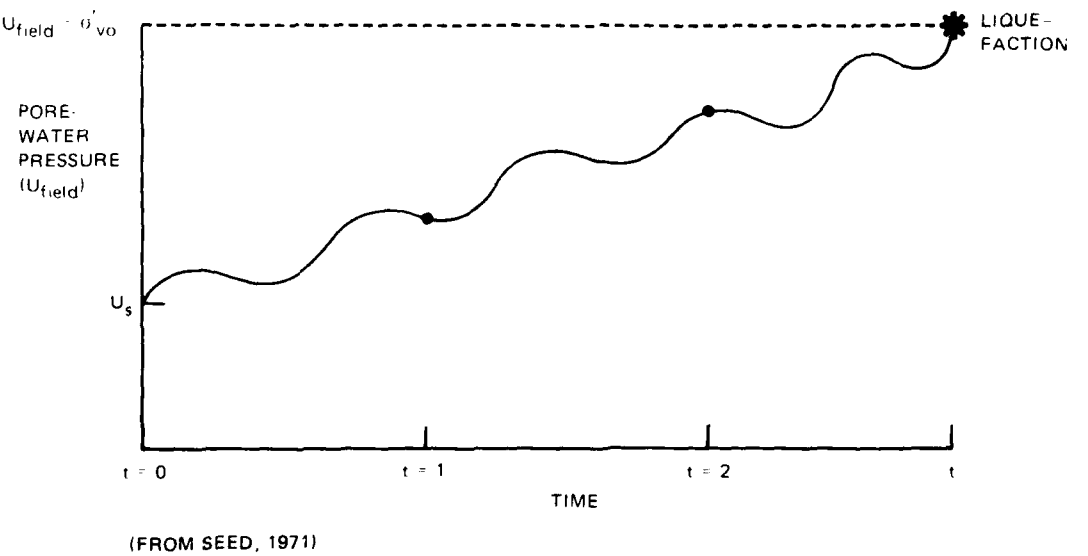

(FROM SEED, 1971)

(b) Pore-water pressure increase versus time.

FIGURE 2.1. Cyclic Stress Loading Due to an Earthquake.

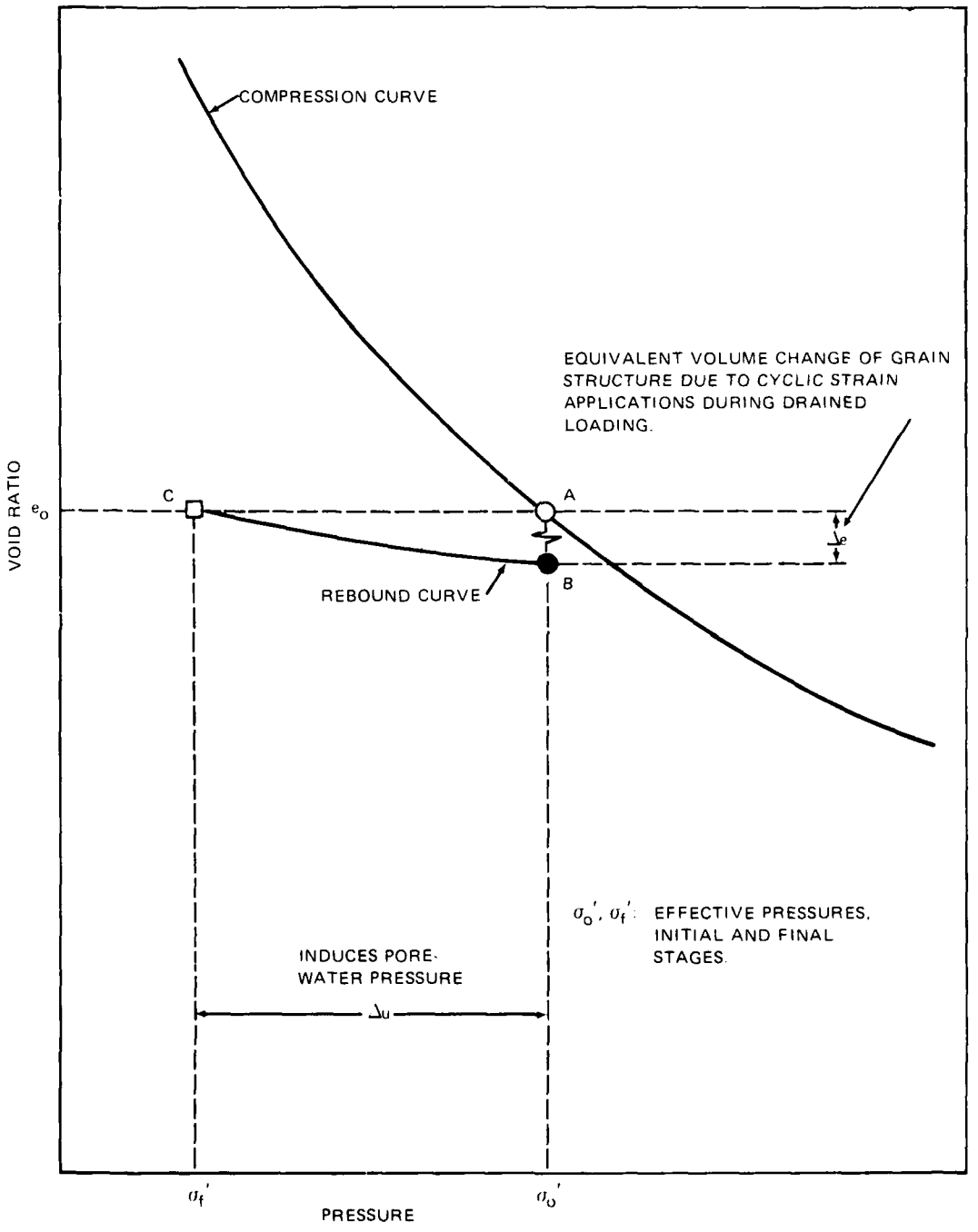

FIGURE 2.2. Schematic Illustration of the Mechanism of Pore Pressure Generation During Cyclic Loading (From Seed, 1976).

Associated with the cyclic loading and soil compacting is the transfer of load to the pore fluid. As the load is released from the soil structure, the soil will tend to rebound along a rebound curve to point C. Under a drained condition the cyclic loading would cause an effect of moving from point A to point B with a net volume decrease. Under undrained conditions, where no volume change can take place, the net effect is moving from point A to point C with a build-up of pore pressure. The net change in pore pressure is determined from the initial and final effective stresses on the soil element.

As described in Chapter 1, Definition of Liquefaction, if the build-up of pore pressure reaches the value of the initial effective confining pressure, the soil will then fail or liquefy. At this point all resistance to deformation has been overcome and the soil will deform under the applied loads. The amount of deformation will depend on the density-state of the soil mass. If the soil is in a loose condition then the deformation could be unlimited. However, if the soil is in a medium to dense state then the soil will begin to dilate. When dilation occurs the pore pressure is reduced and continued deformation is arrested.

FACTORS AFFECTING LIQUEFACTION

GENERAL

When determining the liquefaction potential of a soil profile there are two aspects which need examining. The first is the magnitude of the shearing stresses produced in the profile by a given earthquake. The magnitude of induced shearing stresses is a function of the seismic parameters used in the analysis. The second aspect is the determination of the magnitude of cyclic shearing stresses required to initiate liquefaction in the soil profile. This magnitude is dependent upon the soil properties and other geotechnical parameters. This portion of the chapter will discuss the effect different parameters have on both the induced and required shearing stresses.

INDUCED SHEARING STRESSES — THE SEISMIC PARAMETERS

General. The main parameters generated by earthquakes which are generally discussed in conjunction with liquefaction are:

- Intensity of ground shaking
- Duration of ground shaking
- Magnitude-distance relationship.

Before each of these parameters are explained individually, a brief discussion of their relationship with each other is required. The most common combination of seismic parameters is intensity and duration of ground shaking. These two factors are listed in analysis procedures and case studies by many investigators as the principal seismic parameters (Peacock, 1968), (Seed and Idriss, 1971), (Lee, 1971), (Christian and Swiger, 1975), (Seed, 1976), (Ferritto, 1977), (Dobry, et al, 1979). The third parameter, the magnitude-distance relationship, has been used in place of intensity and duration as the basic seismic factor by Youd and Perkins (1977), and others.

Intensity of Ground Shaking. The intensity of ground shaking, or ground surface acceleration governs the magnitude of the shearing stresses that are applied to the soil elements (Seed and Idriss, 1971). The higher the acceleration of the soil profile the higher the shearing stresses that will be induced. As illustrated by Peacock (1968) in Figure 2.3, under identical confining pressures, the number of cycles required to initiate liquefaction is decreased as the peak shearing stress is increased. In fact, as will be discussed later, a certain threshold acceleration is required to even cause liquefaction.

Ground surface accelerations have been related to magnitude of energy released and distance to causitive faults. Housner (1964) produced a curve utilized for years, however, it was not universally applicable in that it applied only to stiff soil sites. Seed and Idriss (1971) have more recently compiled enough data to create a family of curves with soil type and stiffness also a variable. This relationship is demonstrated in Figure 2.4. Housner and Seed both indicate, however, that the best method to arrive at the intensity of ground acceleration is

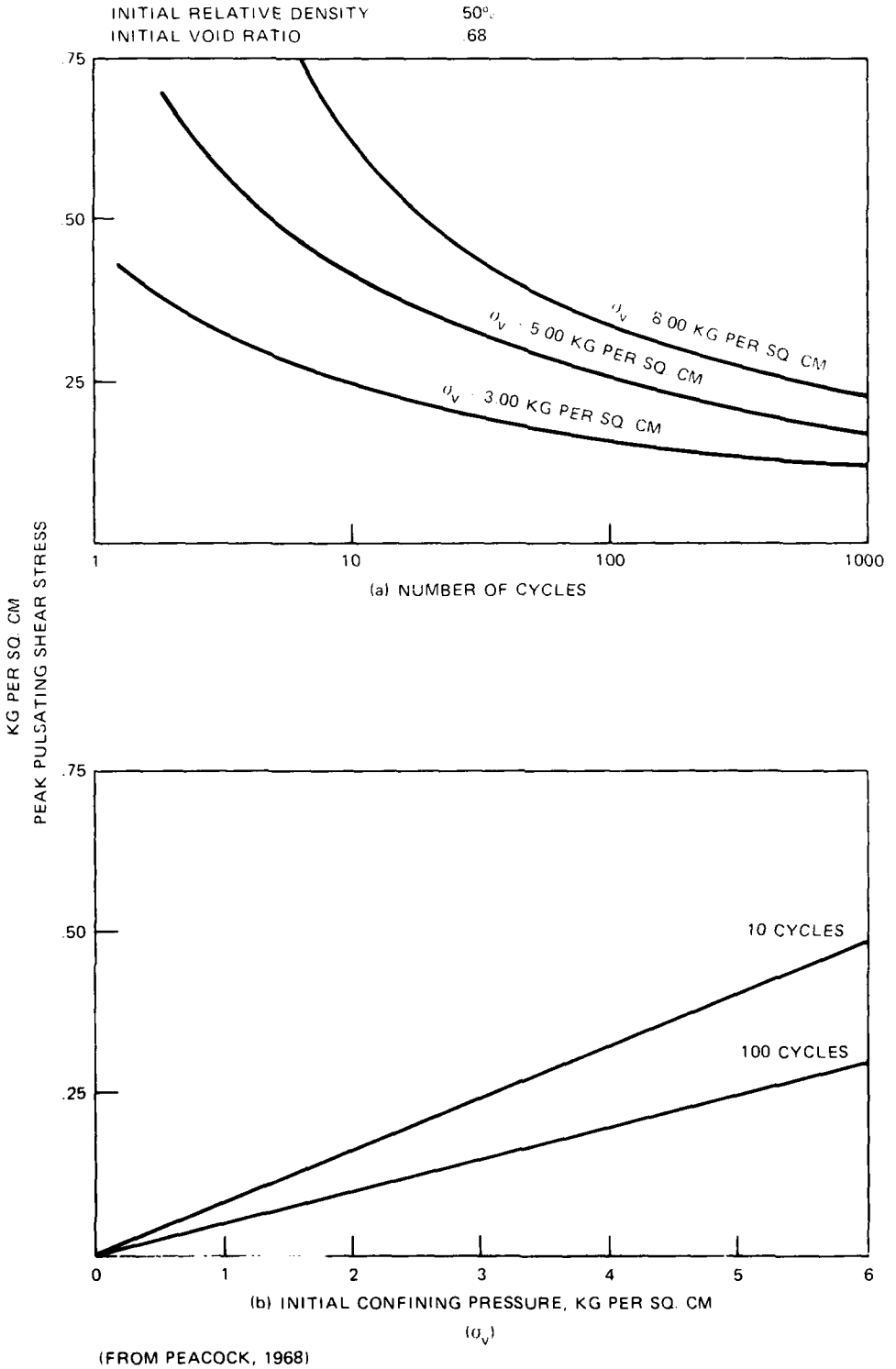

FIGURE 2.3. Effect of Confining Pressure on Cyclic Stress Required to Cause Liquefaction.

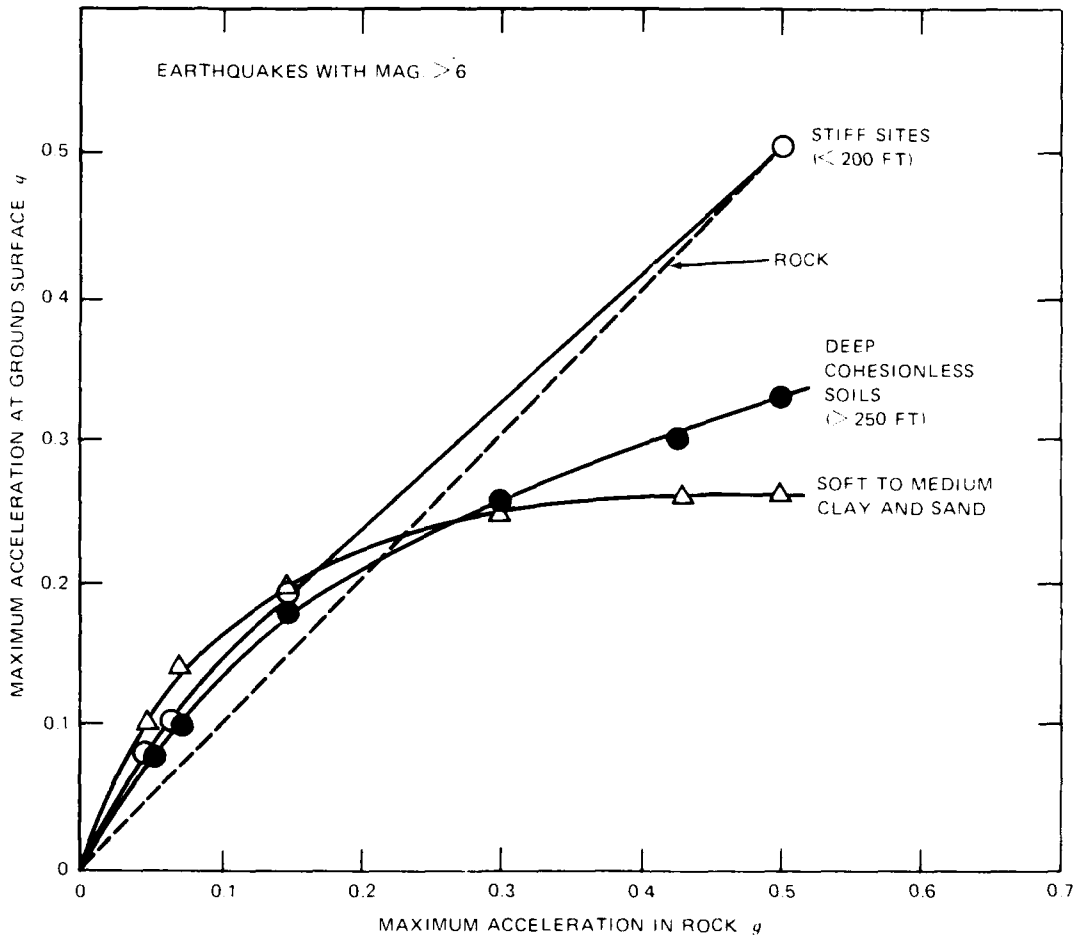

FIGURE 2.4. Approximate Relationships Between Maximum Accelerations for Different Soil Conditions (From Seed and Idriss, 1971).

to measure it with instruments near a seismic source, not necessarily from magnitude-distance relationships.

Because there are only a few recorded acceleration histories, some studies have used earthquake magnitude and distance to causitive sources as their parameters instead of the estimated ground acceleration values. There is much more data on earthquake magnitudes than on earthquake accelerations, therefore, the larger data base on earthquake magnitudes would provide a better solution for development of empirical relationships.

Duration of Ground Shaking. The duration of intense ground shaking has a significant effect on the possibility of liquefaction. It takes time for the pore pressure to build to a

magnitude large enough to overcome the confining pressure and reduce the soil's resistance to deformation. If the duration of strong shaking is not long enough then liquefaction cannot develop. This relationship is seen in Figure 2.3 as, once again, the number of stress cycles to initiate liquefaction is a critical parameter.

Another illustrative example of the importance shaking duration has on liquefaction is pointed out by Seed and Wilson (1967). In their analysis of the *Turnagain Heights landslide* in the 1964 Alaskan earthquake, they report the landslide started approximately 90 seconds after the earthquake began. These authors suggest that had the earthquake lasted only 45 seconds, the slide may never have occurred.

Seed and Idriss (1971) and Lee and Chan (1972) have attempted to standardize the duration of ground shaking by utilizing an equivalent number of significant stress cycles. It is well known that an earthquake produces erratic stress cycles of varying frequencies and magnitudes. These cycles are hard to use in an analysis procedure because of their non-uniform nature. As a result, the above mentioned investigators developed a procedure where the effects of the significant earthquake cycles were simulated by a certain number of uniform stress cycles (called the equivalent number of significant stress cycles). Each uniform stress cycle requires a certain amount of time to oscillate, and so the duration of strong ground shaking is determined by the number of uniform cycles that are applied to the soil. The equivalent number of significant stress cycles is used extensively in laboratory work and computer simulation to model earthquake conditions.

Magnitude-Distance Relationship. The reasons for the development and use of this relationship have already been discussed in the section on Intensity of Ground Shaking. It appears intuitively obvious that waves are attenuated the farther they travel and that the shear stress magnitude subsequently diminishes with the distance from the causitive source.

REQUIRED SHEARING STRESSES — THE GEOTECHNICAL PARAMETER

General. The potential for liquefaction depends, not only on the seismic activity of the region but also on the condition within a soil deposit. Many soil deposits will not liquefy,

regardless of the magnitude and duration of the cyclic shearing stresses that are applied to the soil. The main factors that are considered to influence a soil deposit's resistance to liquefaction are listed below.

- Soil Type
- Relative Density
- Initial Confining Pressure
- Soil Structure or Method of Deposition
- Age of Deposit
- Depth to Groundwater
- Seismic History

Some of the governing factors, such as soil type, density, initial confining pressure, and depth to groundwater are fairly well understood. Their effect on the liquefaction mechanism can be recognized and quantified. The other factors have been recognized as having some effect on the liquefaction mechanism, but they are not fully understood.

Soil Type. Soil type has been established as one of the main contributing factors to liquefaction. Many studies and investigations have pointed to the grain size distribution curves of the soils involved as a major factor in evaluating liquefaction potential. Fine uniformly-graded sands are cited as the most susceptible to liquefaction. This includes, however, a range from large silt particles to medium coarse sands that could also be classified as very susceptible to liquefaction. This range of particle sizes seems to allow the build-up of excess pore pressures more readily than any other size distribution.

Coarse grain sands and gravelly deposits have experienced some cases of liquefaction, but in general have a higher resistance to liquefaction than the finer sands (Wong, et al, 1975), (Ross, et al, 1969). The reason for this is the rapid dissipation of excess pore pressures. Gravelly deposits allow the excess pore pressures to dissipate so rapidly that they do not build up to the effective confining pressures and cause failure.

Clays, while also being exempt from liquefaction, do not maintain stability by pore pressure dissipation while loaded. Their stability is maintained due to their plastic, cohesive nature. Clays maintain their cohesive properties with an electrostatic attraction, rather than the frictional intergranular properties of silts and sands. While friction is obviously reduced by buoyancy, clays maintain their attraction through a significant increase in excess pore-water pressure. Seed (1968) explains that during earthquakes, the cyclic strain developed in elements of sand in the field may not be more than .4%, while the strain in deposits of soft clay may be as large as 1 or 2%. Figures 2.5 and 2.6 show the effects of cyclic strains of these magnitudes on saturated sand and clay. In Figure 2.5 the application of a cyclic strain of about .17% to a sample of saturated sand caused initial liquefaction and total failure after about 16 strain cycles. In contrast, Figure 2.6 shows the loss of strength of a sample of San Francisco Bay mud after 200 strain cycles (Thiers, 1968). Even 200 cycles, with strain amplitudes of up to 2%

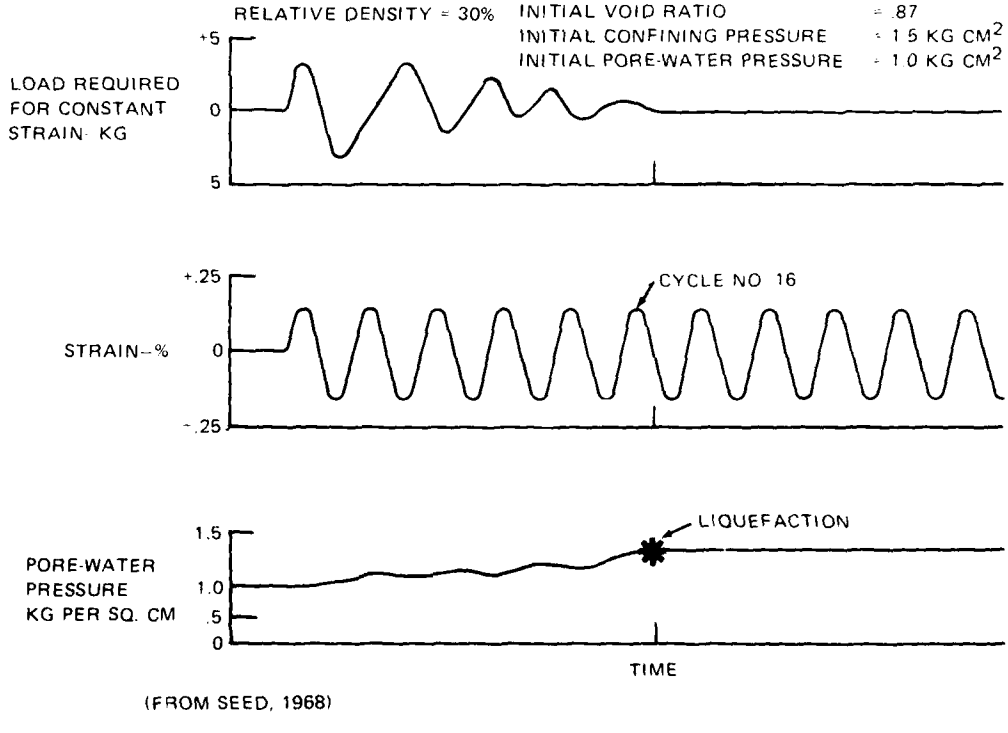

FIGURE 2.5. Cyclic Strain Test on Loose Sand.

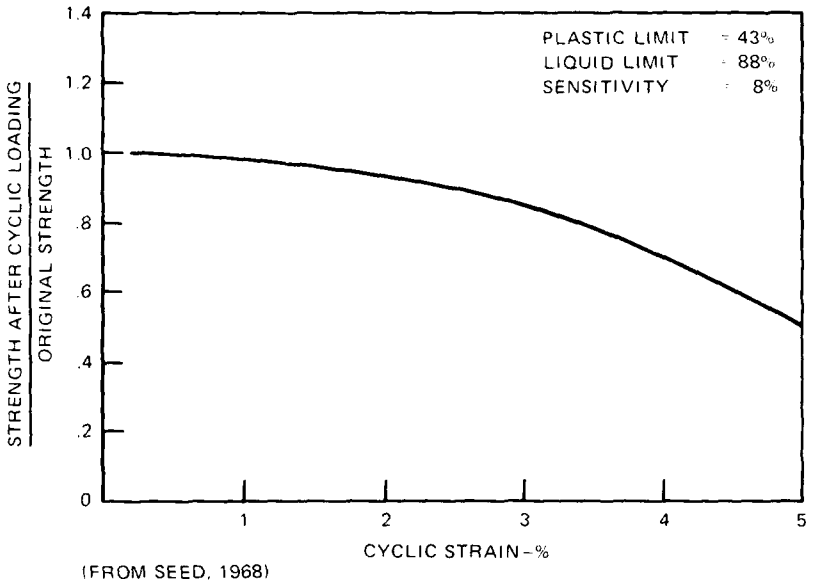

FIGURE 2.6. Effect of 200 Strain Cycles on the Strength of Clay.

caused a strength reduction of only about 5% while exhibiting a continual deformation. This deformation is known to continue as long as the earthquake loading does not exceed the static strength of the clay. Stress in excess of this strength will result in a rupture type failure.

Clays, however, do exhibit another form of dynamic failure. This is a result of the collapse of a previously stable particle structure which is not associated with a pore pressure build-up. A clay susceptible to this phenomenon is termed sensitive and thixotropic.

A new development, even for the most liquefiable soils, are the grain characteristics. Several studies (Annakai, 1975), (Castro and Poulos, 1976) have shown that different types of sands with essentially the same grain size curves, compacted to the same relative density, and compacted with the same compaction methods, differ as to their liquefaction potential. This phenomenon is not completely understood as to what causes the observed difference, but is probably related to grain size.

Relative Density. Relative density has long been recognized as a major factor affecting the liquefaction potential of a deposit. If a deposit is in a relatively loose condition, i.e., low relative density, liquefaction can be initiated by lower shearing stresses or shorter durations of

shaking than if the deposit is at a higher relative density. Figure 2.7 illustrates results of a typical cyclic load test run on loose sand (Seed and Peacock, 1968). In this test a cyclic shear stress of constant amplitude (± .33 kg. per sq. cm.) was applied with a frequency of one cycle per second under a vertical consolidation load of 5 kg. per sq. cm. The resulting changes in horizontal shear strain and pore-water pressure were recorded.

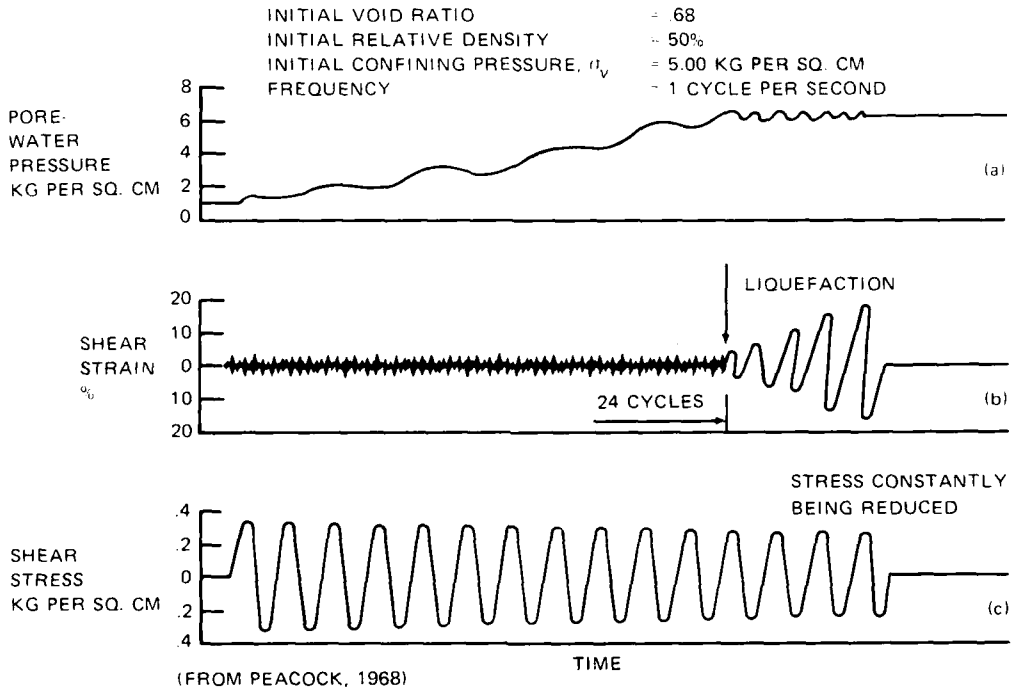

FIGURE 2.7. Pulsating Load Test on Loose Sand—Simple Shear Conditions.

It is interesting to note that in the initial stages of the test (i.e., the first 24 cycles of stress application), the gradual increase in pore-water pressure did not produce a significant increase in the shear deformation, even though the effective stress was constantly being reduced. However, as soon as the effective stress within the sample had been reduced to zero, thereby reducing the shear strength to zero, the deformations increased rapidly and failure due to liquefaction occurred within 2 cycles. This sudden failure appears to be characteristic of loose sands in a variety of dynamic tests.

In contrast, Figure 2.8 exhibits results of the same cyclic load test on dense sand (Seed and Peacock, 1968). An analysis of the pore-water pressure and shear strain curves show that dense sands exhibit somewhat the same behavior as loose sands. Initially, there was no noticeable deformation with increasing pore-water pressure. However, unlike loose sand, the strain amplitude increased more slowly with increasing number of stress cycles. Thus, the dense sand exhibits a gradual build-up of shear strain with the onset of initial liquefaction, but shear strains tend toward a limiting value of about 8% double strain amplitude. A conclusion typified in numerous tests is that dense sand is capable of undergoing "initial liquefaction with a limited strain potential." (Seed, 1976)

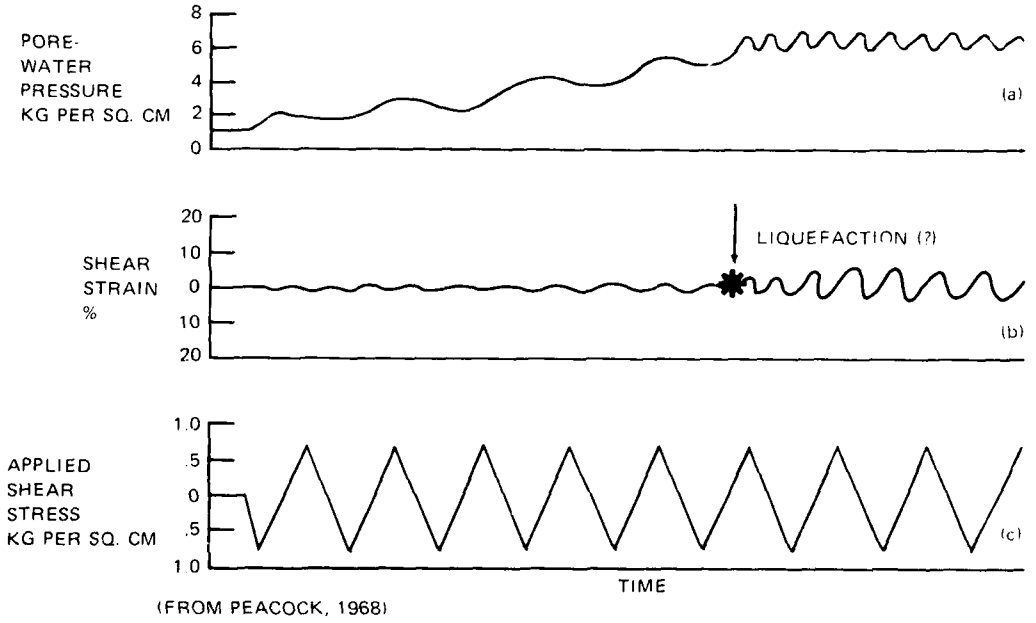

FIGURE 2.8. Pulsating Load Test on Dense Sand—Simple Shear Conditions.

The theories for such a drastic difference in the behavior of sands and silts of different relative density is still being debated. As pointed out by Norris (1980), the arguments between Casegrande and Seed are growing closer together. Norris suggests that Casegrande's critical void ratio theory seems to be a good starting point for debate. As discussed in Mechanisms of Liquefaction, the critical void ratio suggests a void ratio where values less than this ratio (i.e., in a denser state) tend to dilate during shear strain as the particles are forced to "ride up and

over each other." In contrast, void ratios in excess of this value (i.e., in a looser state) tend to collapse into a denser state during shear strain thereby tending toward a total volume decrease. Clearly a decrease in total volume will result in an increase in pore-water pressure when sample drainage and subsequent actual volume change is prevented.

In dense sand and silt, however, as the effective normal stress approaches zero and a significant amount of shear strain is initiated, the tendency is to cause a volume increase, thereby causing a tensional pore-water pressure build-up in the undrained condition. As the shear strain proceeds, the excess pore-water pressure builds in a negative direction and the normal effective stress increases ($\sigma' = \sigma - (-\mu$ excess)). As a result, with each cycle only a certain amount of deformation can occur before sufficient resistance is mobilized, thereby realizing Seed's "limited strain potential."

It is with regard to the effective stress approaching zero, and whether dense sands actually liquefy that Casegrande and Seed founded their debate. Casegrande, using his critical void ratio concept, argued that any sand existing at a void ratio below the critical value tends to dilate during dynamic shear stress, thereby negating any pore pressure build-up as the sample would be in tension. Seed, on the other hand, argues that the critical void ratio is applicable to static loading, but that it does not deal with the possible volume decrease tendency of dense sand during the pore pressure build-up phase occurring prior to the shear strains causing dilation.

Initial Confining Pressure. The confining pressure that a soil element is under is of significant importance in determining its liquefaction potential. The higher the effective confining pressures the higher the excess pore pressures need to be to overcome the strength of the soil that prevents deformation.

Regarding the overburden pressure, the deeper the liquefiable material is in the profile, the higher the overburden pressure and the more resistant the soil becomes (Seed and Lee, 1966). Meslov (1957) and Ambraseys and Sarma (1969) use this to suggest that the presence of a surcharge will reduce the tendency of a deposit to liquefy.

Another important confining pressure, the lateral earth pressures, can be a function of either present overburden pressures or the geologic history of the deposit. If a deposit has been subjected to higher overburden pressures than now exists on the deposit, it has been overconsolidated to a degree. By increasing the overconsolidation ratio (ratio of highest past overburden pressure to present overburden pressure), an increase in lateral earth pressure is also produced. The result of increasing the lateral pressure is the same as increasing the overburden pressure, a more resistant soil deposit to liquefaction (Seed and Peacock, 1971).

Lemuk (1966) and Shannon (1966) illustrate the effects of initial confining pressures as they describe the Seward, Alaska flowslide utilizing eyewitness accounts coupled with a detailed geotechnical analysis. In short, liquefaction occurred at depths of 50 feet or less causing flowslides downhill into the harbor. When one such layer slid away, the reduction in confining pressure permitted liquefaction of the underlying layer and this procedure could repeat progressively during the earthquake.

Seed, Lee, and Idriss (1969) suggest their laboratory tests show that the larger the ratio of initial shear stress to initial normal confining pressures acting on a horizontal surface of a soil element, the greater is the horizontal cyclic shear stress required to induce liquefaction in a given number of stress cycles. This relationship leads directly to the conclusion that other factors being equal, liquefaction will be induced more easily under level ground conditions than is sloping zones of a deposit.

The parameter that many laboratory studies base their results on is the cyclic stress ratio. The cyclic stress ratio is the shearing stress required to cause liquefaction to the effective confining stress on the sample. The cyclic stress ratio is usually plotted versus the number of equivalent uniform stress cycles that is required to cause liquefaction. The shearing stress is proportionate to the confining stress so the cyclic stress ratio provides a convenient dimensionless parameter that includes two factors that influence the liquefaction characteristics of a soil deposit.

Soil Structure (Method of Deposition). Soil structure and the effect that it has on the liquefaction characteristics of a soil is a fairly recent finding. Mulilius, et al (1975) clearly show that the method in which a soil deposit has been laid down makes a difference in its liquefaction characteristics. Their report deals mainly with different methods of preparing laboratory samples, but the conclusions are easily extrapolated to field conditions. This means that a cohesionless deposit probably will have different potentials for liquefaction depending on whether it was deposited by fluvial deposition, direct sedimentation, or by eolian deposition. Each soil structure would be different and would produce different susceptibilities to liquefaction.

The exact nature of what the soil structure does to alter liquefaction potential is not completely understood. It is, therefore, hard to quantify and to indicate how the soil structure could be considered in an analysis procedure.

Age of Deposit. The length of time that a soil deposit has been in place also has an effect on its liquefaction characteristics. The older a soil deposit is the less chance there seems to be that it will liquefy. Holocene (recent) and late Pleistocene deposits are cited as the most likely deposits to liquefy. This conclusion is based on numerous case studies that determine the age of deposits that were known to liquefy during a seismic event (Youd and Hoose, 1977), (Youd and Perkins, 1977). Recent laboratory studies have also shown that the longer a sample is allowed to sit before testing the more resistant the samples becomes to liquefaction. Lee (1975) indicates that this increase in resistance might be the result of cementation between the contact points of sand grains, or the development of a more stable structure resulting from secondary compression.

Depth to Groundwater. The depth to the groundwater level plays a major role in liquefaction susceptibility. If a soil is not fully saturated then it is impossible to develop excess pore-water pressure.

The depth to the water table also affects the confining pressure on the soil element. The higher the water level in the soil profile, the lower will be the effective confining pressure at

any depth below the water level. This indicates that a high water table in a soil deposit not only saturates the deposit, making liquefaction possible, but also reduces the effective pressures on the soil elements below the water level. If the effective confining pressures are reduced on the soil elements, then the deposit is more susceptible to liquefaction.

Seismic History. Although not completely understood, seismic or strain history has a significant effect on the susceptibility of a soil deposit to liquefaction. Seed, et al (1977) and Youd (1977) states that this change in liquefaction susceptibility could possibly result from a volume change, i.e., interparticle packing or structural changes caused by previous earthquakes that change the pore pressure build-up mechanism or ability. The effects were first presented by Finn, et al (1970), but later studies have shown some of the same results (Lee and Focht, 1975), (Seed, et al, 1977), (Youd, 1977).

Youd (1977) summarizes the results by stating 4 conclusions. (1) Drained prestraining generally produces a packing in sandy materials that is more resistant to liquefaction than was the original packing. (2) Undrained prestraining, not producing liquefaction, with subsequent pore-pressure relief also produces a packing that is more resistant to liquefaction than the original packing. (3) Undrained prestraining producing liquefaction and limited flow deformation leaves a packing highly susceptible to liquefaction even after reconsolidation. (4) Following a loading phase, which produces liquefaction, and a limited flow deformation and reconsolidation phase as outlined in number 3, additional drained loading cycles produce significant increases in the liquefaction resistance of previously liquefied sand (Youd, 1977). Suggested causes of increased liquefaction susceptibility with previously liquefied soil include a loss of strengthening from cementation, prior strain history, and lost grain structure.

METHOD OF ANALYSIS

GENERAL

With all the information now being generated concerning liquefaction, some authors have attempted to form a rational method of analysis. Each different method is based on the seismic

and geotechnical parameters previously discussed. Individual authors may weigh individual parameters differently, depending on their feelings of importance to the situation. No one method is clearly better, nor has one method been universally accepted. Only with numerous trial and error situations, with the final test being actual case histories, will the most accurate method of analysis be accepted. Currently, some methods might be used more than others, but it's generally only because they have been in existance longer.

LABORATORY TESTING PARAMETERS

A large amount of laboratory work has been carried out by investigators in the analysis of the dynamic stress field in soil during liquefaction. Many of the testing procedures, together with the subsequent results, have been used as a springboard for other field methods for analyzing liquefaction potential. This laboratory testing section is meant to provide an understanding of the stress field and discuss two of the more major soil dynamic tests and the potential problems of each. It must first of all be realized that whenever laboratory testing is carried out on soil, disturbances of the in-situ soil structure is inevitable and therefore understood to be a problem.

It has previously been suggested (Seed and Peacock, 1971) that in many cases it appears that the main forces acting on soil elements in the field during earthquakes are those resulting from an upward propagation of shear motions from underlying rock formations. The result is that a soil element in a deposit, with a horizontal ground surface, is subjected to the sequence of stress application illustrated in Figure 2.9. Before the earthquake the soil element is subjected to the principal stress (σ') and $k_o\sigma'$, in which k_o is the coefficient of lateral earth pressure at rest. During the earthquake the element will be deformed through the development of a shear stress (τ_{hv}) which will reverse directions many times during the cyclic loading.

Utilizing analytical methods, such as the program SHAKE (Schnabel, et al, 1972) which predicts ground motion acceleration, the values of τ_{hv} and σ' can be evaluated for different soil elements in the profile. The magnitude of this shear stress will vary somewhat erratically

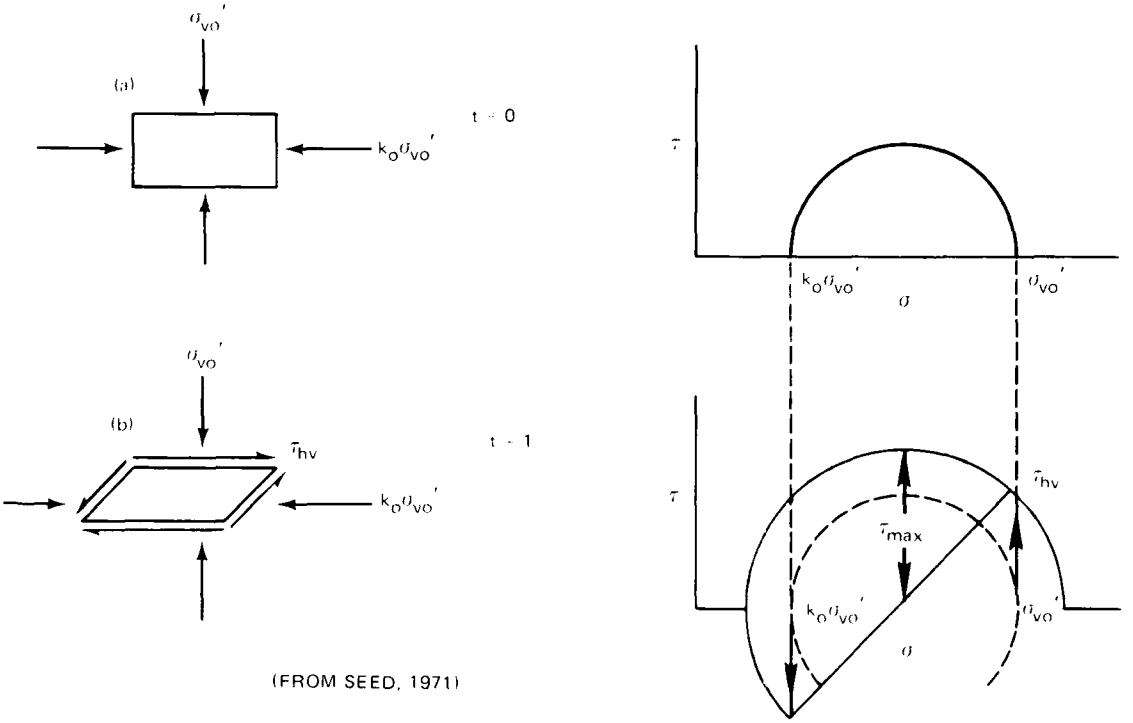

FIGURE 2.9. Cyclic Stress Loading—Simple Shear Test.

from one cycle to the next. As mentioned in the discussion on Duration of Shaking, by appropriately weighing the different cyclic stress amplitudes this loading pattern can be converted to an equivalent number of uniform stress cycles. It is this pattern to which the samples are subjected during laboratory testing. The objective, therefore, of the test procedure is to determine the magnitude of the cyclic shear stress (τ_{hv}) which will cause liquefaction of representative samples for different values of the initial effective normal stress (σ_v').

CYCLIC SIMPLE SHEAR TEST

Seed and Peacock (1971) note that the laboratory cyclic simple shear test is considered to correctly simulate the field loading condition (Figure 2.9). Both field and laboratory elements are first consolidated under an effective overburden pressure (σ_v'), and because the sample is restrained (see Figure 2.10 for test apparatus) from lateral deformation, a lateral earth pressure is modeled equal to $k_o\sigma_v'$, yielding the stress condition as shown in Figure 2.9. During an

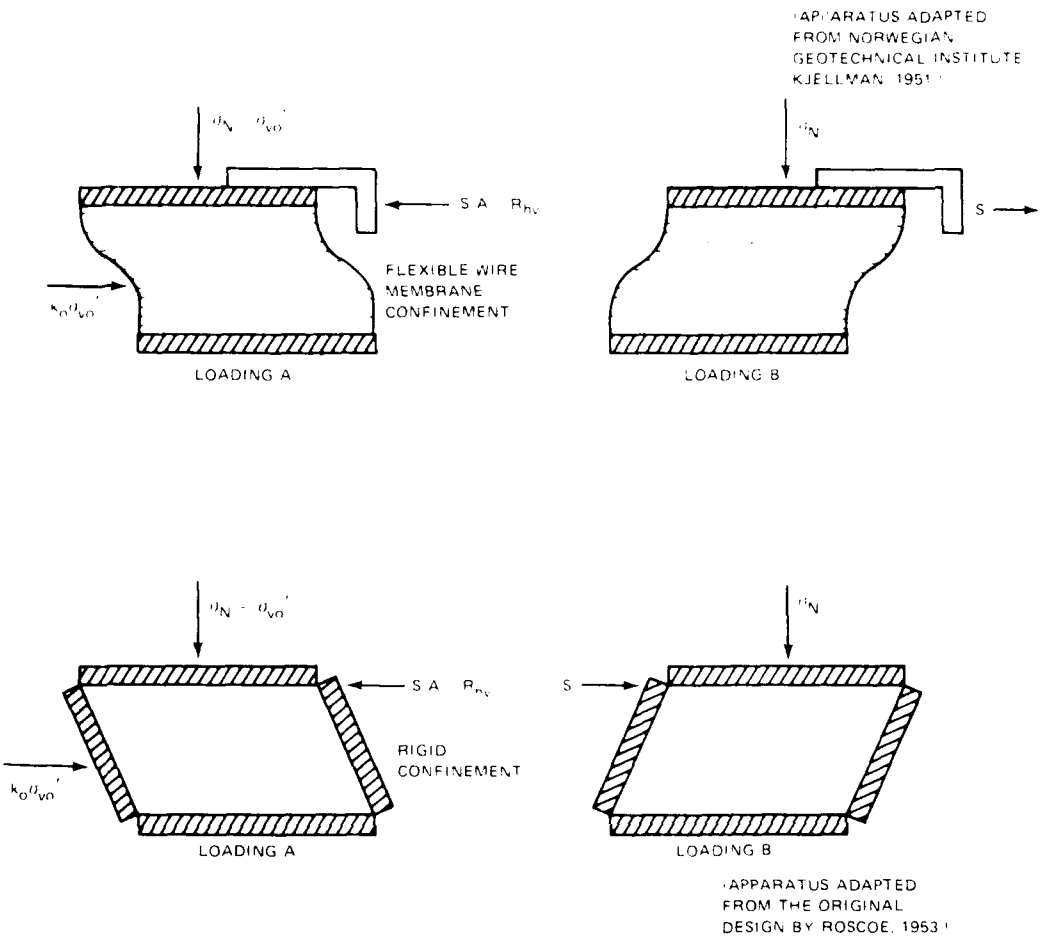

FIGURE 2.10. Laboratory Cyclic Simple Shear Test Apparatus.

earthquake, or as a result of stress applications in the laboratory, the soil element is subjected to a horizontal and vertical shear stress (τ_{hv}). This stress condition changes as shown by Figure 2.9's accompanying Mohr's circle. Note that as τ_{hv} is applied in a cyclic manner, the maximum shear stress (τ_{max}) in the sample increases, and in fact is always greater than τ_{hv} when k_o is less than 1. Note also that the shear stress required to cause failure increases with increasing k_o or confining pressure. This further illustrates the importance of confining stress.

It has therefore been established that the application of stress in the cyclic simple shear test is similar to that in the field. Note, however, that when modeling liquefaction phenomena in the laboratory, testers are interested in working at or near a failing condition at all times.

From this we can clearly see that the effects of nonuniform behavior can be very detrimental to the results.

Seed and Peacock point out that accurate simulation of field stress conditions are limited by the following factors:

1. Because of the difficulties in enclosing test specimens to maintain constant volume or uniform strain, it is difficult to prepare test specimens in a uniform condition, i.e., uniform specimen densities, representative of field conditions.

2. Difficulties are encountered in ensuring a uniform application of shear stress across the width of the sample, the uniformity depending to a considerable extent on the stress transfer mechanism between the cap, base, and the sample.

3. Roscoe (1953), who has worked to refine the testing apparatus, notes difficulties in developing complementary shear stresses along the vertical faces of a test specimen; the absence of which leads to nonuniformities in stress and strain conditions near the edges of the sample and to some rocking of the cap and base under cyclic shear stress application.

4. Unless the specimen is specially constrained, concentrated zones of stress and subsequent strain are likely to develop at the points of application, i.e., the cap and base.

Seed and Peacock have found that the net effect of the limitations on both the apparatus and testing procedures, and the subsequent nonuniformities in stress conditions cause samples to fail up to 35% lower than would be required in the field.

CYCLIC TRIAXIAL TEST

Because of its more widespread availability and simplified procedures, the cyclic triaxial compression test is a popular tool for use in evaluating liquefaction potential. It must be noted, however, that the stress conditions in this test are not readily comparable to those for normal earthquake loading conditions (Seed and Peacock, 1971). This difference in effective stresses can best be exemplified by looking at the variations in total stresses on a particular plane at inclination α. Figure 2.11(a) illustrates the method of loading employed by the cyclic triaxial test with a superimposed plane at inclination α. The accompanying Mohr circles (Figure 2.11(b)) show the stress directions involved. In comparing times 1 and 2, as also seen in actual

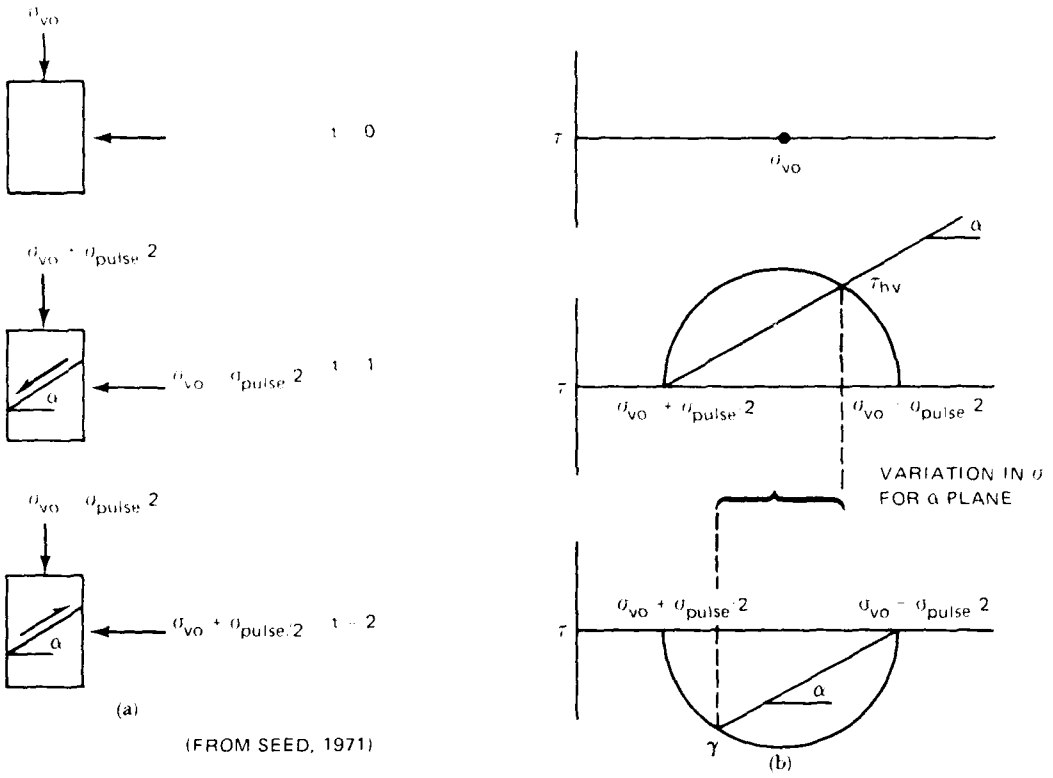

FIGURE 2.11. Cyclic Stress Loading—Cyclic Triaxial Test.

field conditions, the shear stress magnitudes are equal but their directions are opposite. Unlike the actual field conditions we wish to model, note the variations in total normal stress occurring between the two intervals. As noted in the discussion of the cyclic simple shear test, a typical seismically loaded field element is subjected to a relatively constant normal load with the cyclic shear component being opposite in direction but equal in peak magnitude. Figure 2.11 suggests that only when $\alpha = 45°$ (or $2\alpha = 90°$) will the modeled laboratory stress conditions be similar to those expected in the field.

Seed and Peacock (1971) caution that it is only possible to produce the desired stress changes isotropically by consolidating the sample, i.e., under a lateral pressure coefficient equal to 1 ($k_o = 1$). If any other initial stress condition is used, there is no plane in the sample which receives the desired symmetrical changes in shear stress corresponding to those on the horizontal plane in the field. This factor further alienates the triaxial model from the desired field conditions as the accepted in-situ k_o value usually ranges from .4 to .5.

Seed and Peacock's (1971) further observations regarding the cyclic triaxial test include the following factors potentially affecting the accuracy:

1. Under field loading conditions, the direction of the major principal stress will vary from about 0° to 40° on each side of the vertical, but in the triaxial compression test the direction of the major principal stress may rotate through an angle of 90° on each stress cycle.

2. Unless special precautions are taken, friction between the cap and base of the test specimen can cause stress concentrations which can lead to premature failure of the specimen (Castro, 1969).

3. During the lateral compression part of the stress cycle, the sample will tend to "neck" as failure approaches, and it is difficult to determine the stress condition on the sample once this occurs (i.e., the area is constantly changing). The effect is not likely to be very significant for relatively loose samples in which liquefaction and the development of large strains occur almost simultaneously, but it can have a significant effect on the behavior of dense samples, which in turn would lead to apparently larger deformation than would otherwise be the case.

4. There appears to be evidence that stresses causing liquefaction in triaxial compression tests are influenced by the diameter of the specimen, where the smaller diameter specimens require higher stresses to cause liquefaction.

The effects of the first three limitations are likely to cause test specimens to liquefy or fail at stresses lower than those which would be required under corresponding field conditions. However, Seed and Peacock (1971) also advise that utilizing a $k_o = 1$ condition in the laboratory will cause stresses inducing failure or liquefaction to be higher than those inducing failure in the field.

As an increasing amount of laboratory analysis is undertaken regarding liquefaction, the relationships between cyclic simple shear tests, cyclic triaxial tests, and actual field conditions are constantly being updated. It is recognized that there are numerous problems in attempting an accurate field model. The employment of correction factors, the derivations of which are beyond the scope of this paper, are now being received with an increasing amount of confidence as the potential for catastrophes due to liquefaction is being realized.

SIMPLIFIED PROCEDURE

Over a period of time, the experienced gained from the rigorous analysis employing the shear stress histories computed via SHAKE (Schnabel, et al, 1972), or any other appropriate program has led Seed and Idriss (1971) to propose a simplified method which eliminates:

1. the need to determine the variation in shear stress history with depth, and
2. the need to perform laboratory tests.

This method is, of course, not as accurate as the more rigorous analysis. If indications from the method reveal no danger of liquefaction by a wide margin, a safe condition can be indicated. If the procedure is either safe by a narrow margin, or unsafe, a more detailed analysis should be employed.

This method is operational due to some simplifying assumptions. The basic premise is to compare the cyclic stresses that an earthquake will cause in a soil profile to the cyclic stresses that are required to cause liquefaction in that same profile, as illustrated in Figure 2.12. The overlap region on the figure is the area of concern.

The stresses induced by an earthquake are estimated by a simplified equation of the form:

$$\tau_{ave} = .65 \frac{\gamma h}{g} a_{max}\ rd \qquad (2.1)$$

where

τ_{ave} = average shearing stress caused by the earthquake

γ = unit weight of the soil

g = acceleration of gravity

a_{max} = maximum ground surface acceleration

rd = stress reduction coefficient

The average shearing stress is based on the amount of stress that will be realized beneath a rigid column of soil at a depth h. The stress reduction coefficient, rd, is used because the soil column is not truly rigid. The multiplier constant is an assumption that the average stress is 65% of the maximum stress induced by the irregular stress history. Figure 2.12 is based on numerous calculations of equivalent uniform shearing stresses for different stress histories. The

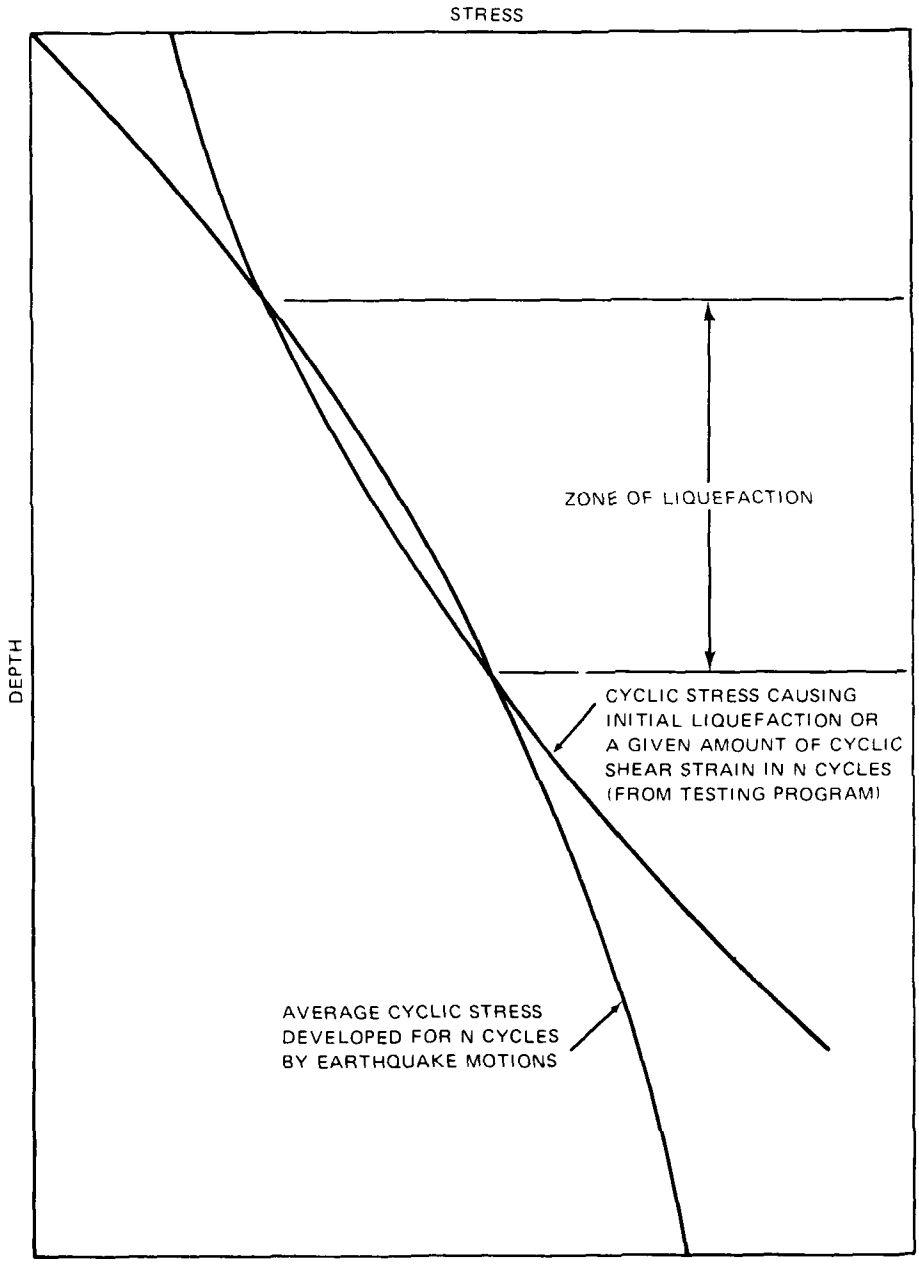

FIGURE 2.12. Method of Evaluating Liquefaction Potential (From Seed and Idriss, 1971).

maximum ground surface acceleration is taken from a family of curves proposed by Seed, who integrated a known bedrock acceleration with a known type of soil profile to yield a surface acceleration. (See Figure 2.4)

The duration of ground shaking is accounted for by adjusting the number of equivalent uniform cycles that are assumed to be applied to the soil profile by the earthquake. This value can be obtained from Seed and Idriss' recommendation which is totally a function of earthquake magnitude.

Shearing stresses required to cause liquefaction in the soil profile are usually determined on the basis of laboratory tests. Dynamic triaxial shearing tests, like those previously described, are usually run to determine the cyclic stress ratio required to cause liquefaction in a given number of cycles and at a given relative density. Stress ratio also depends on the mean grain size diameter, D_{50}.

If dynamic tests are not performed, then a cyclic stress ratio can be estimated for a given D_{50} value at a given relative density and at a given number of uniform stress cycles from dynamic test data run on other samples. The form of the equation used for estimating stresses required to cause liquefaction is

$$\left(\frac{\tau}{\sigma'_o}\right) \text{ l Dr} \cong \left(\frac{\sigma dc}{2\sigma a}\right) \text{l Dr' Cr} \frac{\text{Dr}}{\text{Dr'}} \tag{2.2}$$

where

$\left(\frac{\tau}{\sigma'_o}\right)$l Dr = cyclic stress ratio causing liquefaction at a relative density of Dr

$\left(\frac{\sigma dc}{2\sigma a}\right)$ l Dr' = ratio of the deviator stress to the initial ambient pressure that causes liquefaction at a relative density equal to Dr'; from cyclic triaxial test.

Cr = correction factor to correct triaxial data to field conditions.

$\frac{\text{Dr}}{\text{Dr'}}$ = relative density ratio, to change data from a relative density of Dr' to a given relative density of Dr (Dr' = 50% for Seed's data).

This form of the equation is valid for relative densities to 80%.

If the average shearing stress (τ_{ave}) from equation 2.1 is set equal to the shearing stress (τ) from equation 2.2, then the maximum acceleration (a_{max}) can be determined. Both equations must relate to the same number of shearing stress cycles. The value of a_{max} can be plotted versus the value of Dr for that set of data. Different relative densities can be used to arrive at

different values of a_{max}. The plot forms a boundary between liquefaction and non-liquefaction conditions. An example of this type of plot is shown in Figure 2.13.

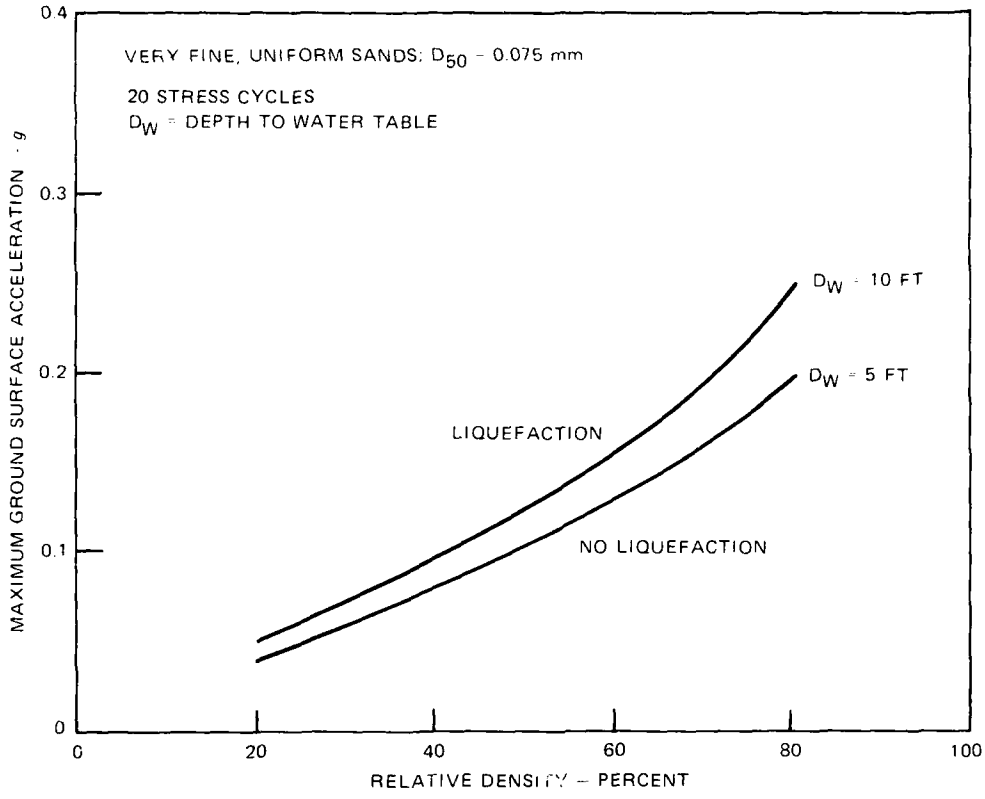

FIGURE 2.13. Evaluation of Liquefaction Potential for Very Fine Sand—20 Stress Cycles (From Seed and Idriss, 1971).

EMPIRICAL METHODS

Another method that is becoming widely known is presented in its most recent form by Seed, et al (1977). This method is based on empirical data of sites that have been studied where liquefaction has or has not occurred. The cyclic stress ratio causing liquefaction was plotted versus blow count data from the standard penetration test, corrected to an effective overburden pressure of 1 ton/sq. ft. A lower bound curve was established that separates the liquefaction conditions from the non-liquefaction conditions, as depicted in Figure 2.14.

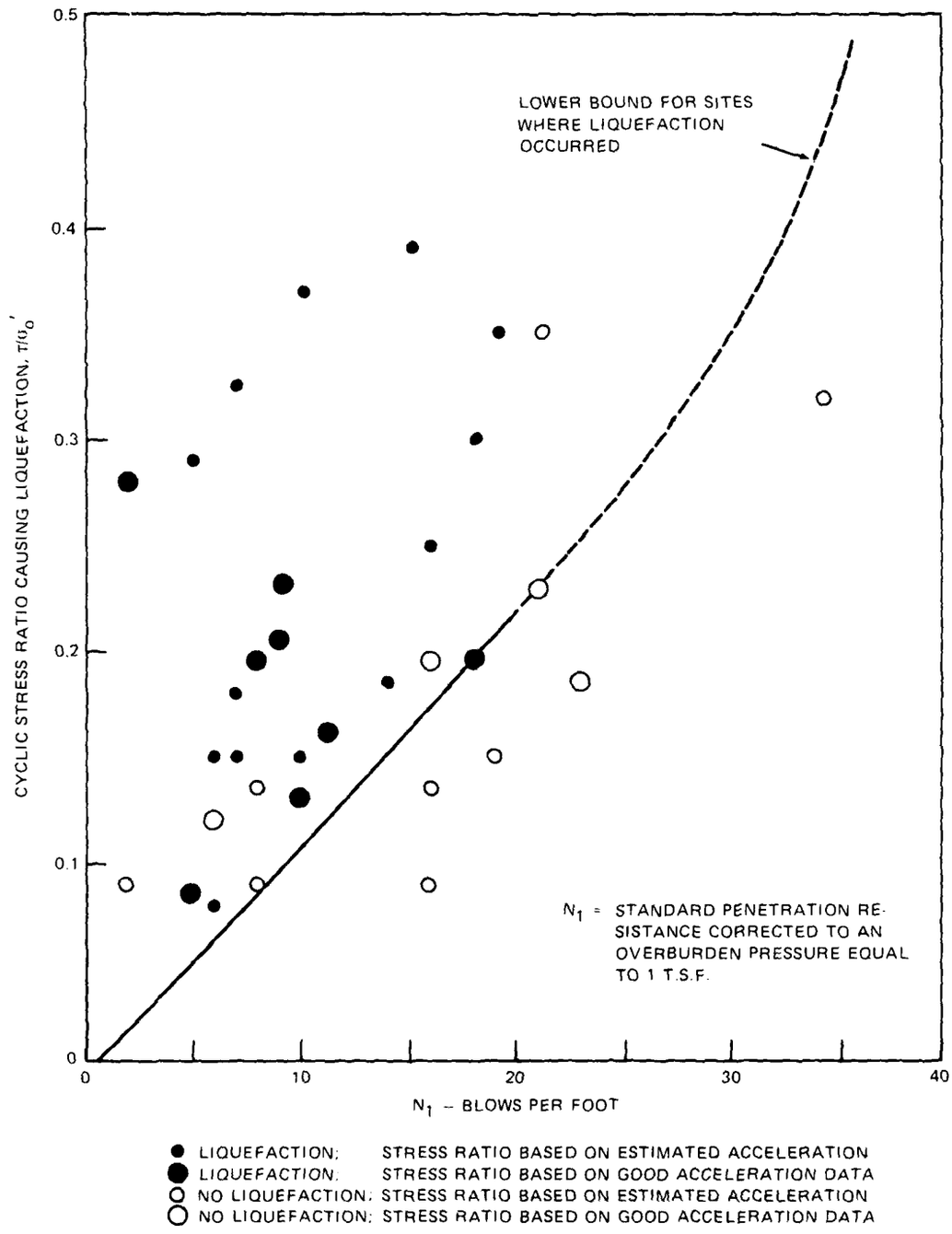

FIGURE 2.14. Correlation Between Stress Ratio Causing Liquefaction in the Field and Penetration Resistance of Sand (From Seed, Mori, and Chan, 1977).

To use the figure, the cyclic stress ratio must be determined. First, the shearing stresses that would be created in a soil profile by an earthquake need to be predicted. This can be accomplished using the same equation 2.1 as given for the simplified procedure for evaluating soil liquefaction potential. Then, the initial effective confining stress used to form the ratio can be determined from boring data taken at the site. The ratio of the shearing stress to the initial confining stress is plotted on the chart versus the corrected blow count also obtained from boring data. If the point is above the boundary line then liquefaction is a possibility. If the point plots below the line then liquefaction probably will not develop. If the point plots close to the line, on either side, then a closer look at the data using a different, more detailed method of analysis is probably justified. This type of approach could be used to pick out the sites and profile layers that might need more attention.

Whitman (1971) presented a method very similar to the above empirical method. He also used data from earthquakes that have caused liquefaction, as well as from a few that did not. The data that he plotted was the stress ratio versus relative density. He pointed out that the data is not sufficient to define a trend or a boundary line, but with more information on other earthquakes some type of distinction could be made between liquefiable and non-liquefiable deposits.

The main difference between Whitman's chart and Figure 2.14 is the plotting of relative densities instead of blow count data. The relative densities are determined using standard penetration results and relationships from Gibbs and Holtz (1957). It is, however, more appropriate to plot the standard penetration results rather than the relative densities. The blow count data in some ways accounts for more of the factors that influence a soil's liquefaction potential than does relative density alone. As the factors such as relative density, soil particle cementation, lateral earth pressure, and prior seismic histories affect liquefaction potential they similarly affect blow count data. It is, therefore, suggested that the blow count data gives a better representation of true strength resulting from many influencing factors and not just one (Seed, et al, 1977).

Donovan and Singh (1976) presented a method for determining liquefaction susceptibility along the Trans Alaskan Pipeline corridor. Their work was a collection of many other investigators' data and results. Simplifications of the data presentations was made for many of the parameters. Donovan and Singh (1976) explain that each of these changes, which were made so that the procedures could be understood and applied by geotechnical engineers with little or no prior soil dynamics experience, was compared with empirical data from cases where liquefaction had been observed before it was implemented.

The first criteria for decision making was an examination of the ground slope along the route. Areas of slope less than 2% were not considered further for liquefaction potential. The reason for this is due to the nature of the construction project. Bearing capacity failures due to liquefaction was not considered a potential problem. Bearing capacity failures were also not considered problems of environmental concern, unlike the potential for flow-slides. Slopes in excess of 2% were evaluated with the following non-liquefiable criteria:

1. Soils consisting of clays and some fine grained silts with sufficient cohesive strength to resist grain movement which could result in the development of excess pore pressures. This condition is considered to be satisfied when the plasticity index number is greater than 5.
2. Soils are very coarse (large gravel, cobbles, and boulders) with sufficiently high permeability and close proximity to drainage areas facilitating rapid enough flow of excess water to prevent build-up of pore pressures.
3. Soils are not, or cannot become saturated.
4. Frozen soils stay frozen.
5. Rock.

A flowchart is made up, and if the soil still remains potentially liquefiable after the 5 criteria mentioned, an empirical chart, relating dry density to relative density by soil type is used to find relative density.

At this point there are five seismic zones or regions separated by maximum magnitude earthquakes and expected duration of the ground shaking. Each zone has a lower bound relative density where liquefaction potential is considered "high". If a density reading is determined, design engineers are brought in to further determine the liquefaction susceptibility.

A Code of Aseismic Design of Hydraulic Structures for this country states that any silty soil which contains less than 15 to 20% clay particles (the clay particle is defined as less than .005 mm in diameter) and has a plasticity index greater than 3, is possible to reach liquefaction during a strong earthquake. The code further qualifies this by saying the water content must also be higher than nine-tenths of the soil's liquid limit.

The newest empirical method, and still in its infant stage, is the use of the cone penetrometer for liquefaction potential analysis. Martin and Douglas (1981) suggest the profiling of a site using the cone penetrometer test, as opposed to the standard penetration test (SPT), provides more information faster, more reliably and at a lower cost than any other method now available. Unlike the SPT, where the actual strength property of the soil being measured is uncertain (Seed, 1979), they also insist that the qualitative determination of strength variation throughout the site profile is immediately obtained from the field records due to side friction measurements along the cone as well as end bearing.

Due to the length of existence of the standard penetration test, and the subsequent broad data base, research is now aimed at the cone penetrometer test—standard penetration test conversion. This emphasis is being focused on the use of the SPT and liquefaction potential relationship, the methods of the cone penetration analysis, and the reliability of the cone penetration (CPT)—SPT correlations. Martin and Douglas (1981) have found that data scatter in the CPT, in relation to the SPT, stems primarily from the scatter in the SPT results or from the finite measurement intervals of the SPT as compared to the essentially continuous CPT measurements. Even with scatter in comparative relations, the CPT method is so rapid that a large statistical data base can be developed, allowing precise definitions of average site characteristics.

PROBABILISTIC AND STATISTICAL METHODS

Some of the most recent approaches to the problem contain concepts of statistical and probability analysis. Christian and Swiger (1975) presented a statistical approach that involves the apparent relative densities and ground accelerations at sites where liquefaction did and did not occur during an earthquake. The basic data was used in a statistical analysis that determined whether the soil would fit into a liquefiable or non-liquefiable category. Confidence levels or probability levels were also included within the analysis to determine how good their procedure was. It was pointed out that their probability levels were not the probability of liquefaction, but the level of confidence in their dividing lines between liquefiable and non-liquefiable sites.

Yegian and Whitman (1977) presented a method of analysis based on a probabilistic model. They developed a parameter in their analysis that is basically the ratio of the induced cyclic shearing stress to the available strength of the soil. The basic inputs into the parameter are the magnitude of the earthquake and the hypocentral distance from the site to the causitive source. They include this liquefaction parameter in their probability model. The probability model gives the probability that a site will liquefy under any earthquake loading. This is a function of the probability that a site will liquefy given a certain magnitude earthquake and the probability of the magnitude earthquake occurring.

Youd and Perkins (1977) have also developed a procedure that is based on probability concepts. The technique develops a liquefaction potential map that gives the relative potential of a site developing liquefaction. The potential map is a combination of two base maps, a susceptibility map and an opportunity map. The susceptibility map outlines the soil deposits within a study area that are most likely to liquefy. The factors used to classify the susceptibility of each deposit were the soil type of the deposit, grain size distribution, and the age of the deposit. A general statement concerning water table depth was also considered in their analysis.

A liquefaction opportunity map provided the seismicity of the study area. The seismicity was determined from the seismic history of the study area. Using the seismic data and a magnitude-distance relationship, a contour map showing the return periods of earthquakes large enough to cause liquefaction was developed. The development of the return period contours were based on concepts from probability analysis.

The final potential map was the combination of the susceptibility and opportunity maps. This type of analysis is a preliminary guide for a given study area. It is not intended to be used as a site-specific analysis that could be included in design calculations. It can, however, help in planning and site location decisions.

STIFFNESS METHOD UTILIZING IN-SITU TESTING PARAMETERS

Although the mechanism of liquefaction has been agreed on, Dobry and Swiger (1979) have presented a method of analysis which may eliminate the previously described problems of laboratory soil preparation for tests involving dynamic stress analysis. An alternative strain approach has been proposed with the main advantages being that the shear modulus at small strains, G_{max} = shear stress/shear strain, can be measured in-situ by geophysical techniques, thus providing a direct measure of the stiffness of the sand deposit ($G_{max} = \varrho V_S^2$, where ϱ = mass density, V_S = shear wave velocity). The basis of this approach is that, other things being equal, stiffer sands are more resistant to liquefaction.

As is described in more detail in a later section of this thesis, a threshold strain, below which no soil densification or subsequent pore pressure build-up can occur, is utilized to predict a threshold acceleration of a soil layer or deposit. Predicted design earthquake accelerations can be determined by computer analysis, or any other means, and then compared to the calculated threshold accelerations to determine the potential for pore pressure build-up. When threshold accelerations are greater than predicted design accelerations, pore pressure build-up will occur and the potential for liquefaction should be further investigated on a site-specific basis.

OTHER METHODS

Two other methods that do not fit into the other categories are presented by Donovan (1971) and Ghaboussi and Dikmen (1978). Donovan (1971) presented a method referred to as a cumulative damage approach. The method makes use of Miner's damage equation and sums up the damage to the soil structure by the cyclic loading of an earthquake. This is analogous to the fatigue failure in structures. A factor of safety is determined to indicate liquefaction or no liquefaction at a particular site.

Ghaboussi and Dikmen (1978) presented a procedure that models the soil profile as a two-phase fluid-solid system. The method was based on the differential equation of motion of a lumped mass system. The solution of the equation of motion included the nonlinear properties of the soil and two separate types of damping. Pore pressure distribution was monitored at different depths by the equations of motion to determine when and where liquefaction would occur.

Chapter 3
SOIL SUSCEPTIBILITY — THE QUALITATIVE STEP

GENERAL

A liquefaction susceptibility map was developed for utilization in determining liquefaction potential. Youd (1978) describes liquefaction susceptibility as the relative ease with which the material under a particular site can be liquefied during strong seismic shaking and permanent ground displacement can ensue. The parameters considered in the development of the liquefaction susceptibility map were the geotechnically related parameters of the unit.

GEOLOGIC SETTING

LOCATION

The China Lake Naval Weapons Center is located in two areas. The southernmost area, Randsburg Wash, is located south and east of Searles Lake and Searles Valley. Due to a groundwater level in excess of 40 feet below ground surface, this area was not considered in this study.

The second area, unofficially referred to as main site, encompasses some 1000 square miles. The boundaries form a rectangle, approximately 42 miles in the north-south and 26 miles in the east-west directions. The northern half of the naval reservation is located in the southern extension of the Coso Range while the eastern third of the lower half reaches into the Argus Range. While there may be plans for the construction of major facilities in these mountainous regions, the excessive depths to groundwater eliminates any liquefaction potential.

The remaining southwest quarter of the Weapons Center is located in Indian Wells Valley and extends west to the base of the Sierra Nevada Mountain Range. It is in these lowlands where a majority of the base's present and future development lies. The designated study area for this investigation includes only the southernmost portion of the described rectangular area. This area covers approximately 260 square miles. (See Figure 3.1.)

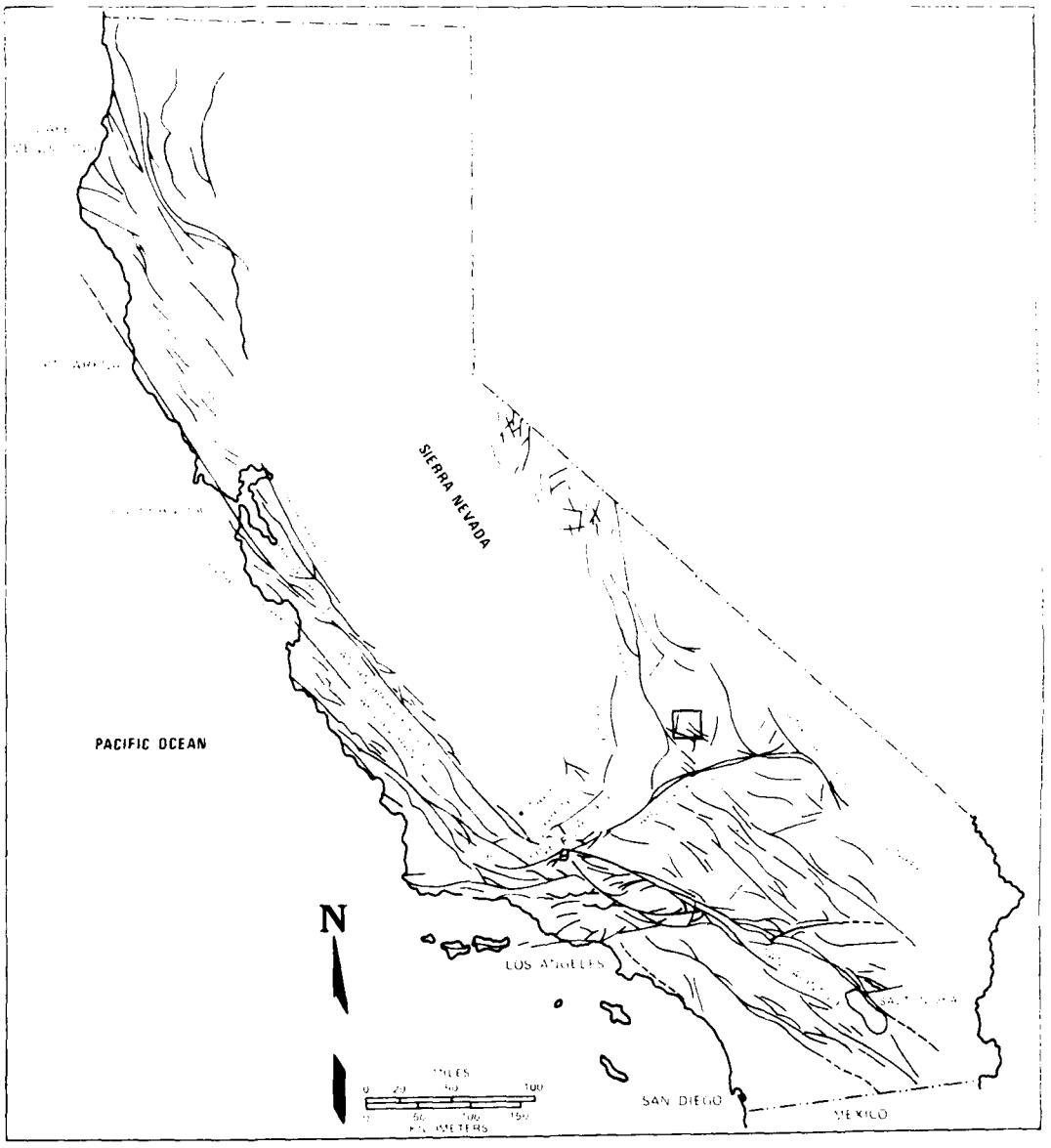

FIGURE 3.1. Study Area Location Map.

GENERAL GEOLOGY

Indian Wells Valley, including the China Lake Naval Weapons Center, now consists of playas and alluvial fans. During Pleistocene this area was occupied by perennial lakes and streams. The coalescing alluvial fans extend from the mouths of the surrounding mountain ranges and form gradually decreasing alluvial plains several miles wide. The Sierra Nevadas, being the major range in the area, offer the majority of the material making up these fans, thus the decreasing slope is to the east.

Zbur (1963) utilized geophysical methods to determine the thickness of the alluvium in the central part of the valley to be nearly 2000 feet. These deposits consist mainly of moderate to well sorted sands with some gravels in the higher regions of the valley, but grade to silt and silty clay in the lower elevations where the lakes were confined in more recent time. Dutcher and Moyle (1973) interpret the seismic data as revealing four main layers of rocks and deposits, which, from deepest to shallowest, have average seismic velocities of 15,600-16,000 fps; 9,600 fps; 7,300-7,400 fps; and 5,700-6,100 fps. The authors describe these layers as the highest velocity representing the basement complex, probably of similar composition to the Sierra Nevada range, the 9,600 fps layer corresponding to the continental deposits, and the alluvium consisting of two layers, the upper of which has a velocity considerably less than the lower. Dutcher and Moyle (1973) point out that a refracting horizon between the deeper and shallower parts of the alluvium was found consistently throughout the valley and proved to be a reliable marker. The authors theorize that the average velocity differences are caused by compaction or consolidation of the deeper alluvium.

Dutcher and Moyle (1973) describe the groundwater basin as being recharged entirely by internal surface drainage. The major sources of this drainage are the numerous small intermittent streams flowing from the canyons of the Sierra Nevadas. The authors suggest that these streams convey runoff to the fans where, after crossing the Sierra Nevada fault zone, the seepage recharges the groundwater body. Additional recharge is generated from the runoff in the Argus Range.

FAULT SYSTEMS

Indian Wells Valley, specifically the China Lake Naval Weapons Center, lies in a very seismically active region. Fault systems lying within the valley, or nearby, are the main sources of this seismic activity. As described in Chapter 5, background seismicity generated at a distance from the study area is also considered, but to a lesser degree. This section will give a brief description of each local fault considered for this study.

The major source of local seismicity is the Sierra Nevada frontal fault. This fault system visibly extends a majority of the length of the Sierra Nevada Range. This system can be traced by shutter ridges, off-set streams, and other typical frontal fault geomorphic features. Because of its proximity to the study area, only 26 miles of the feature was considered as a local source while probabilistic seismicity generated by the remainder of the fault was considered in the background seismicity evaluation.

The next local source used for this study was the Little Lake fault. As described by St. Amand (1958), von Huene (1960), and Roquemore (1981), the Little Lake fault splays eastward from the Sierra Nevada frontal fault and continues south across Indian Wells Valley to the Garlock fault. The trace of the fault used in this study was 38 miles long and extends directly through the Naval Weapons Center and this study area.

The third local source of seismicity used for this study was the Airport Lake fault. Von Huene (1960) indicates this fault extends some 18 miles from the north, where its southernmost trace joins the Little Lake trace within the Naval Weapons Center boundary. Both the Little Lake and Airport Lake faults are considered to have experienced motion within the last 10,000 years, thereby being classified as "active". (Roquemore, 1981)

The fourth localized source was the Argus fault. This sytem appears as a series of splays located on the eastern side of the naval range area at the base of the Argus Mountain range. This splay region was traced for 20 miles, encompassing a wide band which vanishes just north of the actual study area.

The fifth, and last local source utilized in this study was the Garlock fault. This major east-west trending fault extends approximately 175 miles from the San Andreas eastward to the Death Valley fault system. This feature is considered to separate the Mojave Desert and the Basin and Range provinces (Allen, et al, 1965). Hill and Dibblee (1953) consider the Garlock to be merely an offset extension of one of the major Transverse Range faults. The Garlock trace is located 5 miles south of the study area.

SOIL TYPES

GENERAL

A soil susceptibility map shows the areas with soils that are likely to liquefy given a sufficient magnitude of ground shaking. As discussed in Chapter 2, soil type is a very important parameter in analyzing liquefaction potential. A map showing soil deposits in the Indian Wells Valley was prepared by Moyle (1963) and was utilized in this study to give the information on soil type required for analysis.

MOYLE'S MAP

Moyle (1963) presented a detailed map of the surface soils in the Indian Wells Valley showing different geologic formations from Miocene to Holocene. This map provided the major source of soil data for this study. Moyle is noted as a particularly detailed mapper and during the field checking for this study there were no discrepancies noted in his work. Plate 2 shows the results of the map that was developed by Moyle in the study area.

Tertiary volcanics occur as local hills and smaller outcrops to the northern regions of the study area. These volcanics extend from the low lying foothills back into the Coso and Argus ranges.

Quaternary deposits comprise nearly all of the valley floor region. Moyle identified many locations of deposits that range in age from Pleistocene to Holocene.

Because the age of a deposit affects its liquefaction characteristics, the detailed mapping of the Quaternary units was extremely helpful in developing the susceptibility map. The seven different soil types that Moyle identified from the Quaternary Period in this study area were classified with respect to liquefaction potential and used to produce the susceptibility map. The specific classification for each soil type is discussed later.

Some of the more highly susceptible formations are the sand dunes and playa silts with interbedded sand layers. The dunes in the study area are actively drifting and quite unconsolidated. The younger alluvium features a well sorted sand which is slightly consolidated locally, but still remains uncemented.

GEOTECHNICAL REPORTS

There were only a few geotechnical reports at various sites within the valley that provided information on soil deposits. These reports were compiled in conjunction with previous foundation studies done in the southern portion of the study area. These studies were fairly complete in their information, however, they were few in number and their depth of study was shallow, between 15-20 feet.

Well logs, on the other hand, were plentiful in number and located over a widely distributed area. The problems encountered with these, however, were numerous. First of all, the information on soil type was very sketchy and suspect. Further, the dates of the loggings were in the vicinity of 1945-1959, and the tendency seemed to be to lump a profile into a generalized description. Also, the depths of the borings were rounded off and the personnel involved avoided detailed and consistent descriptions.

The use of the more complete geotechnical reports is one method that could be very helpful in refining classifications of susceptibility to liquefaction. Detailed boring logs in a study area would give more assurance in using surface soil maps for the location of liquefaction susceptible deposits. The reports currently available are useful as a supplement to a detailed surface geologic map, but should not be relied upon past their limited spatial accuracy.

SUSCEPTIBILITY CLASSIFICATION SYSTEM

GENERAL

The development of the liquefaction susceptibility map was based on the factors discussed in Chapter 2 that influence liquefaction potential. The qualitative influence of several of these factors on liquefaction and the ground failure susceptibility of various sedimentary deposits has been estimated by Youd and Hoose (1977) on the basis of data contained in the historical records (Youd and Perkins, 1978). Because of the general nature of the susceptibility map not all of these influencing factors were considered. Most of the geotechnical factors require site-specific characteristics to determine their effect on the liquefaction potential. This prevented their use on a general, large scale map. There were, however, three geotechnical factors used that were of a nature that the soil deposits could be classified as to their relative susceptibility to liquefaction. These three factors were age of deposits, soil type, and depth to groundwater. Each soil deposit was examined in terms of these three factors and classified as to whether it had a high, moderate, low, or no susceptibility to liquefaction.

SOIL TYPE

The first parameter considered was soil type of the deposit. Fine to medium grained sands are the most susceptible to liquefaction. Moyle did not distinguish between grain sizes within sands and silts, such as fine, medium, and coarse grained material, but referred to them only as sand or silt with a general degree of sorting. Therefore, different classifications were given only on the fact that the deposit was either a sand, gravel, silt, or clay.

AGE OF DEPOSIT

After the soil type was considered, the age of each deposit was used to analyze the soil's susceptibility. As pointed out in Chapter 2, relatively recent deposits are the most susceptible to liquefaction. The lower bound of this study was chosen at Quaternary age deposits (1.8 million years old; Pliestocene). Deposits older than this Period were classified as nonsusceptible to

liquefaction. Younger deposits were classified based on when they were deposited within the Quaternary Period. Holocene deposits (less than 11,000 years old) received higher classifications than did Pleistocene deposits (between 11,000 and 1.8 million years old).

DEPTH TO GROUNDWATER

The last geotechnical factor that was considered was the depth to groundwater. The important influence of the water level was discussed in Chapter 2.

Depth to groundwater data was collected from the United States Geological Survey (Lapinski, 1981) after a series of wells were measured for water levels. When data points were scarce, a map, also created by USGS (1976), showing the elevation of groundwater above mean sea level was used in conjunction with a topographic map of the same scale to calculate the depth of the water below ground surface. Latitudinal and longitudinal coordinates were assigned to each data point and used as input into a computerized griding routine. From the resulting grid system, a computer graphic program drew contour lines of equal depths to groundwater. Boundary conditions set for this graphic program included intervals of 2 feet, ranging from +2.00 to −40.00 feet. This process is also described in Chapter 1.

The groundwater contour map, as presented in Plate 1, enabled three depth ranges to be outlined and used to further adjust deposit classification. If the depth to the water level was between 2 feet above and 16 feet below the surface a higher classification was given to a soil deposit than if the water level was between 17 and 40 feet below the surface. The 40-foot level was used a lower bound. If the water level is too deep then the effective initial confining pressures become so large that liquefaction is prevented. This was also discussed in Chapter 2. Youd and Perkins (1978) suggested that a depth of 33 feet might be a lower bound. Other authors (Shannon, 1966) (Seed, 1976) suggest 50 feet as a lower bound. A value of 40 feet was determined to be a conservative yet realistic depth.

INITIAL SUSCEPTIBILITY

A list of the deposits from Moyle's (1963) map is given below with a brief description of

the soils contained in the deposits. A discussion on the classification of liquefaction susceptibility for each soil deposit is also given in this description. These classifications are based only on age of deposit and soil type. Depth to groundwater will be discussed later.

Qof — Older Fan Deposits. These deposits are moderately cemented to moderately indurated boulders, sand and clay, cemented with calcareous tufa. On the basis of soil type and cementation, the susceptibility is given a moderate classification. This soil was deposited during Pleistocene and, on the basis of age, is reduced to a low classification.

Qol — Old Lacustrine Deposits. These deposits are silt, sand, and fresh water marl, cemented with calcareous tufa cement. On the basis of soil types and cementation, this deposit is given a moderate classification with liquefiable lenses. The age of this deposit is Pleistocene which will reduce the final classification to moderate-low.

Qls — Old Lakeshore Deposits. These deposits are silt, sand, clay and lime-cement. On the basis of soil types and cementation, this deposit is given a moderate classification, with some potentially liquefiable lenses. The age of this deposit is Pleistocene which will reduce the final classification to moderate-low.

Qos — Old Dune Sand. These deposits are dunal sands of moderate consolidation. On the basis of soil types and consolidation, this deposit is given a moderate classification. The age of these dunes is Pleistocene which will reduce the final classification to moderate-low.

Qv — Unnamed Volcanic Rocks. These deposits are flows of extrusive basalts, vesicular to dense and occurring in the higher regions of the study area. These flows are Pleistocene and recent. Volcanic flows are not susceptible to liquefaction.

Qya — Younger Alluvium. These deposits are unconsolidated, moderately to well sorted sand, clay and gravel, and carried only a moderate distance from the source area. On the basis of soil type and consolidation, this deposit is given a high classification. These deposits are Holocene, which according to the age maintain the classification of this deposit as high.

Qyf — Younger Fan Deposits. These deposits are unconsolidated, poorly to moderately sorted gravel, sand, silt and mud flow debris locally derived. On the basis of the presence of

gravel and mud flow debris (i.e., fine silt and clay), this deposit is given a moderate classification. The age of these deposits are Holocene, thus maintaining the susceptibility classification of moderate.

Qp — Playa Deposits. These deposits are unconsolidated sand, silt and clay beneath small lake beds. On the basis of soil types, i.e., large quantities of silt and clay with localized sand layers, this deposit is given a high to moderate classification. The age of these deposits is Holocene, thus maintaining the susceptibility classification of high-moderate.

Qds — Dune Sand Deposits. These deposits are unconsolidated sand dunes which are actively drifting. On the basis of the soil type and unconsolidation, this deposit is given a high classification. The age of this deposit is Holocene, thereby maintaining a high classification.

Qsp — Sand and Interdune Playa Deposits. These deposits are small playas surrounded by sand dunes which are actively drifting. Each of these deposits have been previously described. On the basis of the soil types and frequent occurrences of unconsolidated sands and silts, these deposits are given a high classification. The age of these deposits is Holocene, thereby maintaining the high classification.

FINAL SUSCEPTIBILITY

Two of the three geotechnical parameters influencing the liquefaction susceptibility of a soil deposit have now been accounted for in the previous description. The logic for each decision, as suggested by Youd and Perkins (1978), is illustrated in Appendix I.

The third geotechnical parameter, the depth to groundwater, was considered separately from the other two factors. This parameter depended on the location of the soil deposit in relation to the depth to groundwater contours. The same soil deposit may receive a high susceptibility classification in the middle of the study area where the water is near the surface, and receive a moderate or low classification in another region where the water level is substantially deeper.

The groundwater criteria set previously (0-16', 17-40', >40') was then combined with the classification results from the age of deposition and the soil type to form a liquefaction

susceptibility table. Table 3.1 shows this susceptibility matrix. This table illustrates how the depth to groundwater affected the final classification of a soil deposit.

TABLE 3.1. Susceptibility Matrix—Estimated Susceptibility of Soil Deposits to Liquefaction, Based on Age of Deposits, Soil Type, and Depth to Groundwater.

Depth to Groundwater (feet)	Tertiary	Quaternary									
	Pre-Pleistocene	Pleistocene					Holocene				
		Qof	Qol	Qls	Qos	Qv	Qya	Qyf	Qp	Qsp	Qds
+2 - 16	N	L	M	M	M	N	H	M	H/M	H	H
17 - 40	N	N	M/L	M/L	M/L	N	M	L	M/L	M	H/M
>40	N	N	N	N	N	N	N	N	N	N	N

H – HIGH SUSCEPTIBILITY
H/M – HIGH TO MODERATE SUSCEPTIBILITY
M – MODERATE SUSCEPTIBILITY
L – LOW SUSCEPTIBILITY
N – NO SUSCEPTIBILITY

LIQUEFACTION SUSCEPTIBILITY MAP

By using Moyle's (1963) surface geologic map and transposing the computer generated depth to groundwater contour map over it, the soil susceptibility map was laid out. At this point the soil susceptibility matrix was used to classify areas of high, moderate, and low probable liquefaction potential. The liquefaction susceptibility map is presented in Plate 2 and shows the areas of relative liquefaction susceptibility.

Chapter 4

SOIL SUSCEPTIBILITY — THE QUANTITATIVE STEP

GENERAL

The qualitative step for determination of soil susceptibility to liquefaction (Chapter 3) outlined areas of high, moderate, and low susceptibility. In this chapter, the areas designated as highly or moderately susceptible are investigated further in a more quantitative way to formulate a liquefaction potential map.

The procedure for developing this more quantitative analysis was, in part, discussed by Dobry and Swiger (1979). The procedure, as Dobry refers to it, is called the Stiffness Method. As previously mentioned in Chapter 2, the basis for this analysis is, other things being equal, stiffer sand and silt deposits are less likely to liquefy. Dobry (1980) indicates that this increased stiffness of the deposits can arise from a combination of the different parameters previously discussed, such as increased relative density, increased overconsolidation, stronger fabric, cementation due to geologic aging under pressure, or prestraining due to prior seismic history.

There have been previous attempts at quantifying liquefaction investigations for the purpose of learning the size of an earthquake required to increase pore pressure. Any actual testing for these results, unless purely empirical, required either standard penetration tests in the field or laboratory tests in an effort to determine the cyclic stress ratio (τ/σ'_v) needed to cause liquefaction. As discussed earlier in Chapter 2, and as discussed in detail by Seed (1979) and Feck (1979), the determination of this stress ratio is riddled with uncertainties.

Dobry and Swiger (1979) proposed, based on laboratory evidence, that shear strains rather than exclusively shear stresses control settlement and pore pressure build-up in silts and sands

during cyclic loading. They note the soil parameters which increase stiffness are the same which have been shown to increase the cyclic strengths of sands under dynamic stresses in the laboratory. These detailed in-situ parameters, which are nearly impossible to duplicate in the laboratory, need not necessarily be known for a particular site as the stiffness (shear modulus, or G_{max}) of the soil at small strains can be measured directly in the field using geophysical techniques.

The primary information required for generation of the quantitative susceptibility map is the shear wave velocity of the soil profile, the mass density, and the depth to groundwater. The shear wave velocity and mass density were combined to determine the shear modulus, while the depth to groundwater was used to outline the potentially liquefiable areas (as discussed in Chapter 3) and aid in the determination of the total vertical stress due to overburden.

It is not the goal of this chapter to yield an absolute threshold ground surface acceleration capable of use for design at a particular site. Certain limitations and assumptions will be implemented in order to economically investigate a large geographic area, rather than a site-by-site detailed analysis. The end result of this chapter will be a grid system on 1/2-mile centers indicating a threshold acceleration capable of increasing pore pressures at a depth of 30 feet below the ground surface. The reasons for investigating liquefaction potential at 30 feet will be discussed in Chapter 7.

CONCEPT OF THRESHOLD STRAIN

Recently, an increasing amount of experimental evidence has accumulated on the behavior of stressed soil at the individual particle level. What does soil undergo when strained? Figure 4.1 illustrates the behavior of two spheres when a normal load (N) and a tangential load (T) are applied. The application of the tangential load results in a strain, $\gamma = \frac{\Delta}{R_1 + R_2}$, however, as long as $T < f\,N$ (where f = coefficient of friction), the particles do not slide past each other. Mindlin and Deresiewiez (1953) illustrate this load-displacement behavior in

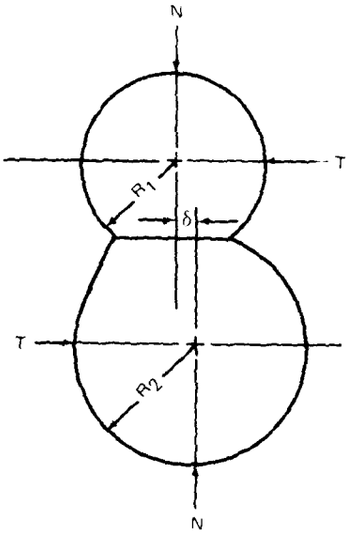

FIGURE 4.1. Elastic Spheres Under Normal and Tangential Loads (*From* Mindlin and Deresiewicz, 1953).

Figure 4.2. Under cyclicly loaded T, oscillating between fixed T^* and $-T^*$ (with $T^* < f\,N$), the behavior is nonlinear *hysteretic*, *strain-rate* independent, and stable (Mindlin and

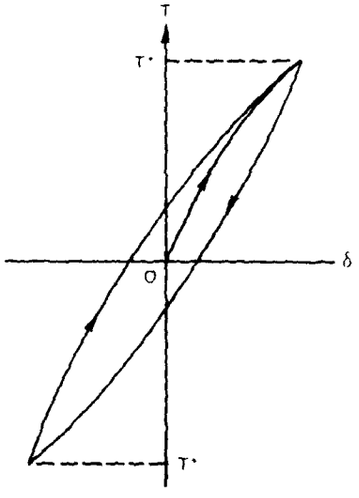

FIGURE 4.2. Theoretical Hysteresis Loop Due *to* Oscillating Tangential Force for Two Spheres *in* Contact (From Mindlin and Deresiewicz, 1953).

Deresiewiez, 1953), or, simply stated, the hysteresis loop does not change with the number of cycles (Dobry and Swiger, 1979). This model is considered representative of granular soils at small strains. Dobry and Swiger (1979) suggest that the value of the threshold strain for a mass of soil is related to the fact that, when the imposed strain equals the threshold strain ($\gamma = \gamma_t$), $T = f N$ and sliding occurs at a significant number of grain contacts. In a similar graphical illustration of this, when $\gamma \geq \gamma_t$, a nonlinear, unstable curve would result and rotate the loop in a clockwise direction with an increasing number of cycles. The physical result of this model is a collapse of the soil structure into a denser configuration until the experienced strain is less than the threshold strain, at which time the hysteresis loop will again become stable. This behavior, for $\gamma \leq \gamma_t$, can best be simulated by kinematic strain hardening. This model suggests, (1) γ_t is independent of grain size, (2) γ_t increases with σ_v, or N, (3) γ_t can be partially dependent on particle sorting, and (4) γ_t is quite dependent on the coefficient of friction and on particle shape.

Dobry and Swiger (1979) related typical tests performed by Ortigosa (1972) and Seed and Silver (1972) on dry sand. A shaking table apparatus subjects a 1-foot-thick layer of sand to a few thousand cycles of base acceleration and the compaction of the sand layer is measured. It has been found that for each relative density (Dr) of sand there is a "critical acceleration" value (a_c), with a_c increasing as Dr increases. If $a > a_c$, the sand densifies and Dr increases, but the densification stops when the condition $a = a_c$ is satisfied.

Dobry and Swiger (1979) suggest that this behavior can be explained by the threshold strain concept. In these tests, the maximum cyclic strain occurs at the base of the sand layer and is equal to $\gamma = (a\sigma_v)/(gG)$, where a = base acceleration, g = acceleration of gravity, σ_v = vertical stress, and G = shear modulus of the sand (to be explained in more detail later). The product $(a/g)\sigma_v$ is constant during the test, but G increases as the sand densifies. As this is the case, γ decreases during the test and densification stops when $\gamma = \gamma_t$. To restart densification, a larger value of a/g is needed so that $\gamma > \gamma_t$ again. In this explanation, if a/g is large enough, γ is always greater than γ_t and the sand should keep densifying until it reaches

Dr = 100%. This occurrence has been reported by Pyke, et al (1974) during actual shaking table tests.

CONCEPT OF MAXIMUM SHEAR MODULUS

The seismic shear strain, γ, induced in the sand layer is $\gamma = \tau G$, where G is the shear modulus of the soil. This value of G, however, is not constant in the soil throughout an earthquake, as it varies with both the level of strain and increasing pore water pressure. It can be assumed, however, that for $\gamma < \gamma_t$ there is no increase in the pore pressure in the soil. Dobry, et al (1981) describes for the limiting case of $\gamma = \gamma_t$ the corresponding peak acceleration is defined as the threshold acceleration $(a_p)_t$. The threshold strain and the threshold acceleration are then related as follows:

$$\gamma_t = \frac{(a_p)_t/g}{G_t} \sigma_v \, rd \tag{4.1}$$

where G_t is the secant shear modulus of the soil associated with the strain γ_t, and $rd \leq 1$ is the soil flexibility coefficient defined by Seed and Idriss (1971). This coefficient ranges from rd = 1 at the surface to rd = .92 at a depth of 30 feet.

This secant shear modulus is more conveniently expressed as follows:

$$G_t = G_{max} \, (G/G_{max})_t \tag{4.2}$$

where G_{max} is the shear modulus of the soil measured at very small strains (i.e., $\gamma \leq 10^{-4}\%$), and (G/G_{max}) is the modulus reduction factor at the threshold strain, γ_t.

Dobry (1978) suggests that nondestructive geophysical methods for field measurements of the soil's shear wave velocity (V_s) induce very small strains in the soil, approximately the same order of those used to define G_{max} in the laboratory. Therefore, V_s and G_{max} are related by the basic wave propagation relationship:

$$G_{max} = \varrho V_s^2 \tag{4.3}$$

where ϱ is the mass density of the soil (total unit weight/acceleration of gravity).

DERIVATION OF THE THRESHOLD ACCELERATION EQUATION

Dobry (1980) uses a simplified soil model of a level sand site to develop the proposed equation (see Figure 4.3). Seed and Idriss (1971) and Seed (1979) used this same model as part of their stress approach to liquefaction. The static state of stress on a soil element at depth (z)

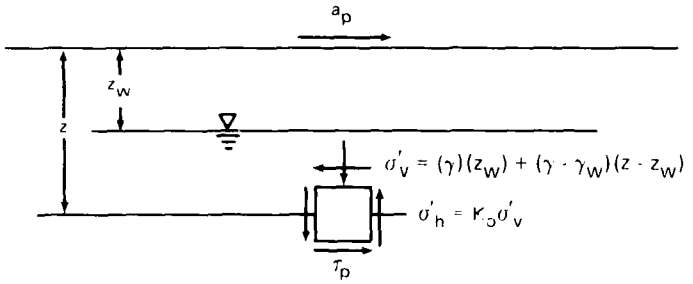

FIGURE 4.3. Simplified Soil Profile (From Seed and Indriss, 1971).

is defined by the effective vertical pressure, σ'_v, by the effective horizontal pressure, $\sigma'_h = k_o \sigma'_v$, and by the total vertical pressure, $\sigma'_v = (\gamma)(z_w) + (\gamma - \gamma_w)(z - z_w)$, where $\gamma_w = 62.4$ lbs/ft^3 is the unit of weight of water. The peak horizontal ground surface acceleration, a_p, and the peak shear stress, τ_p, acting on the horizontal and vertical planes of the soil element are related by:

$$\tau_p = \frac{a_p}{g} \sigma'_v \, rd \tag{4.4}$$

As discussed by Seed (1979), a representative cyclic shear stress caused by the earthquake, τ_e, can be estimated to be about 65% of the peak value, τ_p, (Dobry, 1980). Therefore,

$$\tau_e = .65 \frac{a_p}{g} \sigma'_v \, rd \tag{4.5}$$

and by $\gamma_e = \tau_e/G$, the associated cyclic shear strain is:

$$\gamma_e = .65 \frac{a_p}{g} \frac{\sigma_v \, rd}{G_{max}(G/G_{max})\gamma_e} \tag{4.6}$$

where G and G_{max} are as described in the previous section.

A key experimental fact used in the strain approach is the existence in sands of a threshold strain (γ_t). Several authors have discussed this strain level (Dobry, et al. 1981) (Park and Seed, 1980) (Dobry, 1980) (Powell, 1979) (Dobry and Swiger, 1979) (Dobry and Grivas, 1978) (Seed, 1977) which will be discussed in the next section.

By incorporating this threshold strain, γ_t, into equation 4.6, equation 4.7 becomes:

$$\gamma_t = .65 \frac{(a_p)_t}{g} \frac{\sigma_v' \, rd}{G_{max}(G/G_{max})\gamma_t} \tag{4.7}$$

Rearranging terms to obtain a threshold acceleration we get equation 4.8.

$$(a_p)_t = \frac{\gamma_t \, G_{max}(G/G_{max})\gamma_t}{.65 \, \sigma_v' \, rd} \tag{4.8}$$

Dobry (1980) describes equation 4.8 as the basis of the stiffness method. If the value of G_{max} corresponding to the soil layer at depth z is measured in the field, then equation 4.8 can be used to determine the threshold peak ground surface acceleration, $(a_p)_t$, needed to start the development of excess pore pressure at that depth. A condition of the design earthquake acceleration, $(a_p) < (a_p)_t$, will indicate no pore pressure build-up. The opposite, $(a_p) > (a_p)_t$, will indicate the design earthquake will induce a pore pressure build-up at the indicated depth and further liquefaction studies are necessary.

Dobry, Yokel, et al (1980) have studied numerous sites that had liquefied. Earthquake peak accelerations and threshold peak accelerations were calculated using existing standard penetration blow counts. For each case studied, it was determined that $(a_p) \geq (a_p)_t$. The only two sites for which $(a_p) \approx (a_p)_t$ corresponded to a large magnitude (M = 8.3) earthquake which caused a very long duration of shaking and eventually also liquefied.

SUSCEPTIBILITY CLASSIFICATION SYSTEM

GENERAL

The theory and procedure utilized for obtaining a peak threshold ground surface acceleration has been previously discussed. The task then was to pick values to fulfill

equation 4.8 through field test results and/or literature searches for previously established values applicable to the conditions at the study area. Engineering judgement and assumptions based on the limited data obtained from the field test program were a fundamental step in the application of this method over a large area. The determination of each variable in equation 4.8 is discussed in this section with the judgement and assumptions outlined. The variables determined are the maximum shear modulus, G_{max}, of the layer, the threshold strain, γ_t, the shear modulus reduction coefficient at the threshold strain, $(G/G_{max})\gamma_t$, the total vertical effective pressure at the layer, σ'_v, and the soil flexibility coefficient, rd.

DETERMINATION OF G_{max}

G_{max} is the maximum shear modulus of the soil at small strains, and is defined as the relationship of shear stress, τ, divided by shear strain, γ. This modulus is a direct indication of the stiffness of a soil layer, i.e., the layer's reaction in terms of shear strain to applied shear stress. Clearly, the higher the G_{max} value, the stiffer the soil profile. This stiffness coefficient can be measured in the field by the basic wave propagation relationship, as discussed in equation 4.3 ($G_{max} = \varrho V_S^2$).

In this study, the shear wave velocity was determined using the surface refraction method. A 12-channel, signal enhancing engineering geophone (ES 1200) apparatus was used for this determination. The source for the energy impulse was a 16-pound sledge hammer striking an end-bearing steel plated railroad tie. A pickup truck was driven onto the railroad tie to enhance the contact with the ground (see Figure 4.4). As each end of the beam was struck, the seismograph recorded the seismogram on film. Right and left end impacts generated polarized shear waves of a sinuate nature which were 180° out of phase of each other. Shear wave velocities were chosen at points where these sinuous traces crossed each other.

Forty-five sites were tested for shear wave velocity in an effort to obtain an average velocity for each geologic unit. The more surface area a geologic unit covered, the more shots were taken in that unit for the determination of this velocity.

FIGURE 4.4. Generating Shear Waves for the Geophysical Apparatus.

To better compare individual localities within this large study area, a standard depth of 30 feet below the surface was chosen for analysis of susceptibility. The reasons for this are discussed in detail in Chapter 7.

In the determination of the shear wave velocity of the layer at this depth, certain assumptions are made. First, it is known that surface refraction is capable of measuring to a depth of 1/3 to 1/4 the length of the string of geophones in a uniform, horizontal profile (Norris, personal communications, 1980). The string utilized in this study was 120 feet long (12 geophones), thereby allowing for a 30 to 40 foot depth range. The assumption made at this point was that there was no "shadow zone" in the profile. Briefly, a shadow zone is a layer overlaid by another layer of higher velocity. In this condition, the shear velocity of the slower deep layer will not be detected by the surface geophones as the waves will remain in the

upper, faster layer. The accuracy of this assumption was enhanced by reviewing the available geotechnical boring logs in a potential shot area for the possible existence of such a condition. When this condition was noticed, the locality was not used in the testing program.

With this assumption implemented, the velocities at 30 feet could be measured. In the case of a constant velocity with depth, the calculated velocity was used for the value at the desired depth. In the case of two or more velocities measured in a profile, the deepest velocity (i.e., fastest) was assumed to be that of the layer at 30 feet. This assumption was verified by calculating the depth of the velocity increase and ensuring that this increase was not below the desired 30-foot layer. Equation 4.9 was used to calculate the depth of the velocity change (H).

$$H = \frac{D}{2}\sqrt{\frac{V_2 - V_1}{V_2 + V_1}} \tag{4.9}$$

where D is the "critical distance," or distance from energy source where velocities change (from seismogram), V_2 is the faster velocity, and V_1 is the slower velocity.

It is realized that in reviewing the literature most authors agree that the most popular methods presently being used for determining V_S are, in order of preference, (1) crosshold method, (2) downhole method, and (3) surface refraction method (Dobry, 1981) (Campbell, et al, 1979) (Stokoe and Hoar, 1978) (Hoar and Stokoe, 1977). However, due to the large area covered in this study and the potential astronomical costs of drilling a representative number of boreholes across the Weapons Center, the two more popular methods will be restricted to future site-specific investigations. Table 4.1 illustrates the measured shear wave velocities at 30 feet for the study area.

The second component of the G_{max} equation 4.3 is mass density (ϱ). As already discussed, mass density is defined as the total unit weight divided by the acceleration of gravity. Unit weights were determined in two ways. The most reliable method was, of course, referring to the existing geotechnical logs. Studies done for foundation investigations had accurate measurements at depths. The second method involved the use of the sand cone apparatus and the existing well log data (see Figure 4.5). The well logs, sketchy as they were, did give an

TABLE 4.1. Measured Shear Wave Velocities at a Depth of 30 Feet.
By surface refraction method.

Deposit	V_s (fps)	$\overline{V_s}$ (fps)	Deposit	$\overline{V_s}$ (fps)	V_s (fps)
Qol	1000	1037	Qsp	1111.11	1088
	888.9			1162.8	
	1222.2			1428.6	
				757.6	
Qls	1100	1100		1400	
				921	
Qos	1100	1213.9		1250	
	1041.7			1052.6	
	1500			941.2	
				800	
Qya	1375	1348.7		1142.8	
	1408.5				
	1666.7		Qds	1481	1126.1
	1250			852	
	1315.8			1333	
	808			1123.6	
	1168.8			947.4	
	1463.4			1111	
	1031			1034.5	
	2000				
Qp	873.8	915.4			
	1081				
	880				
	833				
	909				

indication of the uniformity of the profile. Where it could be determined that the layer at 30 feet was approximately the same soil type as that on the surface, the sand cone method was utilized for determination of unit weight. The very rare condition involving a drastically nonuniform profile located in an area without available geotechnical foundation studies for reference required engineering judgement.

DETERMINATION OF γ_t

γ_t is the threshold cyclic shear strain discussed by many authors, as previously noted. Most of these authors agree that the key to the strain approach to liquefaction analysis is the development of an accurate value for γ_t. Richard Ladd of Woodward-Clyde Consultants, and Ricardo Dobry have worked on identifying this threshold strain (Powell, 1979). They

FIGURE 4 5. Sand Cone Apparatus for Mass Density Determination.

conducted cyclic triaxial strain controlled tests on Monterey No. 0 sand. In these tests, they gradually increased the cyclic strain of the test until pore pressure started to develop. Their data clearly indicated the existence of a threshold strain value of between $1 \times 10^{-2}\%$ and $3 \times 10^{-2}\%$, independent of relative density (Powell, 1979). Stoll and Kald (1976) suggested the value for the threshold strain for saturated silts is slightly lower ($\gamma_t = .5 \times 10^{-2}\%$). In reviewing the available detailed geotechnical logs, the sandy soil in the studied layer contains a moderate amount of silt. During personal communications with Dobry (1981), a $\gamma_t = .9 \times 10^{-2}\%$ was suggested for the described conditions in the study area and he agreed the value would be representative.

DETERMINATION OF $(G/G_{max})\gamma_t$

$(G/G_{max})\gamma_t$ has been previously described as the modulus reduction factor at the threshold strain ($\gamma_t = 10^{-2}\%$), where G is the secant shear modulus of the soil associated with the threshold strain and G_{max} is the modulus of the soil measured at very small strains ($\gamma \leq 10^{-4}\%$). Recent laboratory testing of shear stress versus shear strain relationships for determination of G values for different strains has resulted in a range of variations for G/G_{max}. It was determined that for $\gamma_t = 1 \times 10^{-2}\%$, $(G/G_{max})\gamma_t$ is between .65 and .95, while for $\gamma_t = 3 \times 10^{-2}\%$, $(G/G_{max})\gamma_t$ is between .45 and .65 (Dobry, et al, 1981) (Iwasaki, 1978) (Seed and Idriss, 1970). For the previously determined $\gamma_t = .9 \times 10^{-2}\%$ for this study, a value of $(G/G_{max})\gamma_t = .80$ was selected.

DETERMINATION OF σ'_v

σ'_v is defined as the total effective vertical pressure, or $(\gamma)(z_w) + (\gamma - \gamma_w)(z - z_w) = \sigma'_v$, where z_w is the depth to groundwater, z is the depth to the soil element in question (30 feet), γ is the unit weight of the soil above the water table, γ_w is the unit weight of water, or 62.4 lbs/ft^3.

The unit weight of the soil was determined as discussed in the section regarding determination of G_{max}. Depths to groundwater levels were read off of the water contour map generated as discussed in Chapter 3.

DETERMINATION OF rd

As previously mentioned, rd is the soil flexibility coefficient defined by Seed and Idriss (1971). At the ground surface, rd = 1 and at a depth z = 30 feet, rd = .92. It has been explained that shear stresses at any level are due to the upward propagation of shear waves. If the soil column above a given depth can be considered to act as a rigid body, the τ_{max} at bedrock would correspond to the surface acceleration $(a)_s$:

$$\tau_{max}\ _{rigid} = \varrho \times (a)_s \tag{4.10}$$

(force = mass × acceleration)

But the soil column acts as a deformable body, therefore

$$\tau_{max}\ _{deformable} = rd\ \tau_{max}\ _{rigid} \tag{4.11}$$

rd is therefore ≤ 1

Figure 4.6 contains the values of rd Seed and Idriss (1971) have determined for a wide variety of earthquakes and soil conditions.

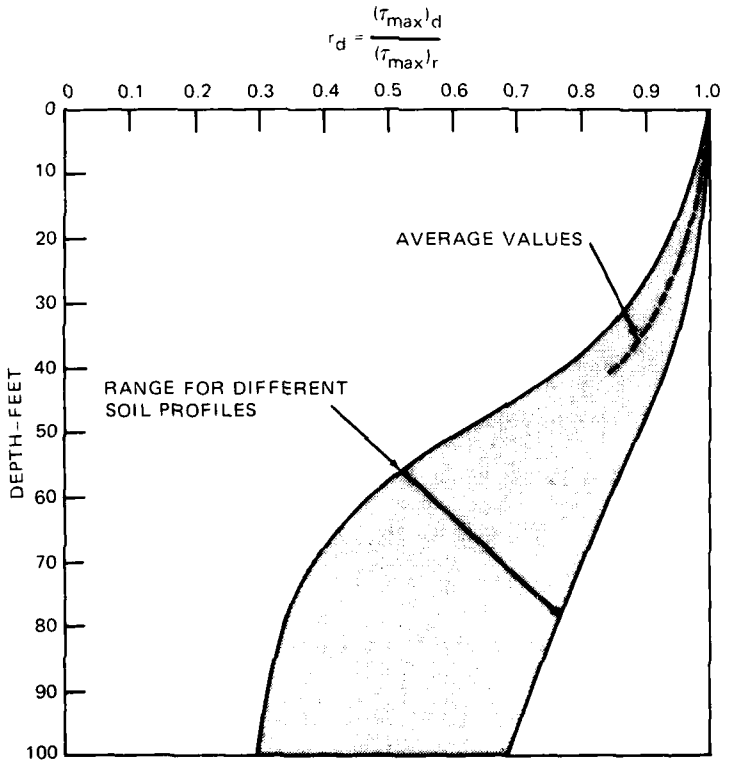

FIGURE 4.6. Range of Values of r_d for Different Soil Profiles (From Seed and Idriss, 1971).

MAP OF THRESHOLD ACCELERATIONS

By utilizing equation 4.8, with the variables as described above, the first state of the liquefaction potential map was prepared for the study area showing the calculated peak threshold ground surface accelerations required to initiate excess pore pressure at a depth of 30 feet. Again, due to the limitations in available geophysical techniques and other assumptions as outlined previously, the acceleration figures are not intended to be used in design calculations. Their function, when combined with the design ground accelerations to be discussed in Chapter 5, is to relate a relative susceptibility as to localities and approximate return intervals for the conditions at the Naval Weapons Center. The threshold acceleration map is presented in Plate 3.

Chapter 5
DESIGN PEAK EARTHQUAKE ACCELERATIONS

GENERAL

The second phase in the development of the liquefaction potential map was the inclusion of the seismicity of the study area. Seismic data was included by way of a computer program called EQRISK (McGuire, 1976). The purpose of this chapter is not to write a user's guide to the program, or even to attempt to explain the theory behind the calculations in determining predicted accelerations. The reader should be able to surmise (1) basically, what the program does, (2) the purpose for using EQRISK in this study, (3) what the input requirements for the program are, and (4) most importantly, what the output means and how it was used in this study.

McGuire (1976) indicates that the theory on which this seismic-risk-analysis program is based has been developed over several years (Cornell, 1968, 1971) (Merz and Cornell, 1973). In short, the program takes, as input, a series of peak ground surface accelerations to be analyzed at each given site, or grid point, as in this study. The algorithm calculates the probability or risk that the given acceleration will be exceeded by a larger acceleration at each particular grid point. Once the risk is calculated, the number of earthquakes per year for each given fault that could produce accelerations in excess of those inputed for analysis are calculated. The total number of expected earthquakes at each site producing these excessive accelerations is the sum of the number of events from all the fault sources analyzed.

The advantages of using EQRISK are threefold. First, EQRISK employs an easy, general, and convenient method of specifying source-area (fault) geometry, which is totally independent

of the site at which seismic risk is to be calculated. The use of this program, in conjunction with this study, negates the task of having to input the proximity of over 600 grid points (sites) to the five major source areas (faults) to be discussed later. Secondly, EQRISK performs risk analysis at individual and specific sites, rather than analyzing regions or large localities. These individual sites of risk analysis can then be compared to the already calculated threshold accelerations at the same particular site in the form of a ratio, $(a_p)/(a_p)_t$ (design acceleration divided by threshold acceleration). The number and location of grid sites is totally up to the program user. Lastly, EQRISK calculates the actual number of earthquakes per year which may exceed any design accelerations. This was useful in this study as it was then very simple to calculate recurrence intervals, in years, of the potential for liquefaction at each site.

The last two important factors to be understood about EQRISK are the input and the output generated by the program. The following two sections will explain these points in more detail.

INPUT REQUIRED

The complex input requirements for EQRISK are outlined in great detail by McGuire (1976), therefore, this section will merely mention the basic parameters involved and then concentrate on the inputed source areas, or faults. The importance and complexity of these remaining parameters should not be underestimated, however, understanding the complete program algorithm and functions of each input variable were not the intent of this thesis. The input listing is located in Appendix II.

Another advantage of EQRISK, though not mentioned previously because it does not directly effect the use of the program results, was the ability to make a simple and intelligent trade off between efficiency and accuracy. The variable NSTEP was used to establish an "iteration" number for calculating the seismic potential of a source area by its gross area. Simply put, the higher NSTEP will give a more accurate spatial distribution, and correspondingly a more accurate seismicity, while increasing the cost of the computer run time.

The second input parameter was a list of "intensities" to be examined. EQRISK, being strictly a probabilistic algorithm, has the capability of examining Modified Mercalli intensity, peak ground acceleration, spectral velocity, or many other output parameters. The term intensity is a general term referring to the form of the desired output. The form of the intensities for this study, as seen in the input listing in the appendix, was the natural logarithm of the peak ground surface acceleration. The range of this list encompasses the range of threshold accelerations, as calculated in Chapter 4. EQRISK calculates the probability of occurrence of some acceleration in excess of each of these input accelerations, as will be discussed further in the next section.

The input list, titled "Risks Desired," simply works backwards from the input accelerations to be examined. This methodology assumes risks to be a design parameter. This output was not used in this study.

The "Attenuation Data" variables have the ability to manually weight attenuation due to distance from the source area in the probabilistic calculations. This spatial consideration was automatically utilized in the calculations, however, these variables give the user additional capabilities in simulating his specific study area conditions.

The input variables labled "No. of Gross Sources" and "No. of Subsources in Gross Source" list the number of energy sources in the region the user wants to consider for potential peak surface accelerations. Each gross source, five in this study, may be divided into a number of rectangular or triangular subsources, depending on the geometry of the gross source boundaries. Subsources aid in the creation of a more definitive outline for the gross source area.

The next set of input statements was the most influential to the program's output. As mentioned, five gross sources had been outlined for this study. The exact latitudinal and longitudinal coordinates of a polygon enclosing each fault were read into the computer. From this point, descriptive variables were inputed dictating specific characteristics about the fault and how each source was to be treated statistically.

The variable COEF is a coefficient allowing subjective input by the user to modify a source area with known parameters. For instance, a coefficient value of -1 may be used to subtract areas of known low seismicity that happen to be located in a large quadralateral enclosing a fault. A coefficient of 1, such as used in this study, is the variable waiving this capability.

The variable AM0 and AM1 are the variables indicating the lower-bound and upper-bound Richter magnitude for each gross source. These will be identified later in this section as each fault is discussed.

The variable BETA(β) is likened to a characteristic "fingerprint" of the seismicity of an area in that it describes the relative distribution of small and large magnitude events. BETA is defined as the natural logarithm of 10, multiplied by the Richter b value for the source. The larger values of b imply relatively fewer large shocks, and visa versa. Values for b are relatively constant for different areas, ranging from .67 to 1.29 for the continental United States (Evernda, 1970). A value of .88 is quite consistent with the data of southern California (Allen and others, 1965) (California Institute of Technology Seismological Laboratory data, 1981).

The variable RATE is the rate of occurrences of events having magnitudes greater than the previously established lower-bound magnitude (AM0) for each gross source area. This variable effectively describes the seismic activity rate of the fault. For each gross source area, RATE is in units of the number of events per year.

Parameter values to indicate "background seismicity" may also be input to the program. McGuire (1976) describes this as seismicity that cannot be associated with a specific source area. This activity-rate input is that of a 10,000 km^2 area, i.e., an area encompassing a circle around the study area with a radius of 150 km.

This activity-rate, unlike the activity-rates for gross source areas being the number of events per year, is in units of number of events per year per 10,000 km^2. This calculation was made once, and the contribution to the expected number of occurrences of peak ground surface

accelerations greater than those in the list to be examined was added to the expected number for each site examined.

In order to calculate rate for both individual faults and background seismicity, a minimum magnitude earthquake to be considered and a design earthquake must be determined. A design earthquake is defined as the earthquake of highest credible magnitude a given fault can produce based on either statistics of the length or the displacement of faults that have historical earthquakes, or both (Roquemore, 1981). This data is represented in the form of curves that plot the parameters of magnitude versus length, magnitude versus displacement, as well as other modifications (Toucher, 1958) (Iida, 1959, 1965) (Albee and Smith, 1966) (Bonilla, 1967, 1970) (Bonilla and Buchanan, 1970).

Presented is a list of the five gross sources, or faults considered for this study, as well as the background seismicity. The data required for the calculation of RATE is also listed.

Gross source	Minimum earthquake magnitude	Design earthquake magnitude	Recurrence interval (yrs)	Reference
1. Sierra Nevada	2.5	8.00	300	Roquemore, personal comm.
2. Little Lake	2.5	6.80	1680	Roquemore, 1981
3. Airport Lake	2.5	6.56	2080	Roquemore, 1981
4. Argus	2.5	6.50	1860	Roquemore, personal comm.
5. Garlock	2.5	8.00	1200	Roquemore, personal comm.
Background seismicity	2.5	8.00	4138	Cal. Tech., 1981

From the above data, the calculations for RATE start with a relationship first presented by Richter (1958).

$$\log n_M = a - bM \tag{5.1}$$

Simply put, equation 5.1 is an expression for the number, n_M, of earthquakes per year having magnitude greater than M occurring in a particular source area, where a is a constant characteristic of the source area and b was previously described.

Step one was to determine a value for the constant a by using what is known about the design earthquake. For example, RATE was calculated for the Sierra Nevada fault as follows:

$$\log 1/300 = a - (.88)(8.0) \tag{5.1}$$

$$4.56 = a$$

The value for a will remain a constant for the particular source area while the recurrence interval for the lower-bound earthquakes were evaluated (RATE):

$$\log \text{RATE} = 4.56 - (.88)(2.5) \tag{5.1}$$

$$\text{RATE} = 230.61$$

Therefore, it was determined that the Sierra Nevada fault would produce 230.61 earthquakes per year of magnitude greater than 2.5. These calculations were repeated for each gross source and incorporated into the program as input.

OUTPUT GENERATED

The form of the generated output is a grid point by grid point analysis of the probability that an arbitrary peak ground surface acceleration will exceed that acceleration listed to be examined (see Appendix III for output). To exemplify this, the first grid point will be discussed for a listed acceleration to be examined.

The first site location (grid point), located after the background seismicity in the output is 117.5568° longitude and 35.6404° latitude. For illustration, the intensity 4.83 will be discussed. It is this list of intensities that is input to be examined. The natural antilog of this input (4.83) is calculated to be 125.21, which represents a fraction of 1 gal (980 cm/sec^2), or the acceleration of gravity $\frac{125.21}{980}$. Therefore, this acceleration to be examined may be more commonly written as .13 g, or thirteen hundredths the acceleration of gravity.

The next line of the output format may be a "caution" statement, which is the result of a computer run-time cost versus efficiency trade off made by the user in the input mode. Briefly, the caution statement suggests that the value for the variable NSTEP does not allow a sufficient number of arc sweeps, or "iterations" to include at least 95% of the total seismic gross area. If

the integration error in the area is greater than 5%, the caution statement informs the user. The appearance of this statement merely reflects a slight reduction in the probabilistic accuracy, but is not a critical factor in obtaining reliable output. McGuire (1976) covers the reason for this statement and the steps leading to it in great detail.

The next line of output is the total number of earthquakes expected to be generated annually which will produce peak ground surface accelerations equal to or greater than the listed accelerations to be examined. As discussed earlier, EQRISK calculates risk or probability associated with the acceleration to be examined. McGuire (1976) explains that once the risk associated with a given acceleration at a site has been calculated for the occurrence of one earthquake of arbitrary magnitude and location in a source area, the annual expected number of events from that source area that cause the given acceleration or greater is obtained by multiplying the single-event risk by the expected number of events during one year. The total expected number of events causing the given acceleration or greater at the site is then obtained by summing the expected number from each source area. It is this, the total expected number, that is reflected in the output.

The illustrative example used previously indicates .146 E + 00 (.146) earthquakes per year are expected with accelerations of at least .13 g (125.21/980). Another way of stating this is that at least 1 event of .13 g acceleration will occur every 6.85 years (1/.146 = 6.85).

The next output line is not used in this study. This line simply states the risk or probability of a random event having a peak ground surface acceleration equal to or greater than the one specified to be examined. In the example, there is a .136 probability (or 13.6% chance) that an event having an acceleration greater than or equal to .13 g will occur each year.

The last three lines are also not used in this study. The risks listed here are "input risks" to be examined. The intensities are the logarithms of the peak ground surface accelerations back figured from these given risks. Percent gravity is figured the same way as was previously described $\left(\frac{\text{Antilog(Intensity)}}{980\ \text{cm/sec}^2}\right)$.

The design peak earthquake accelerations are added to the threshold acceleration map (Plate 3). These design accelerations listed on the map are those of an examined 100-year interval. Should the reader desire an alternative interval, the same output from EQRISK may be utilized as outlined previously in this section.

Chapter 6
LIQUEFACTION POTENTIAL MAP

GENERAL

A liquefaction potential map is developed by dividing the design peak earthquake acceleration for a 100-year return interval, a_p, by the threshold acceleration required for pore pressure build-up at a depth of 30 feet, $(a_p)_t$. The potential map, presented in Plate 3, outlines areas of relative potential for liquefaction by utilizing this ratio, $a_p/(a_p)_t$, over areas of designated high groundwater levels (less than or equal to 40 feet below ground surface) at the Naval Weapons Center, China Lake, California.

Automap II (Environmental Research Institute, 1981) was utilized to graphically illustrate the potential ratio by dividing the determined values into 11 equal subdivisions, as noted in the key. In general, the darker or more detailed graphics pattern corresponds to a higher potential for liquefaction. Blank areas, as noted around the perimeter and in two small regions within the potential zone, correspond to areas of low to nonexistent potential. The two blank regions are labeled such due to the frequency of clay and other non-liquefiable soils as determined by available geotechnical logs. The perimeter region of low potential is defined by a low groundwater level (greater than 40 feet below ground surface).

Chapter 7

SUMMARY

DISCUSSION OF RESULTS

GENERAL

This study identified liquefiable soil deposits at the China Lake Naval Weapons Center and determined the relative potential these deposits have for an increase in pore pressure, and possible liquefaction over a 100-year design interval. This determination was carried out in a three step approach, each step to be discussed individually in this chapter. The locations of soil deposits that are susceptible to liquefaction are shown on a liquefaction susceptibility map. These deposits are identified by utilizing chosen geotechnical parameters as major influencing factors in liquefaction potential. Deposits and areas expected to be highly or moderately susceptible are then subjected to a more detailed engineering-type analysis for a determination of their threshold acceleration; a minimum acceleration required for pore pressure to begin increasing when subjected to continued dynamic loading. Lastly, maximum probable accelerations, for a 100-year return interval, expected in these areas of liquefaction susceptibility are determined for comparison with the threshold accelerations. The end result is a dimensionless number, i.e., a ratio, indicating the anticipated liquefaction potential for a designated area for the given return interval.

SOIL SUSCEPTIBILITY — THE QUALITATIVE STEP

The referenced qualitative step yields a liquefaction susceptibility map which is presented in Plate 2. The map presents general areas where it is highly probable that soil conditions are right for the development of liquefaction. A surface geologic map of Indian Wells Valley,

including the Naval Weapons Center, prepared by Moyle (1963) is used as a major source of reference in locating susceptible soil deposits in the study area. Alternative sources for geologic reference include geotechnical boring logs and well log data. Cross checks with these sources, in conjunction with actual field work performed by this author, are used to verify the accuracy of the geologic information used in this study. It should be realized, however, that there does exist within these susceptible areas places or individual sites where liquefaction would not actually occur. The mapping of susceptible regions on a large scale did not allow for the prevention of misrepresenting specific sites by indicating high classifications when the chance for liquefaction is actually low or nonexistent. This limitation may also apply to specific sites located in an area that received a low susceptibility classification when the probability for liquefaction at the specific site is quite high. This type of misclassification of susceptibility was unavoidable and must be realized.

The importance of the depth to groundwater on liquefaction potential was sufficiently emphasized. Because of this, it must be recognized that the accuracy of the computer generated groundwater contour plot may be another limiting factor. Known depths to groundwater are verified on the contour map; however, the large areas of unknown data are subject to statistical interpretation by the gridding and plotting routines.

Upon completion of the qualitative analysis, some general statements can be made about the susceptible areas at the Weapons Center. The vast majority of the susceptible areas lie within the central portion of the most recent China Lake bed. These areas of high water table are located along G-1 Tower road and Centerline road. Although this lake-bottom material includes nonsusceptible soil such as clay, the presence of silt and sand layers throughout the deposit creates a considerable risk for liquefaction. Another region, which currently supports a considerable amount of development, is within a circle of one mile radius around the Water road and Pole Line road intersection. In addition to playa deposits, the young alluvium consists of unconsolidated sands and silts deposited in a well-sorted state. This material, in all probability, has been transported from the nearby Sierra Nevada mountains by a variety of

AD A124 626 SOIL LIQUEFACTION POTENTIAL AT THE NAVAL WEAPONS CENTER CHINA LAKE CALIFORNIA(U) NAVAL WEAPONS CENTER CHINA LAKE CA E W BANKS SEP 82 NWC-TP-6392 2/2

UNCLASSIFIED F/G 8/13 NL

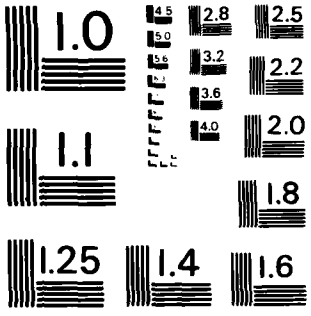

MICROCOPY RESOLUTION TEST CHART
NATIONAL BUREAU OF STANDARDS - 1963 - A

physical mechanisms, the most predominant being water in the form of seasonal runoff or flash flooding.

SOIL SUSCEPTIBILITY — THE QUANTITATIVE STEP

The referenced quantitative step yields a map of threshold accelerations required to initiate pore pressure build-up at a depth of 30 feet. The reason for choosing this seemingly arbitrary depth is twofold. First, by examining the relationship established in equation 4.8, it can be noted that as the analysis increases in depth, the threshold acceleration, $(a_p)_t$, decreases. This may suggest deeper layers are more susceptible to liquefaction. As previously mentioned, this is not necessarily true. Dobry, et al (1981) also recognized this and suggests that in most sites the shear wave velocity also increases with depth. With this in mind, the plots of arrival times versus distances from the source should form a parabolic curve, indicating the velocity gradually increases with depth. In this study, this parabolic tendency was noted in only 25-30% of the shots taken.

As stated in Chapter 4, the surface refraction technique is not widely utilized when attempting to isolate velocity characteristics of a profile, due to the lack of control with depth. It is hypothesized here that the method employed is not precise enough in its arrival times to yield a consistent velocity increase with depth; rather, it yields an accurate approximation of the average profile velocity. Noted abrupt velocity increases are considered a change in soil type. This inconsistency was also noted by Dobry, et al (1981), though to a lesser degree due to his use of crosshole and downhole geophysical methods. Figure 7.1 illustrates 28 in-situ measurements of shear wave velocity for sands and silty sands in California by Campbell, et al (1979), Gibbs, et al (1980), and by Dobry, et al (1981). Twenty of the 28 data points were obtained using downhole techniques; the rest correspond to either crosshole or surface refraction measurements. The figure indicates shear wave velocities for sand can vary greatly, but, more importantly, the data scatter suggests only a relative increase in velocity with depth, and the subsequent potential for deviation from this velocity-depth relationship. It is, therefore, concluded that the inconsistency, though an annoyance, is not uncommon and

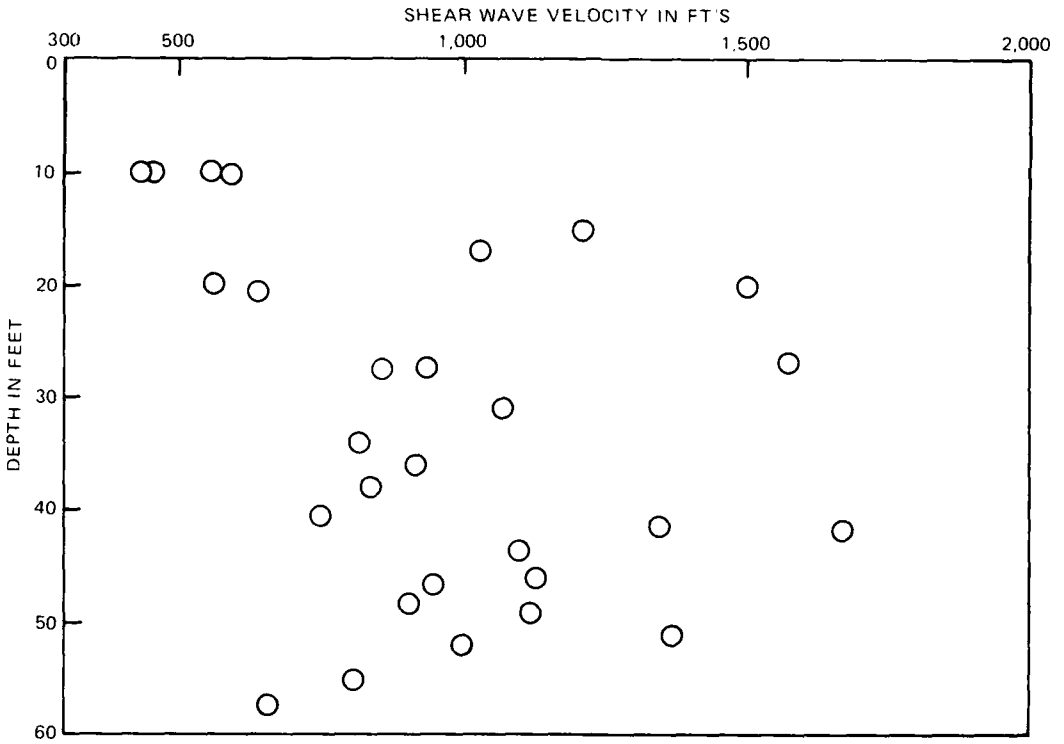

FIGURE 7.1. Twenty-eight In-Situ Measurements of Shear Wave Velocity for Sands and Silty Sands in California. (Campbell, et al (1979), Gibbs, et al (1980), and Dobry, et al (1981)).

accuracy may be enhanced with a more expensive geophysical program. By choosing a common depth to all grid points analyzed, i.e., 30 feet, overburden stress due to increasing depth at a single site would be removed from the list of variables and variations in threshold acceleration, $(a_p)_t$, would become a function of the specific soil properties (mass density, shear wave velocity).

The second reason for choosing this 30-foot depth as a common depth for analysis is, as mentioned in Chapter 4, many authors suggest this as a conservative lower bound for the occurrence of liquefaction. Thus, the groundwater table could be at 30 feet and surface failure could still be initiated. Though this study utilizes 30 feet in its calculations, it is recognized the potential for liquefaction may extend to a depth of 40 feet. This 40-foot depth forms the actual lower bound for the generation of the liquefaction potential map in this study.

As mentioned earlier in this section, the threshold acceleration values are those required to initiate pore pressure build-up at 30 feet. The map presents threshold acceleration calculations

at grid points on 1/2-mile centers throughout the study area. The derivation of equation 4.8 has been explained and the methods of determining individual variables in the equation were outlined. The shear modulus, G_{max}, was singled out as being a very important parameter and was used as the single descriptive variable for each individual deposit. The shear modulus was defined as the mass density, ϱ, multiplied by the square of the shear wave velocity, V_S^2.

The importance of the depth to groundwater on liquefaction potential is pointed out in the previous section. In addition to the accuracy limitations noted, it is important to realize how the presence of the groundwater affects the overburden stress. This effect is described in Chapter 2.

Upon completion of the threshold acceleration calculations, some general statements can be made about the susceptibility in the study area. The lowest threshold accelerations are located in areas of the highest water table. Reasons for this are described in Chapter 2 and include the reduction in effective stress on the examined 30-foot element. Soil deposits typically lower in shear wave velocity also exhibit lower threshold accelerations. These "slower" soils include the playa (Qp) and sand with interdune playa (Qsp) deposits. These regions are in the same areas designated as particularly high risks by the qualitative method of analysis.

DESIGN PEAK EARTHQUAKE ACCELERATIONS

The design peak earthquake accelerations are also illustrated in Plate 3. These calculations represent the maximum expected acceleration at each grid point during a 100-year interval. These figures are determined with the assistance of a probabilistic computer program called EQRISK, developed by Robin K. McGuire (1976). Individual variables used in the program are outlined in Chapter 5. Sources of seismic energy used in the calculations are five major faults in the immediate area, as well as a constant value for background seismicity determined by the California Institute of Technology Seismic Laboratory.

An obvious trend in the design accelerations is a marked increase in expected magnitude progressing in a westward direction. The reason for this trend is that grid points closer to the Sierra Nevada frontal fault are exposed to a fault, not only capable of a maximum magnitude

8.00 event, but also quite active in that it has a substantially shorter recurrence interval than any of the other seismic sources.

THE LIQUEFACTION POTENTIAL MAP

The referenced liquefaction potential map is a graphic representation of the combining of the design peak ground surface earthquake accelerations, a_p, for a 100-year design interval with the peak threshold ground surface accelerations, $(a_p)_t$, necessary for pore pressure build-up at a depth of 30 feet. A dimensionless number, or ratio, $(a_p/(a_p)_t)$, is assigned to each grid point located on 1/2-mile centers throughout the study area. Automap II (Environmental Systems Research Inst., 1981) is utilized as the computer mapping program illustrating zones of increasing liquefaction potential across the Naval Weapons Center.

At this point, it is very important to clearly understand the physical meaning of the "liquefaction potential ratio." This number should not be confused with the standard safety factor in that a safety factor implies the occurrence of failure given a certain value, i.e., less than one. The suggested avoidance of this interpretation is founded on two factors. First, a higher liquefaction potential ratio suggests a situation more prone to ground failure, and thus unsafe. On the other hand, the standard safety factor, which is utilized in many aspects of engineering, indicates failure potential in the opposite manner in that a higher value suggests a safer condition and a value less than one illustrates a driving force greater than the resisting force and ensuing failure. The second factor, and a very important consideration when implementing the results of this study, is the realization that a liquefaction potential ratio greater than one indicates excess pore pressure, or a pore pressure build-up at a depth of 30 feet induced by the design earthquake. The possibility of liquefaction, as it is defined in Chapter 3, and its actual effect on engineered facilities will depend on factors such as duration of shaking, the permeability and drainage boundary conditions of the liquefiable layer, and the dilative or contractive behavior of the soil, which in turn is controlled by the relative density and effective initial confining stresses acting on the soil (Dobry, et al, 1981). Clearly, the

determination of damage potential on a site-specific basis will require detail borings and a layer by layer analysis of the effect the specific soil profile will have on excess pore pressure.

Upon completion of the calculations for liquefaction potential ratios and the liquefaction potential map, some general statements can be made about the possibility for the corresponding hazards in the study area. As also noted on both the liquefaction susceptibility map and in comparing the threshold acceleration values, the greatest potential for liquefaction occurs in the most recent beds of the historic China Lake. Areas along Centerline road and G-2 Tower road are consistently characterized by ratios greater than 3.00, which indicate a strong possibility of liquefaction. Other areas to the west of these roads, also located in the more recently active lake beds of the valley, support ratios in excess of 2.60, also a value indicative of high pore pressures and great potential for damage. Another area previously described as a possible hazardous site, the intersection of Water road and Pole Line road, show localized spots of high damage potential to the north and east of the intersection, while the regions to the west and south are notably lower due to the more competent soil type.

In light of the creation of this liquefaction potential ratio, the need for numerous case studies to help relate the actual damages incurred with varying ranges of this number becomes evident. There are simply not enough cases documented to have an empirical feeling for the damage a ratio of, for instance, 2.00 would actually inflict given a generalized soil profile. This need has only recently been recognized by Ricardo Dobry (Dobry, et al, 1981) and will hopefully be recognized by other investigators in the near future as a valuable tool in quantifying liquefaction potential in an effort to reduce any future life and/or property losses.

RECOMMENDATIONS

The development of this liquefaction potential map provides an important insight into a seismic hazard that exists at the China Lake Naval Weapons Center. It is recommended that the potential map from this project be used, first of all, as a general awareness study of the problem and an indicator that the hazard does exist, and second, that there are zones varying

greatly in their susceptibility across the study area. It is, therefore, considered that the results of this study will be utilized in the planning and development decisions made in connection with the growth of the Weapons Center. It is reiterated that any specific project will require a more detailed analysis for design, dependent on both the magnitude of the structure and the specific site location with respect to the predicted liquefaction potential zones.

A second recommendation is that data for the prediction of liquefaction potential at the Naval Weapons Center be continually updated. Future geotechnical boring logs collected for any number of reasons should be compiled and utilized for updating studies of this type. Depth to groundwater data collected may be used to periodically update the computer contour map generated for this first study. Lastly, as the catalog of seismic data is expanded for the area, it is expected that the prediction of peak ground surface accelerations and their respective recurrence intervals will become increasingly more accurate. Improvements in the probabilistic-type computer programming necessary for these predictions is also expected to become more reliable in the future.

REFERENCES CITED

Albee, A. L. and Smith, J. L., 1966, Earthquake characteristics and fault activity in southern California: Engineering Geology in Southern California, R. Lung and R. Proctor, eds., Association Engineering Geologists, Glendale, California, p. 9-33.

Allen, C. R., St. Amand, P., Richter, C. F. and Nordquist, J. M., 1965, Relationship between seismicity and geologic structure in the southern California region: Seismological Society of America Bulletin, v. 55, no. 4, p. 753-797.

American Geological Institute. 1972. Glossary of geology. Washington, D.C., 857 p.

Annakai, M., 1975, Liquefaction of sand in triaxial tests using uniform and irregular cyclic loading. Ph.D. Dissertation. University of California, Los Angeles.

ASCE, 1958, Glossary of terms and definitions in soil mechanics: Journal of the Soil Mechanics and Foundations Division, ASCE, Vol. 84, No. SM4, pt. 1, pp. 1826-1—1828-43.

Bonilla, M. G., 1967, Historic surface faulting in continental United States and adjacent parts of Mexico: U.S. Geological Survey Open-File Report; also Atomic Energy Commission Report TID-24124.

Bonilla, M. G., 1970, Surface faulting and related effects in earthquake engineering: Earthquake Engineering, Prentice-Hall, Englewood Cliffs, N.J., p. 47-74.

Bonilla, M. G. and Buchanan, J. M., 1970, Interim report on worldwide historic surface faulting: U.S. Geological Survey Open-File Report.

California Institute of Technology Seismological Lab. 1981. Personal communications.

Campbell, K. W., Chieruzzi, R., Duke, C. M., and Lew, M., 1979, Correlation of seismic velocity with depth in southern California: Research Report UCLA-ENG-7965, Earthquake Laboratory, School of Engineering and Applied Science, UCLA, October.

Casegrande, A., 1936, Characteristics of cohesionless soils affecting the stability of earth fills: Journal of the Boston Society of Civil Engineers, January, 1936. Reprinted in Contributions to Soil Mechanics, 1925-1960. Boston Society of Civil Engineers, October, 1940.

Casegrande, A., 1976, Liquefaction and cyclic deformation of sands—a critical review: Harvard Soil Mechanics Series No. 88. Harvard Univ., Cambridge, Massachusetts.

Castro, G., 1969, Liquefaction of sands: Harvard Soil Mechanics Series No. 81. Harvard University, Cambridge, Massachusetts.

Castro, G. and Poulos, S. J., 1977, Factors affecting liquefaction and cyclic mobility: Journal of Geotechnical Engineering Division, ASCE, Vol. 103, No. GT6, June, pp. 501-516.

Christian, J. T. and Swiger, W. F., 1975, Statistics of Liquefaction and SPT results: Journal of the Geotechnical Engineering Division, ASCE, Vol. 101, No. GT11, Proc. Paper 11701. November. pp. 1135-1150.

Cornell, C. A., 1968, Engineering seismic risk analysis: Seismological Society of America Bulletin, v. 58, no. 5, p. 1503-1606.

Cornell, C. A., 1971, Probabilistic analysis of damage to structures under seismic load, in Howell, D. A., Haigh, I. P., and Taylor, C., Dynamic waves in civil engineering: London, Interscience, p. 473-488.

Dixon, S. J. and Burke, J. W., 1973, Liquefaction case history: Journal of the Soil Mechanics and Foundations Division, ASCE, Vol. 99, No. SM 11, Proc. Paper 10133. November. pp. 921-937.

Dobry, Ricardo. 1981. Rensselaer Polytechnic Institute, Dept. of Civil Engineering, Troy, New York. Personal communications.

Dobry, R. and Swiger, W. F., 1979, Threshold strain and cyclic behavior of cohesionless soils: Third ASCE/EMDE Specialty Conference, Sept. 17-19, Austin, Texas.

Dobry, R. and Grivas, D., 1978, Stress-strain relation for soils under earthquake loading—Technical background: Research Report No. 78-2, Department of Civil Engineering, Rensselaer Polytechnic Institute, Troy, New York, July.

Dobry, R., Powell, D. J., Yokel, F. Y. and Ladd, R. S., 1980, Liquefaction potential of saturated sand—the stiffness method: Proceedings of the Seventh World Conference on Earthquake Engineering, Sept. 8-13, Istanbul, Turkey.

Dobry, R., Yokel, F. Y., Ladd, R. S., 1981, Liquefaction potential of overconsolidated sands in areas with moderate seismicity: Conference on Earthquakes and Earthquake Engineering in the Eastern U.S., Sept. 14-16, Knoxville, Tennessee.

Dobry, R., Stokoe, K. H., Ladd, R. S., Youd, T. L., 1981, Liquefaction susceptibility from S-wave velocity: ASCE National Convention, October 27, St. Louis, Missouri.

Donovan, N. C., 1971, A stochastic approach to the seismic liquefaction problem: Proceedings of the 1st International Conference on Applications of Statistics and Probability to Soil and Structural Engineering, September, Hong Kong.

Donovan, N. C., Singh, S., 1976, Development and application of liquefaction criteria for the Trans-Alaska Pipeline: Paper prepared for symposium on Soil Liquefaction, ASCE National Convention, October 2, Philadelphia.

Dutcher, L. C., Moyle, Jr., W. R., 1973, Geologic and hydrologic features of Indian Wells Valley, California: U.S. Geological Survey Water Supply Paper No. 2007, 29 p.

Environmental Systems Research Institute, 1981, Automap II; users manual, Redlands, California, January 1.

Evernda, J. F., 1970, Study of regional seismicity and associated problems: Seismological Society of America Bulletin, vol. 60, no. 2, p. 393-446.

Ferritto, J. M., 1977, Evaluation of probability of seismic liquefaction: Journal of the Technical Councils, ASCE, Vol. 103, No. TC1, Proc. Paper 13387, December, pp. 65-73.

Finn, W. D. L., Bransby, P. L. and Pickering, D. J., 1970, Effect of strain history on liquefaction of sands: Journal of the Soil Mechanics and Foundations Division, ASCE, Vol. 96, No. SM6, Proc. Paper 7670, November, pp. 1917-1934.

Ghaboussi, J. and Dikmen, S. U., 1978, Liquefaction analysis of horizontally layered sands: Journal of the Geotechnical Engineering Division, ASCE, Vol. 104, No. GT3, Proc. Paper 13601, March, pp. 341-356.

Ghaboussi, J. and Wilson, E. L., 1973, Liquefaction and analysis of saturated granular soils: Proceedings of the 5th World Conference on Earthquake Engineering, Vol. 1, pp. 380-389, Rome, Italy.

Gibbs, H. J. and Holtz, W. G., 1957, Research on determining the density of sands by spoon penetration testing: Proceedings of the 4th International Conference on Soil Mechanics and Foundation Engineering, London.

Hill, M. L. and Dibblee, Jr., T. W., 1953, San Andreas, Garlock, and Big Pine faults, California: Bulletin Geol. Soc. America, no. 64, pp. 443-458.

Hoar, R. J. and Stokoe, K. H., 1977, Generation and measurements of shear waves in-situ: Dynamic Geotechnical Testing, ASTM STP 654, June, pp. 3-29.

Housner, G. W., 1965, Intensity of earthquake ground shaking near the causative fault: Proceedings of the 3rd World Conference on Earthquake Engineering, Vol. 1, pp. 94-115, New Zealand.

Iida, K., 1959, Earthquake energy and earthquake fault: Nagoya University, Journal of Earth Science, Vol. 7, No. 2, p. 98-107.

Iwasaki, T., Tatsuoka, F. and Takagi, Y., 1978, Shear moduli of sands under cyclic torsional shear loading: Soils and Foundations, Vol. 18, No. 1, March, pp. 39-56.

Lapinski, P., 1981, U.S. Geological Survey, Personal communications.

Lee, K. L., 1971, Characteristics of liquefaction of level sandy ground during the Tokachioki earthquake, by H. Kishida: Soils and Foundations, Vol. 11, No. 1, pp. 65-68.

Lee, K. L., 1975, Formation of adhesion bands in sands at high pressures: Report No. UCLA-ENG-7586, UCLA School of Engineering and Applied Science, October.

Lee, K. L. and Chan, K., 1972, Number of equivalent significant cycles in strong motion earthquakes: Proceedings of the International Conference on Microzonation, Univ. of Washington, Seattle, October, pp. 609-627.

Lee, K. L. and Focht, J. A., 1975, Liquefaction potential of Ekofisk Tank in North Sea: Journal of the Geotechnical Engineering Division, ASCE, Vol. 100, No. GT1, Proc. Paper 11054, January, pp. 1-18.

Lee, K. L. and Seed, H. B., 1967, Cyclic stress conditions causing liquefaction of sand: Journal of the Soil Mechanics and Foundations Division, ASCE, Vol. 93, No. SM1, Proc. Paper 5058, January, pp. 47-70.

Lemuk, R. W., 1966, Effects of the earthquake of March 27, 1964 at Seward, Alaska: U.S. Geological Survey Proc. Paper No. 542-F.

Lew, H. S., Leyendecker, E. V. and Dikkers, R. D., 1971, Engineering aspects of the 1971 San Fernando Earthquake: Building Science Series 40, U.S. Department of Commerce, National Bureau of Standards, December.

Martin, G. R. and Douglas, B. J., Evaluation of the cone penetrometer for liquefaction hazard assessment: U.S. Geological Survey Open File Report No. 81-284.

McGuire, R. K., 1976, EQRISK—Evaluation of earthquake risk to site: U.S. Geological Survey Open File Report No. 76-67.

Merz, H. A. and Cornell, C. A., 1973, Seismic risk analysis based on a quadratic magnitude—frequency law: Seismological Society of America Bulletin, Vol. 63, No. 6, pt. 1, p. 1999-2006.

Mindlin and Deresiewiez, 1953, Described in "Threshold strain and cyclic behavior of cohesionless soils" by R. Dobry: Third ASCE/EMDE Specialty Conference, Sept. 17-19, 1979, Austin, Texas.

Moyle, W. R., Jr., 1963, Data on water wells in Indian Wells Valley area, Inyo, Kern, and San Bernardino Counties, California: California Department of Water Resources Bulletin 91-9, 243 p.

Moyle, W. R., Jr. and Fenzel, F. W., 1965, Map described in "Geologic and hydrologic features of Indian Wells Valleys, California," by L. C. Dutcher and W. R. Moyle, Jr.: U.S. Geological Survey Water Supply Paper No. 2007, 29 p.

Mulilis, J. P., Chan, C. K. and Seed, H. B., 1975, The effects of method of sample preparation on the cyclic stress-strain behavior of sands: Report No. EERC 75-18, Earthquake Engineering Research Center, University of California, Berkeley.

Norris, G., 1981, University of Nevada, Reno, Personal communcation.

Ortigosa, P., 1972, Described in "Threshold strain and cyclic behavior of cohesionless soils" by R. Dobry and W. F. Swiger: Third ASCE/EMDE Specialty Conference, September 17-19, 1979, Austin, Texas.

Peacock, W. H. and Seed, H. B., 1968, Sand liquefaction under cyclic loading simple shear conditions: Journal of Soil Mechanics and Foundation Division, ASCE, Vol. 94, No. SM3.

Peck, R. B., 1979, Liquefaction potential: science versus practice: Journal of the Geotechnical Engineering Division, Vol. 105, No. GT3, March, pp. 393-398.

Peck, R. B., Hanson, W. E. and Thornburn, T. H., 1974. Foundation Engineering, John Wiley and Sons, Inc., New York, 514 p.

Powell, D. J., 1979, A cyclic strain approach to liquefaction of level sand sites: M.S. Thesis, Rensselaer Polytechnic Institute, Troy New York.

Pyke, R., Chan, C. K. and Seed, H. B., 1974, Settlement and liquefaction of sands under multi-directional shaking: Report No. EERC 74-2, University of California, Berkeley, February.

Richter, C. F., 1958, Elementary seismology: W. H. Freeman and Company, San Francisco, 768 p.

Roquemore, G. R., 1981, U.S. Naval Weapons Center, China Lake, California, Personal communications.

Roquemore, G. R., 1981, Active faults and associated tectonic stress in the Coso Range, Calif.: Ph.D. Dissertation, University of Nevada, Reno, Nevada.

Ross, G. A., Seed, H. B. and Migliaccio, R. R., 1969, Bridge foundation behavior in Alaska Earthquake: Journal of the Soil Mechanics and Foundations Division, ASCE, Vol. 95, No. SM4, Proc. Paper 6664, July, pp. 1007-1036.

Schnabel, P. B., Lysmer, J., Seed, H. B., 1972, SHAKE—A computer program for earthquake response analysis of horizontally layered sites: Earthquake Engineering Research Report EERC 72-12, University of California, Berkeley.

Seed, H. B., 1968, Landslides during earthquakes due to soil liquefaction: Journal of Soil Mechanics and Foundations Division, Vol. 94, No. SM5, September.

Seed, H. B., 1969, The influence of local soil conditions on earthquake damage: Seventh International Conference on Soil Mechanics and Foundation Engineering, August, Mexico City.

Seed, H. B., 1976, Evaluation of soil liquefaction effects on level ground during earthquakes: Preprint 2752, State-of-the-Art Paper, ASCE Annual Convention and Exposition, September 27-October 1, Philadelphia.

Seed, H. B., 1979, Soil liquefaction and cyclic mobility evaluation for level ground during earthquakes: Journal of the Geotechnical Engineering Division, ASCE, Vol. 105, No. GT2, February, pp. 201-255.

Seed, H. B. and Idriss, I. M., 1967, Analysis of soil liquefaction Niigata Earthquake: Journal of Soil Mechanics and Foundations Division, ASCE, Vol. 93, No. SM3, May.

Seed, H. B. and Idriss, I. M., 1970, Soil moduli and damping factors for dynamic response analysis: Report No. EERC 70-10, Earthquake Engineering Research Center, Univ. of California, Berkeley, December.

Seed, H. B. and Idriss, I. M., 1971, Simplified procedure for evaluating soil liquefaction potential: Journal of Soil Mechanics and Foundations Division, ASCE, Vol. 97, No. SM9, Proc. Paper 8371, September, pp. 1249-1273.

Seed, H. B. and Lee, K. L., 1966, Liquefaction of saturated sands during cyclic loading: Journal of Soil Mechanics and Foundations Division, ASCE, Vol. 92, No. SM6, November.

Seed, H. B., Mori, K. and Chan, C. K., 1977, Influence of seismic history on liquefaction of sands: Journal of the Geotechnical Engineering Division, ASCE, Vol. 103, No. GT4, Proc. Paper 12841, April, pp. 257-270.

Seed, H. B., Lee, K. L., Idriss, I. M. and Makdisi, F., 1975, Dynamic analysis of the slide in the lower San Fernando dam during the earthquake of February 9, 1971: Journal of the Geotechnical Engineering Division, ASCE, Vol. 101, September, pp. 381-397.

Seed, H. B. and Peacock, W. H., 1968, Sand liquefaction under cyclic loading simple shear conditions: Journal of Soil Mechanics and Foundations Division, ASCE, Vol. 94, No. SM3, pp. 698-708.

Seed, H. B. and Peacock, W. H., 1971, Test procedures for measuring soil liquefaction characteristics: Journal of Soil Mechanics and Foundations Division, Vol. 97, No. SM8, August.

Seed, H. B. and Silver, M. L., 1972, Settlement of dry sands during earthquakes: Journal of Soil Mechanics and Foundations Division, ASCE, Vol. 98, No. SM4, April, pp. 381-397.

Seed, H. B. and Wilson, S. D., 1967, The turnagain heights landslide, Anchorage, Alaska: Journal of Soil Mechanics and Foundations Division, ASCE, Vol. 93, No. SM4, Proc. Paper 5320, pp. 325-353.

Shannon, W. L., 1966, Slope failures at Seward, Alaska: ASCE Conference on Stability and Performances of Slopes and Embankments, Berkeley, California.

St. Amand, P., 1958, Circum-Pacific orogeny: Publication of The Dominion Observatory, Vol. 20, No. 2, p. 403-411.

St. Amand, P., 1981, U.S. Naval Weapons Center, China Lake, California, Personal communcations.

Stokoe, K. H. and Hoar, R. J., 1978, Variables affecting in-situ seismic measurements: Proceedings of the Geotechnical Engineering Specialty Conference on Earthquake Engineering and Soil Dynamics, ASCE, June, Pasadena, California, pp. 919-939.

Stoll, R. and Kalb, L., 1976, The threshold of dilation under cyclic loading: Proceedings, Specialty Session on Liquefaction Problems in Geotechnical Engineering, ASCE Annual Convention, Sept. 27-October 1, Philadelphia.

Terzaghi, K. and Peck, R. B., 1948, Soil mechanics in engineering practice. John Wiley and Sons, Inc., New York, 566 p.

Thiers, G. R. and Seed, H. B., 1968, Cyclic stress-strain characteristics of clay: Journal of Soil Mechanics and Foundations Division, ASCE, January.

Toucher, D., 1958, Earthquake energy and ground breakage: Seismological Society of America Bulletin, Vol. 48, No. 2, p. 147-153.

United States Dept. of Interior, 1974, Earth manual, a water resources publication, Bureau of Reclamation, Washington, D.C.

von Huene, R. W., 1960, Structural geology and gravimetry of Indian Wells Valley, southeastern California: Ph.D. Dissertation, University of California, Los Angeles, p. 138.

Wang, W., 1979, Some findings in soil liquefaction: Code of Aseismic Design of Hydraulic Structures, Earthquake Engineering Research Laboratory, Richmond, California.

Whitman, R. V., 1971, Resistance of soil to liquefaction and settlement: Soils and Foundations, Vol. 11, No. 4, pp. 59-68.

Wong, R. T., Seed, H. B. and Chan, C. K., 1975, Cyclic loading liquefaction of gravelly soils: Journal of the Geotechnical Engineering Division, ASCE, Vol. 101, No. GT6, Proc. Paper 11396, June.

Yegian, M. K. and Whitman, R. V., 1977, Risk analysis for ground failure by liquefaction: ASCE Fall Convention and exhibit, October 17-21, San Francisco, California.

Youd, T. L., 1971, Landsliding in the vicinity of the Van Norman Lakes in the San Fernando Earthquakes of 1971: U.S. Geological Survey Professional Paper 733, Washington, D.C.

Youd, T. L., 1975, Liquefaction, flow and associated ground failure: Proceedings of U.S. National Conference on Earthquake Engineering, June 18-20, Ann Arbor, Michigan.

Youd, T. L., 1977, Packing chances and liquefaction susceptibility: Journal of Geotechnical Engineering Division, ASCE, Vol. 103, No. GT8, Proc. Paper 13101, August, pp. 897-922.

Youd, T. L., 1978, Major causes of earthquake damage is ground failure: Information paper published by ASCE—Civil Engineering, April.

Youd, T. L. and Hoose, S. N., 1976, Liquefaction during the 1906 San Francisco earthquake: Journal of Geotechnical Engineering Division, ASCE, Vol. 102, No. GT5, Proc. Paper 12143, May, pp. 425-439.

Youd, T. L. and Hoose, S. N., 1977, Liquefaction susceptibility and geologic setting: Proceedings of the 6th World Conference on Earthquake Engineering, January 10-14, New Delhi, India.

Youd, T. L. and Perkins, D. M., 1977, Mapping of liquefaction potential using probability concepts: ASCE fall convention and exhibit, October 17-21, San Francisco, California.

Youd, T. L. and Perkins, D. M., 1978, Mapping liquefaction-induced ground failure potential: Journal of Geotechnical Engineering Division, ASCE, Vol. 104, No. GT4, Proc. Paper 13659, April, pp. 433-446.

Zbur, R. T., 1963, A geophysical investigation of Indian Wells Valley, California: U.S. Naval Ordnance Test Station, China Lake, NWC TP 2795, p. 98.

Appendix I

SUSCEPTIBILITY TABLE

TABLE A.1. Estimated Susceptibility of Sedimentary Deposits to Liquefaction During Strong Seismic Shaking (From Youd, 1978).

Type of deposit (1)	General distribution of cohesionless sediments in deposits (2)	Likelihood that Cohesionless Sediments, When Saturated, Would Be Susceptible to Liquefaction (by Age of Deposit)			
		< 500 yr (3)	Holocene (4)	Pleistocene (5)	Pre-pleistocene (6)
(a) Continental Deposits					
River channel	Locally variable	Very high	High	Low	Very low
Flood plain	Locally variable	High	Moderate	Low	Very low
Alluvial fan and plain	Widespread	Moderate	Low	Low	Very low
Marine terraces and plains	Widespread	—	Low	Very low	Very low
Delta and fan-delta	Widespread	High	Moderate	Low	Very low
Lacustrine and playa	Variable	High	Moderate	Low	Very low
Colluvium	Variable	High	Moderate	Low	Very low
Talus	Widespread	Low	Low	Very low	Very low
Dunes	Widespread	High	Moderate	Low	Very low
Loess	Variable	High	High	High	Unknown
Glacial till	Variable	Low	Low	Very low	Very low
Tuff	Rare	Low	Low	Very low	Very low
Tephra	Widespread	High	High	?	?
Residual soils	Rare	Low	Low	Very low	Very low
Sebka	Locally variable	High	Moderate	Low	Very low
(b) Coastal Zone					
Delta	Widespread	Very high	High	Low	Very low
Esturine	Locally variable	High	Moderate	Low	Very low
Beach					
High wave energy	Widespread	Moderate	Low	Very low	Very low
Low wave energy	Widespread	High	Moderate	Low	Very low
Lagoonal	Locally variable	High	Moderate	Low	Very low
Fore shore	Locally variable	High	Moderate	Low	Very low
(c) Artificial					
Uncompacted fill	Variable	Very high	—	—	—
Compacted fill	Variable	Low	—	—	—

RT-118 (8) V04.00

Appendix II

DESIGN GROUND ACCELERATIONS FOR LIQUEFACTION POTENTIAL, CHINA LAKE NWC

NSTEP = 15 OCALC = 0 JPRNT = 0

List of examined intensities 4.45 4.58 4.70 4.83 4.95 5.08 5.20 5.33 5.45 5.58 5.70

Risks desired 0.2000 0.1500 0.1000 0.0500 0.0100 0.0050 0.0030 0.0000

Attenuation data =	C1	C2	C3	SIGMA	RZERO	RONE	AAA	BBB
	6.16	0.60	−1.30	0.00	25.00	0.00	2000.00	0.00

No. of gross sources 5
No. of subsources in gross sources 3 4 1 2 7

Gross source	L/S	COEF	MO	M1	BETA	RATE/YR	EDEPTH
1	0	1.00	2.50	8.00	2.0300	230.6100	0.0000
2	0	1.00	2.50	6.80	2.0300	3.6000	0.0000
3	0	1.00	2.50	6.56	2.0300	1.8000	0.0000
4	0	1.00	2.50	6.50	2.0300	1.7800	0.0000
5	0	1.00	2.50	8.00	2.0300	57.6500	0.0000
(Background)	0	1.00	3.00	8.00	2.0300	6.0700	0.0000

Gross source 1	Subsource coordinate data	117.9418	35.5825	117.9108	35.5702
Gross source 1	Subsource coordinate data	117.8846	35.6786	117.8487	35.6753
Gross source 1	Subsource coordinate data	117.9269	35.9298	117.8920	35.9371
Gross source 1	Subsource coordinate data	118.0252	36.0700	117.9973	36.1139
Gross source 2	Subsource coordinate data	117.4685	35.5895	117.4835	35.6162
Gross source 2	Subsource coordinate data	117.5639	35.5610	117.5623	35.5898
Gross source 2	Subsource coordinate data	117.6530	35.5823	117.6237	35.6025
Gross source 2	Subsource coordinate data	117.7573	35.7533	117.7259	35.7678
Gross source 2	Subsource coordinate data	117.8633	35.9273	117.8317	35.9402
Gross source 3	Subsource coordinate data	117.8003	35.8896	117.7695	35.8392
Gross source 3	Subsource coordinate data	117.7771	36.1166	117.7419	36.1140
Gross source 4	Subsource coordinate data	117.6856	35.8748	117.6151	35.8740
Gross source 4	Subsource coordinate data	117.6833	36.0271	117.6129	36.0393
Gross source 4	Subsource coordinate data	117.7389	36.1271	117.6779	36.1537
Gross source 5	Subsource coordinate data	119.0255	34.8238	118.7753	34.7735
Gross source 5	Subsource coordinate data	118.4874	35.0068	118.4771	34.9738
Gross source 5	Subsource coordinate data	118.0766	35.2349	118.0551	35.2149
Gross source 5	Subsource coordinate data	117.9854	35.3590	117.9513	35.3100
Gross source 5	Subsource coordinate data	117.5922	35.4820	117.5841	35.4629
Gross source 5	Subsource coordinate data	117.0167	35.6144	117.0083	35.5881
Gross source 5	Subsource coordinate data	116.6572	35.6413	116.6653	35.5753

Appendix III

Gross source 3 Subsource 7 Exact area 156.1
Gross source 5 Total area 1264.8

Results for Background Seismicity

Intensity =	4.45	4.58	4.70	4.83	4.95	5.08	5.20	5.33	5.45
Antilog (intensity) =	85.63	97.51	109.95	125.21	141.17	160.77	181.27	206.44	232.76
(Background) E(NO/YR) =	0.627E – 01	0.409E – 01	0.274E – 01	0.178E – 01	0.118E – 01	0.755E – 02	0.496E – 02	0.311E – 02	0.201E – 02

Results for site location 117.5568 35.6404

Intensity =	4.45	4.58	4.70	4.83	4.95	5.08	5.20	5.33	5.45
Antilog (intensity) =	85.63	97.51	109.95	125.21	141.17	160.77	181.27	206.44	232.76
All sources E(NO/YR) =	0.501E + 00	0.330E + 00	0.223E + 00	0.146E + 00	0.976E – 01	0.625E – 01	0.409E – 01	0.252E – 01	0.156E – 01
All sources risk =	0.394E + 00	0.281E + 00	0.200E + 00	0.136E + 00	0.930E – 01	0.606E – 01	0.401E – 01	0.249E – 01	0.154E – 01

Risks =	0.200000	0.150000	0.100000	0.050000	0.010000	0.005000	0.003000
Intensity =	4.70	4.80	4.93	5.14	5.55	5.69	5.78
Antilog (intensity) =	109.98	121.06	137.93	170.01	257.06	296.66	322.84

Results for site location 117.5655 35.6404

Intensity =	4.45	4.58	4.70	4.83	4.95	5.08	5.20	5.33	5.45
Antilog (intensity) =	85.63	97.51	109.95	125.21	141.17	160.77	181.27	206.44	232.76
All sources E(NO/YR) =	0.520E + 00	0.342E + 00	0.232E + 00	0.151E + 00	0.101E + 00	0.651E – 01	0.427E – 01	0.264E – 01	0.163E – 01
All sources risk =	0.405E + 00	0.290E + 00	0.207E + 00	0.140E + 00	0.964E – 01	0.630E – 01	0.418E – 01	0.260E – 01	0.162E – 01

Risks =	0.200000	0.150000	0.100000	0.050000	0.010000	0.005000	0.003000
Intensity =	4.71	4.81	4.94	5.15	5.56	5.70	5.79
Antilog (intensity) =	111.21	122.47	139.55	171.99	260.29	300.31	327.07

Results for site location 117.5742 35.6404

Intensity =	4.45	4.58	4.70	4.83	4.95	5.08	5.20	5.33	5.45
Antilog (intensity) =	85.63	97.51	109.95	125.21	141.17	160.77	181.27	206.44	232.76
All sources E(NO/YR) =	0.540E + 00	0.356E + 00	0.241E + 00	0.157E + 00	0.106E + 00	0.678E – 01	0.445E – 01	0.276E – 01	0.172E – 01
All sources risk =	0.417E + 00	0.299E + 00	0.214E + 00	0.146E + 00	0.100E + 00	0.656E – 01	0.436E – 01	0.272E – 01	0.170E – 01

Risks =	0.200000	0.150000	0.100000	0.050000	0.010000	0.005000	0.003000
Intensity =	4.72	4.82	4.95	5.16	5.57	5.72	5.80

INITIAL DISTRIBUTION

3 Naval Air Systems Command
  AIR-00D4 (2)
  AIR-604 (1)
1 Chief of Naval Material (MAT-03T1)
1 Chief of Engineers (B. Hall)
1 Naval Facilities Engineering Command, Western Division, San Bruno
2 Naval Sea Systems Command (SEA-99612)
2 Chief of Naval Research, Arlington
  ONR-460, J. Beacock (1)
  ONR-532, M. Odegard (1)
4 Naval Civil Engineering Laboratory, Port Hueneme
  Code 03 (1)
  Code 045, J. Tyrrell (1)
  Code 07 (1)
  S. L. Bugg (1)
1 Naval Intelligence Support Center (W. T. Peterson)
1 Naval Ocean Research and Development Activity, Bay St. Louis (A. Boward)
1 Naval Ocean Systems Center, San Diego
1 Naval Ocean Systems Center, San Diego (Code 533, G. Wilkins)
1 Naval Research Laboratory (Code 5230, Energy Conservation Branch)
1 Air Force Flight Test Center, Edwards Air Force Base (Chief Scientist)
1 Central Intelligence Agency, Langley Air Force Base
1 Deputy Under Secretary of Defense Research and Engineering
  (Research and Advanced Technology, Capt. G. Smith)
1 Defense Advanced Research Projects Agency, Arlington (S. Ruby)
1 Defense Nuclear Agency, Kirtland Air Force Base (Technical Library)
2 Defense Technical Information Center
1 Arizona Bureau of Mines, University of Arizona, Tucson (Director)
1 Bureau of Land Management, Bakersfield, CA (F. S. Crafts)
1 Bureau of Land Management, Denver, CO (J. D. Juilland)
2 Bureau of Land Management, Sacramento, CA
  Chief, Branch of Minerals (1)
  State Director (1)
2 Bureau of Mines
  Assistant Director for Minerals Research (1)
  Director, Mining Research (1)
2 Department of Energy
  Division of Peaceful Nuclear Explosives
    Director (1)
    A. H. Ewing (1)

1 Department of Energy, Las Vegas (Director, Engineering and Construction Division)
1 Department of the Interior, Bureau of Reclamation (Dr. Chung-Ming Wong, Assistant to the Commissioner for Geothermal Resources)
1 Federal Power Commission (Division of Electrical Resources and Requirements, Bureau of Power, B. B. Chew)
1 National Aeronautics and Space Administration (Earth Observation Program, Earth Sciences Survey)
4 United States Geological Survey, Denver, CO
- D. B. Jackson (1)
- D. R. Mabey (1)
- J. O'Donnell (1)
- J. N. Towle (1)

1 United States Geological Survey, Los Angeles, CA (Oil and Gas Branch, John Fackler)
33 United States Geological Survey, Menlo Park, CA
- C. Bacon (1)
- M. Clark (1)
- B. Dalrymple (1)
- E. du Bray (1)
- W. Duffield (1)
- J. Eaton (1)
- W. Ellsworth (1)
- W. F. Fisher (1)
- R. O. Fournier (1)
- J. D. Friedman (1)
- S. Gowarecki (1)
- W. R. Hemphill (1)
- W. Isherwood (1)
- H. M. Iyer (1)
- V. E. McKelvy (1)
- J. G. Moore (1)
- Dr. D. F. Peck (1)
- D. Plouff (1)
- W. A. Radinski (1)
- P. Reasenberg (1)
- E. Roedder (1)
- G. Rusnak (1)
- G. I. Smith (1)
- P. Snavely (1)
- R. Stone (1)
- J. M. Thompson (1)
- R. von Huene (1)
- R. Wallace (1)
- A. Walter (1)
- R. G. Wayland (1)
- C. Weaver (1)
- D. E. White (1)
- R. S. Williams (1)

2 Battelle Memorial Institute, Pacific Northwest Laboratory, Richland, WA
- D. H. Stewart (1)
- J. Zellmer (1)

1 California Academy of Sciences, San Francisco, CA (Department of Geology, Dr. I. Campbell)
1 California Department of Conservation, Sacramento, CA (L. H. Axtel)
3 California Department of Water Resources, Los Angeles, CA
  Chief, Planning Division (1)
  J. J. Coe (1)
  Technical Library (1)
1 California Department of Water Resources, Sacramento, CA (R. C. Richter, Geology Staff Specialist)
3 California Division of Mines and Geology, Sacramento, CA
  R. H. Chapman, Associate Geophysicist (1)
  J. B. Koenig (1)
  M. C. Woods (1)
4 California Division of Mines and Geology, San Francisco, CA
  R. H. Chapman (1)
  C. Jennings (1)
  M. Stinson (1)
  B. Troxel (1)
3 California Division of Mines and Geology, Santa Ana, CA
  M. Bushnell (1)
  E. W. Kiessling (1)
  P. K. Morton (1)
4 California Institute of Technology, Pasadena
  Professor C. Allen (1)
  Professor K. Seih (1)
  Professor L. T. Silver (1)
  Technical Library (1)
3 California State University, Fresno, CA
  Professor J. Avent (1)
  Professor B. Blackerby (1)
  Library (1)
1 Cornell University, Ithaca, NY (Department of Geology, J. Oliver)
1 Earth Sciences Associates, Palo Alto, CA (L. Alvarez)
1 Lamor-Merrifield Company, Santa Monica, CA (Dr. P. Merrifield)
3 Los Angeles Department of Water and Power, Los Angeles, CA
  J. S. Arlidge (1)
  W. G. Hannah (1)
  H. R. King (1)
2 National Science Foundation, Washington, D. C.
  Dr. J. Denton (1)
  H. Metcalf, Office of Intergovernmental Science Program (1)
2 Nevada Bureau of Mines, University of Nevada, Reno, NV
  J. Schilling (1)
  D. Trexler (1)
1 Office of Science and Technology, Washington, D. C. (Dr. R. Balzhiser, Assistant Director of Energy and Environment)
1 Pennsylvania State University, Department of Geosciences, State College, PA (L. Wright)
1 Rice University, Houston, TX (Department of Geology, B. C. Burchfiel)
1 Roy J. Shlemon and Associates, Inc., Newport Beach, CA (Dr. R. J. Shlemon)

4 Stanford University, Stanford, CA
  Department of Mineral Engineering (1)
  W. R. Dickinson (1)
  R. Johns (1)
  G. H. Thompson (1)
1 Union Oil Company, Los Angeles, CA (Dr. C. Ott)
1 United Nations Resources and Transportation Division, New York, NY (J. McNitt)
1 University of California, Lawrence Livermore National Laboratory, Livermore, CA (Plowshare Division)
2 University of California, Riverside
  Department of Geological Sciences
    R. Furgerson (1)
    Dr. R. Rex (1)
3 University of Nevada, Reno, NV
  Professor W. Peppin (1)
  Professor D. B. Slemmons (1)
  Mackay Library (1)
1 University of Southern California, Los Angeles, CA (Department of Geological Sciences, G. A. Davis)
1 University of Utah, Salt Lake City, UT (R. B. Smith, Director, State Geological Survey)
1 University of Utah Research Institute, Salt Lake City, Utah (J. B. Hulen)
1 Woods Hole Oceanographic Institute, Woods Hole, MA (Department of Geology and Geophysics, S. Thomas Crough)
1 Woodward-Clyde Consultants, San Francisco, CA (W. Page)

DEPTH TO GRO
NAVAL WEAPONS CENT

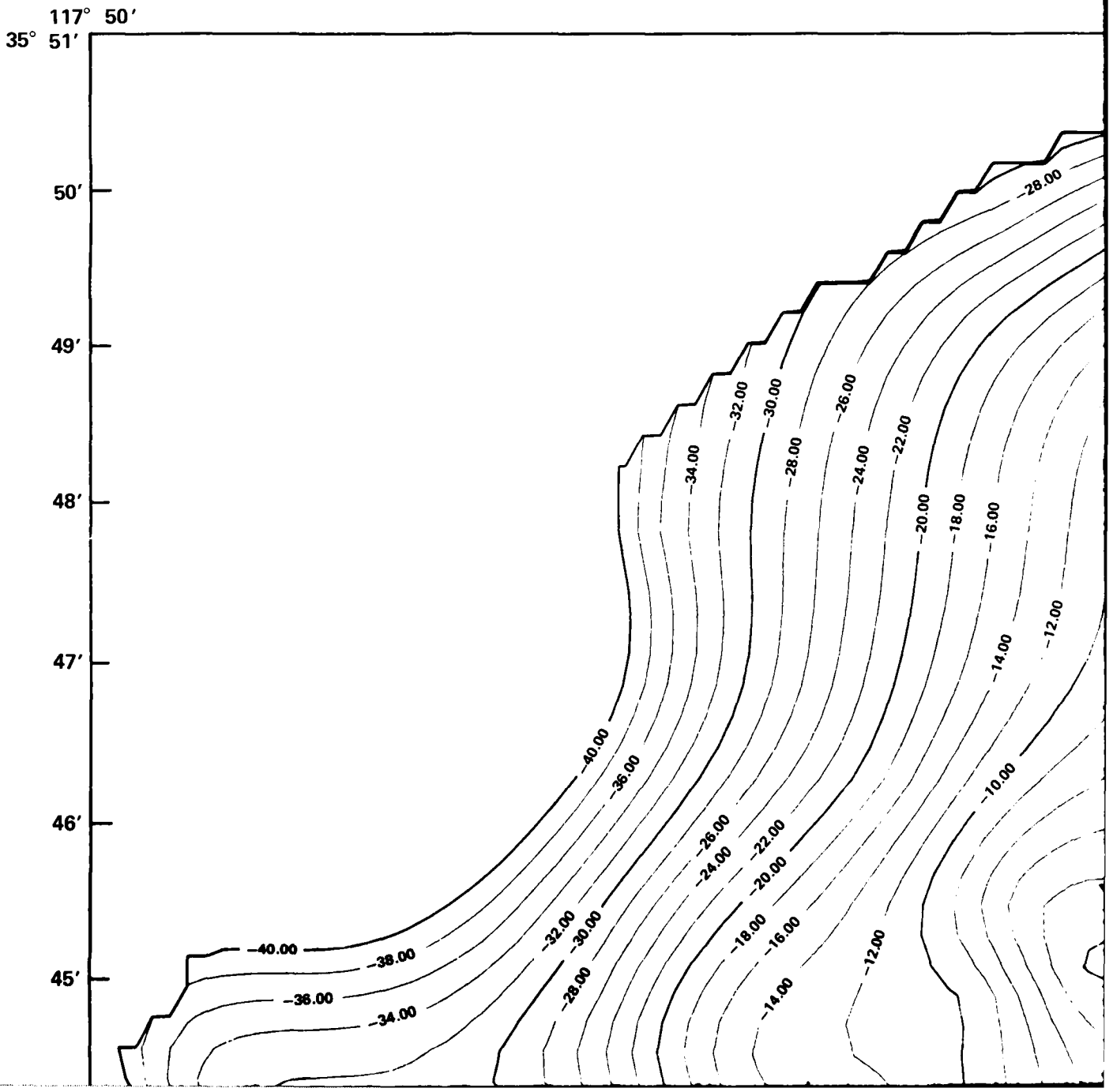

PLATE 1

WATER FOR THE
CHINA LAKE, CALIFORNIA

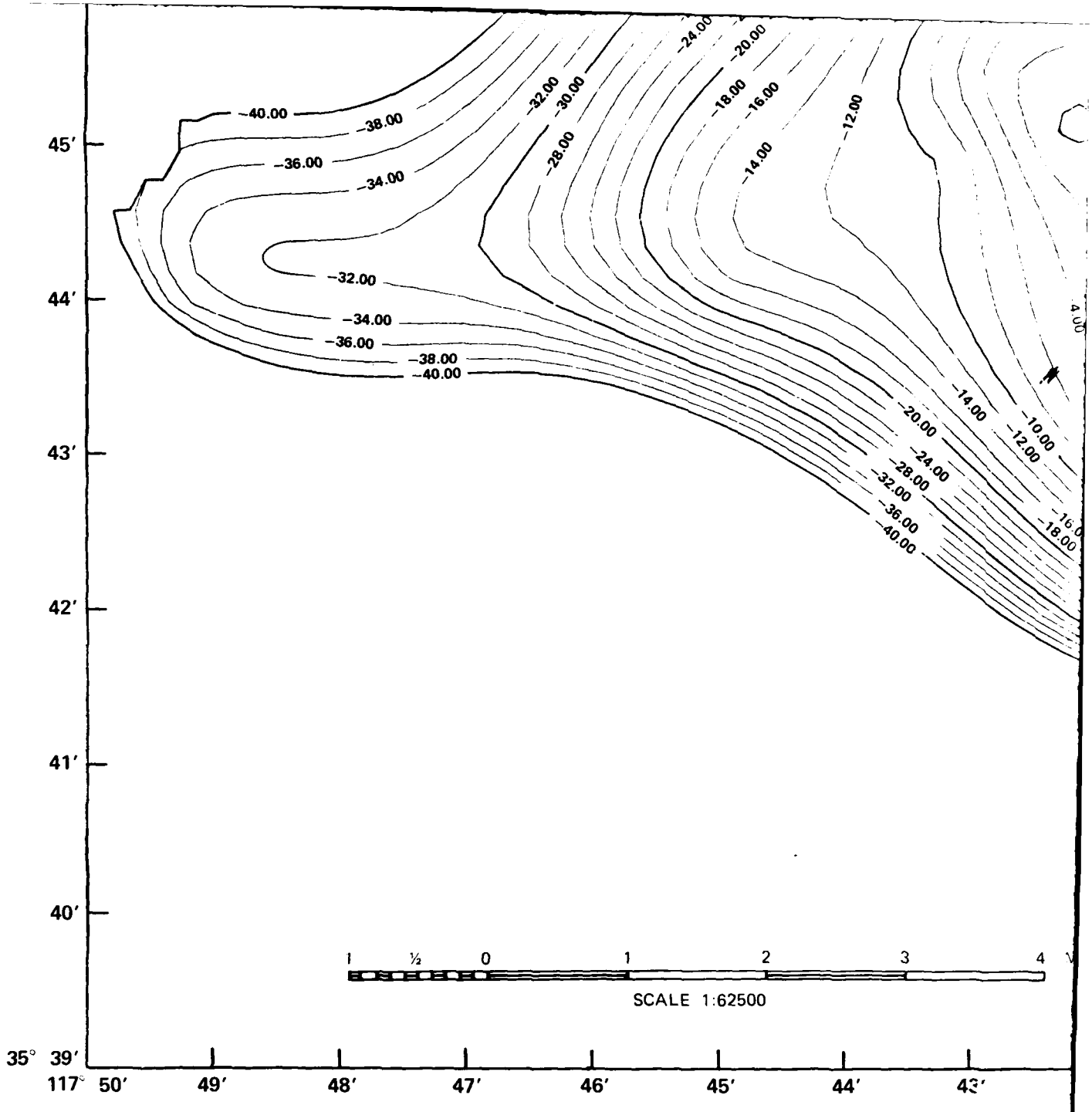
-40.00
-38.00
-36.00
-34.00
-32.00
-30.00
-28.00
-24.00
-20.00
-18.00
-16.00
-14.00
-12.00
-10.00
45′
44′
43′
42′
41′
40′
1 ½ 0 1 2 3 4
SCALE 1:62500
35° 39′
117° 50′
49′
48′
47′
46′
45′
44′
43′

3

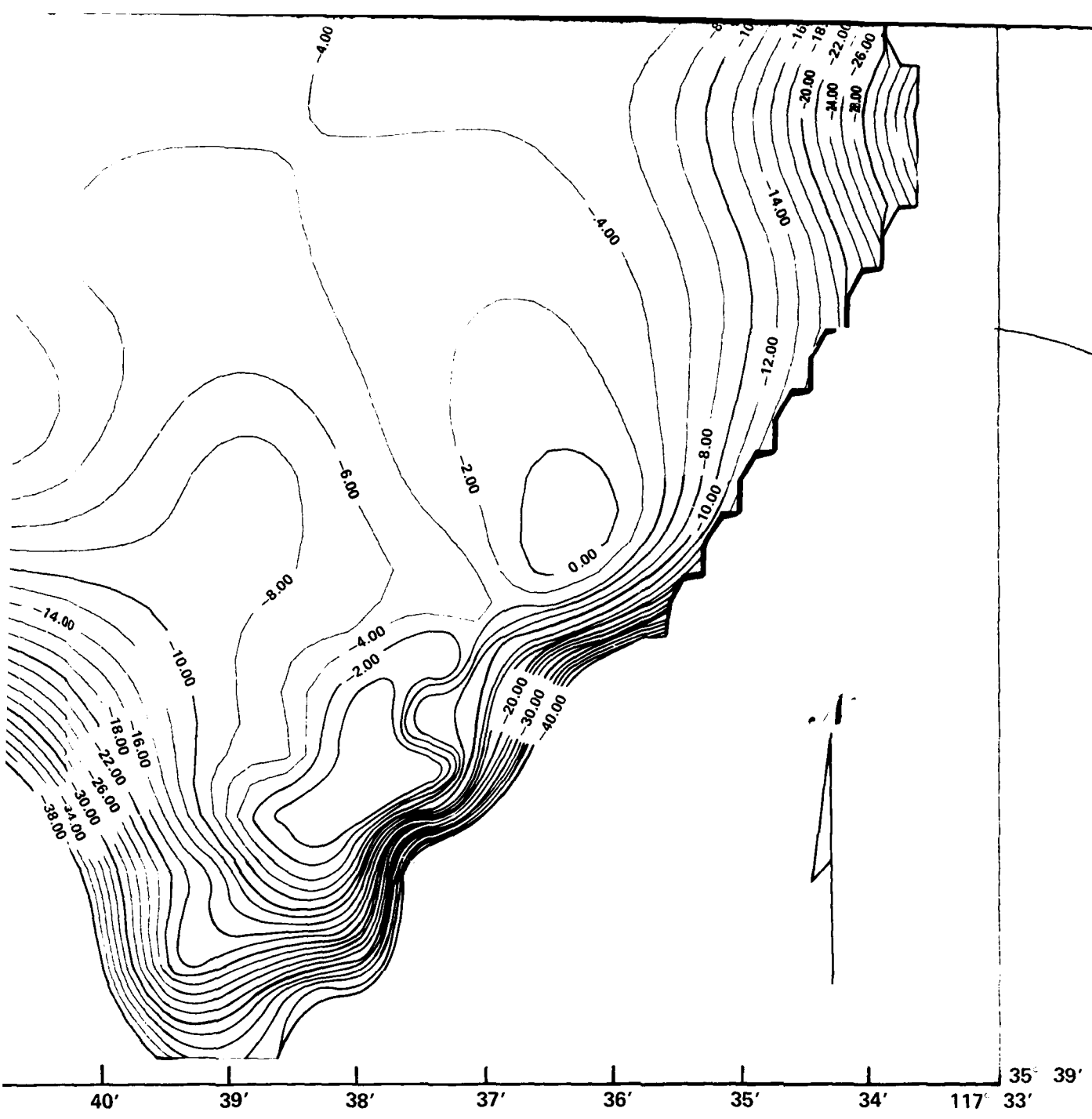
-4.00
-6.00
-8.00
-10.00
-12.00
-14.00
-16.00
-18.00
-20.00
-22.00
-26.00
-30.00
-34.00
-38.00
-40.00
-2.00
0.00
35° 39′
40′
39′
38′
37′
36′
35′
34′
117° 33′

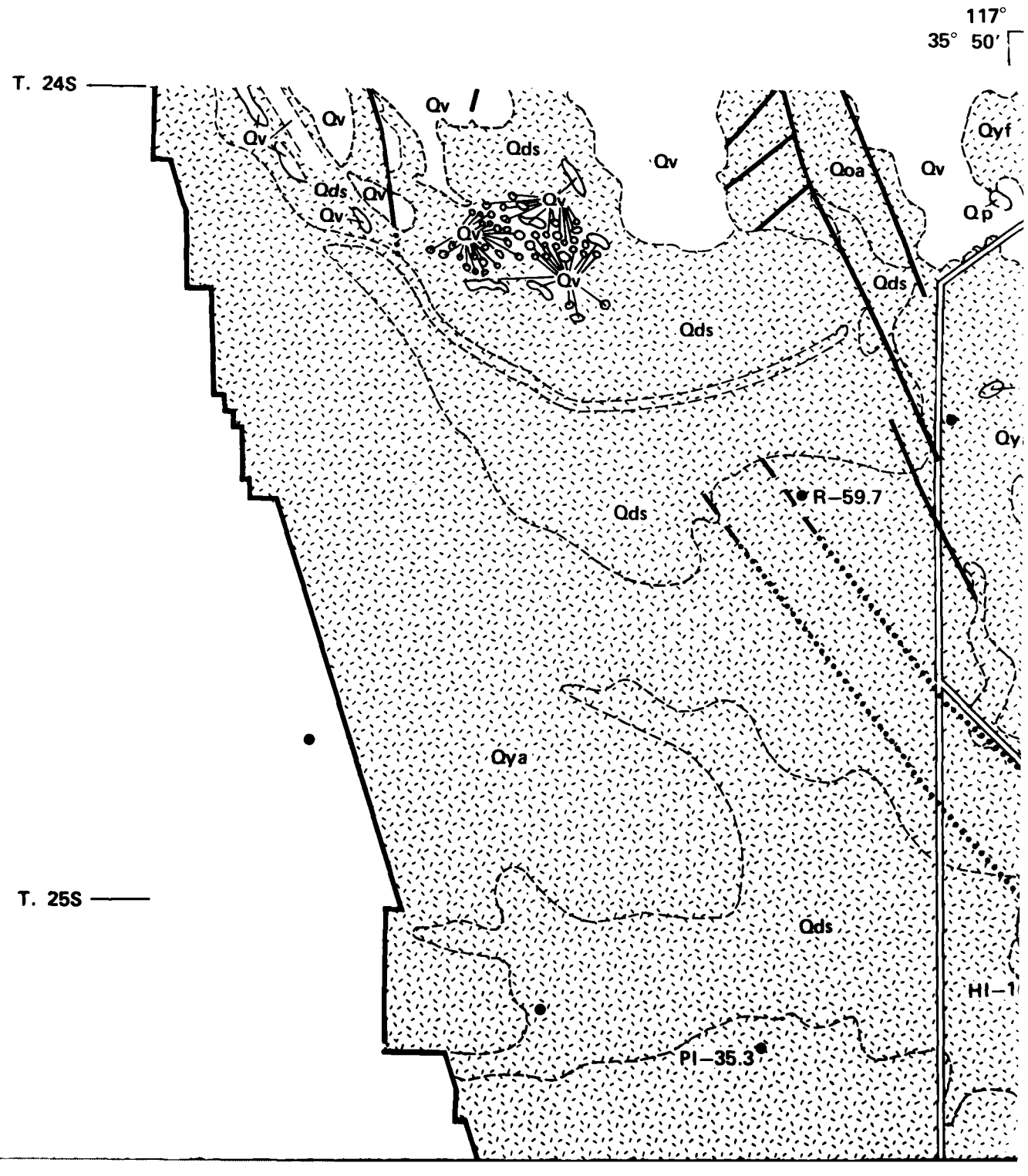
117°
35° 50'
T. 24S
T. 25S
Qv
Qds
Qoa
Qyf
Qp
Qya
R–59.7
PI–35.3

1 2

LIQUEFACTION SUSCEPTIBII
NAVAL WEAPON CENTER, CHI

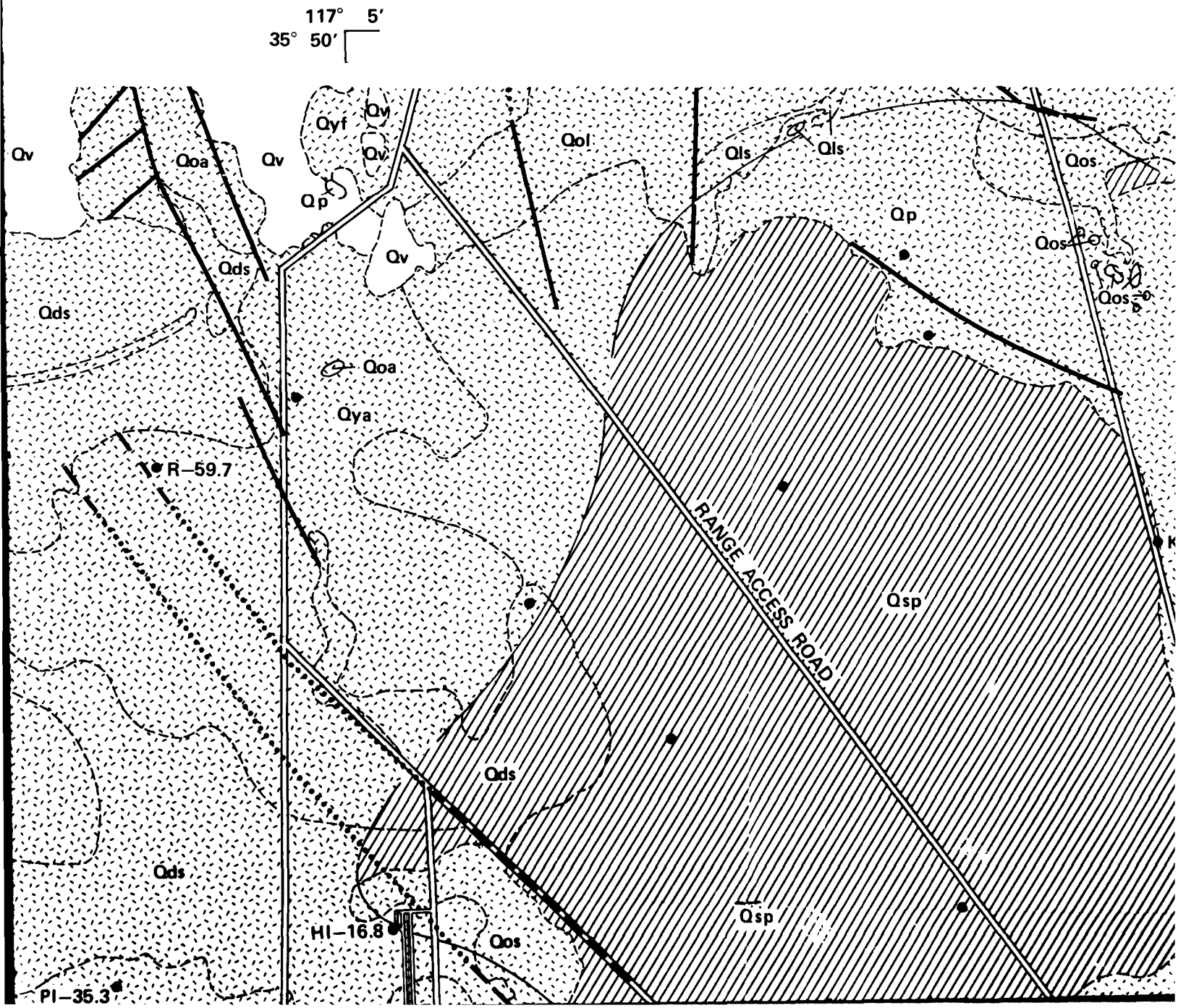

IBILITY MAP FOR THE
HINA LAKE, ,CALIFORNIA

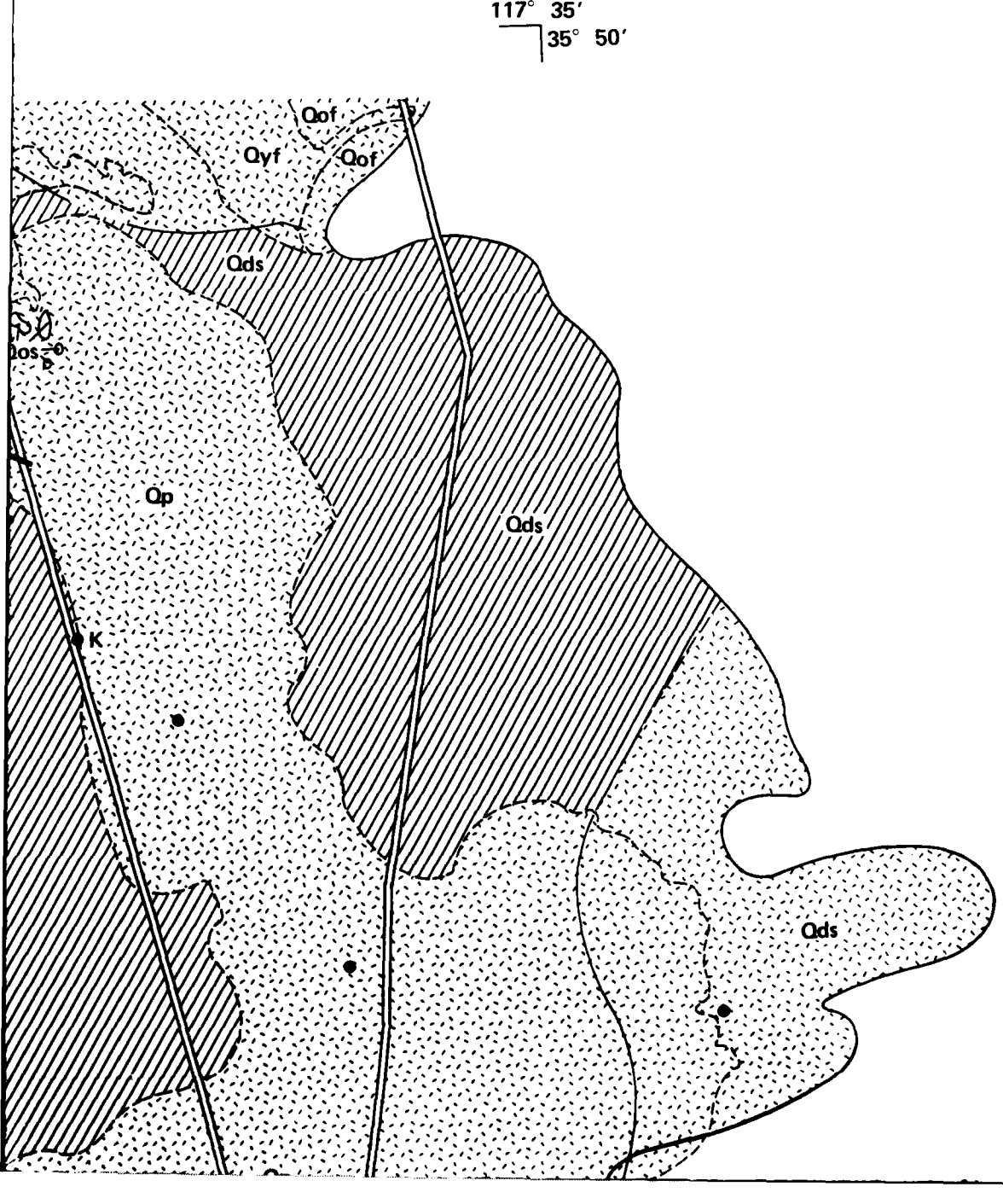

3 1 4

PLATE 2

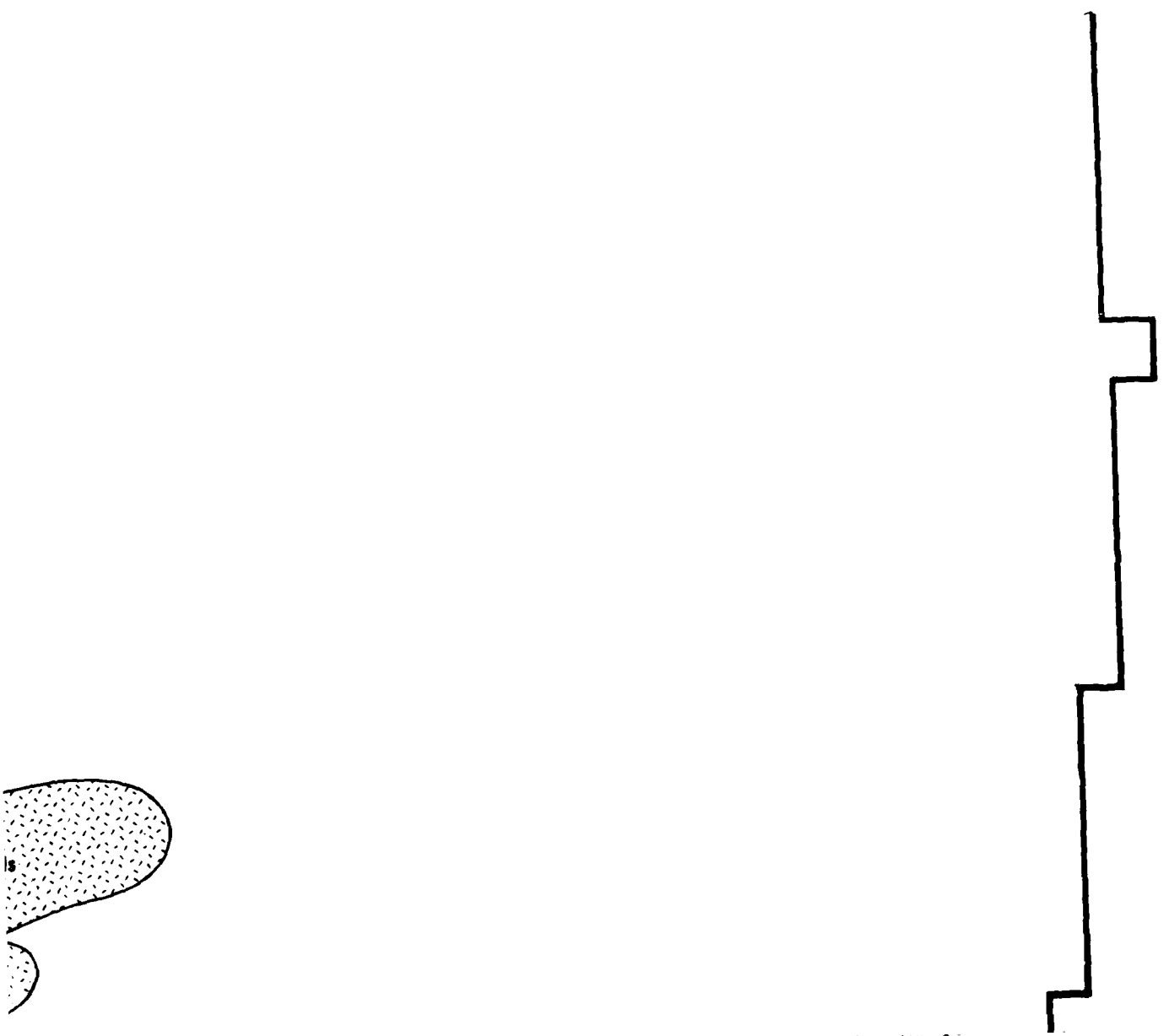

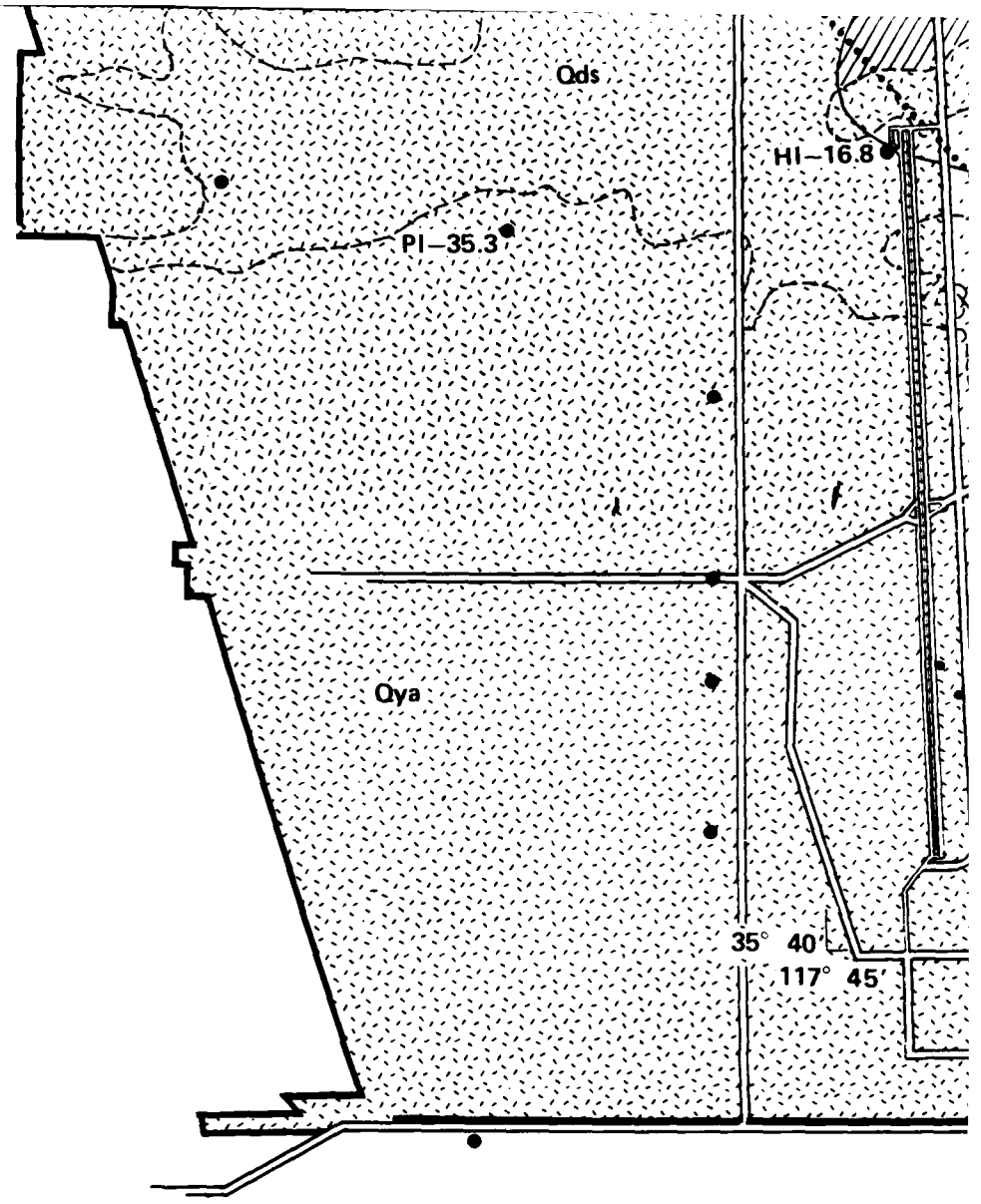

Qof – OLDER FAN DEPOSITS.
Qol – OLD LACUSTRINE DEPOSITS.
Qls – OLD LAKESHORE DEPOSITS.
Qos – OLD DUNE SAND.
Qv – UNNAMED VA VOLCANIC ROCKS.
Qva – YOUNGER ALLUVIUM.
Qyf – YOUNGER FAN DEPOSITS.
Qp – PLAYA DEPOSITS.
Qds – DUNE SAND DEPOSITS.
Qsp – SAND AND INTERDUNE PLAYA DEPOSITS.
● – WELL LOCATIONS

1 ½ 0 1

SCA

R. 39E

5

1

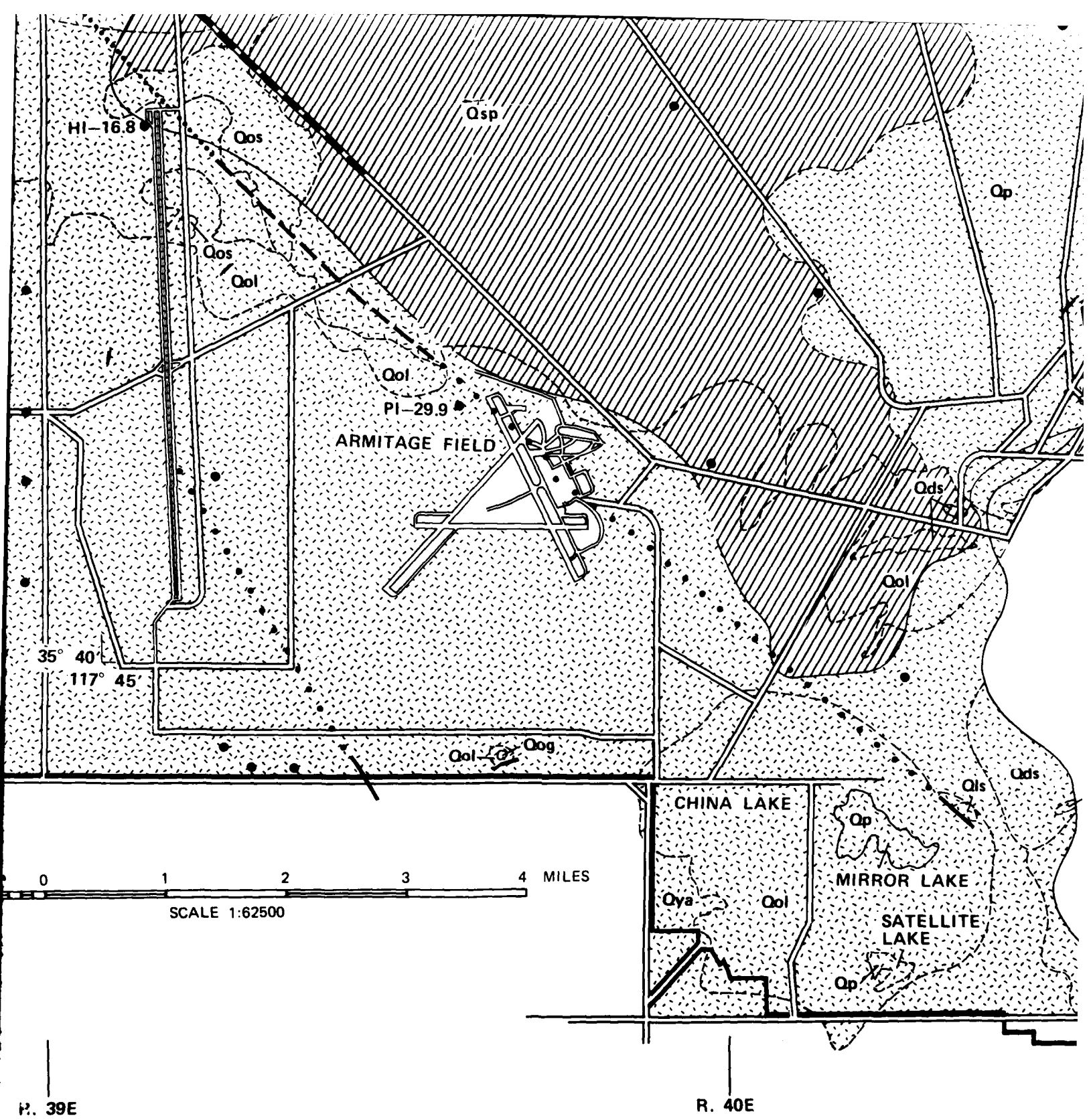
HI–16.8
Qos
Qsp
Qp
Qos
Qol
Qol
PI–29.9
ARMITAGE FIELD
Qds
Qol
35° 40'
117° 45'
Qol
Qog
Qds
Qls
CHINA LAKE
Qp
MIRROR LAKE
Qya
Qol
SATELLITE LAKE
Qp
0 1 2 3 4 MILES
SCALE 1:62500
R. 39E
R. 40E

1 6


35° 40′
117° 35′
Qds
Qog
HIGH CLASSIFICATION
MODERATE CLASSIFICATION
NOT SUSCEPTIBLE

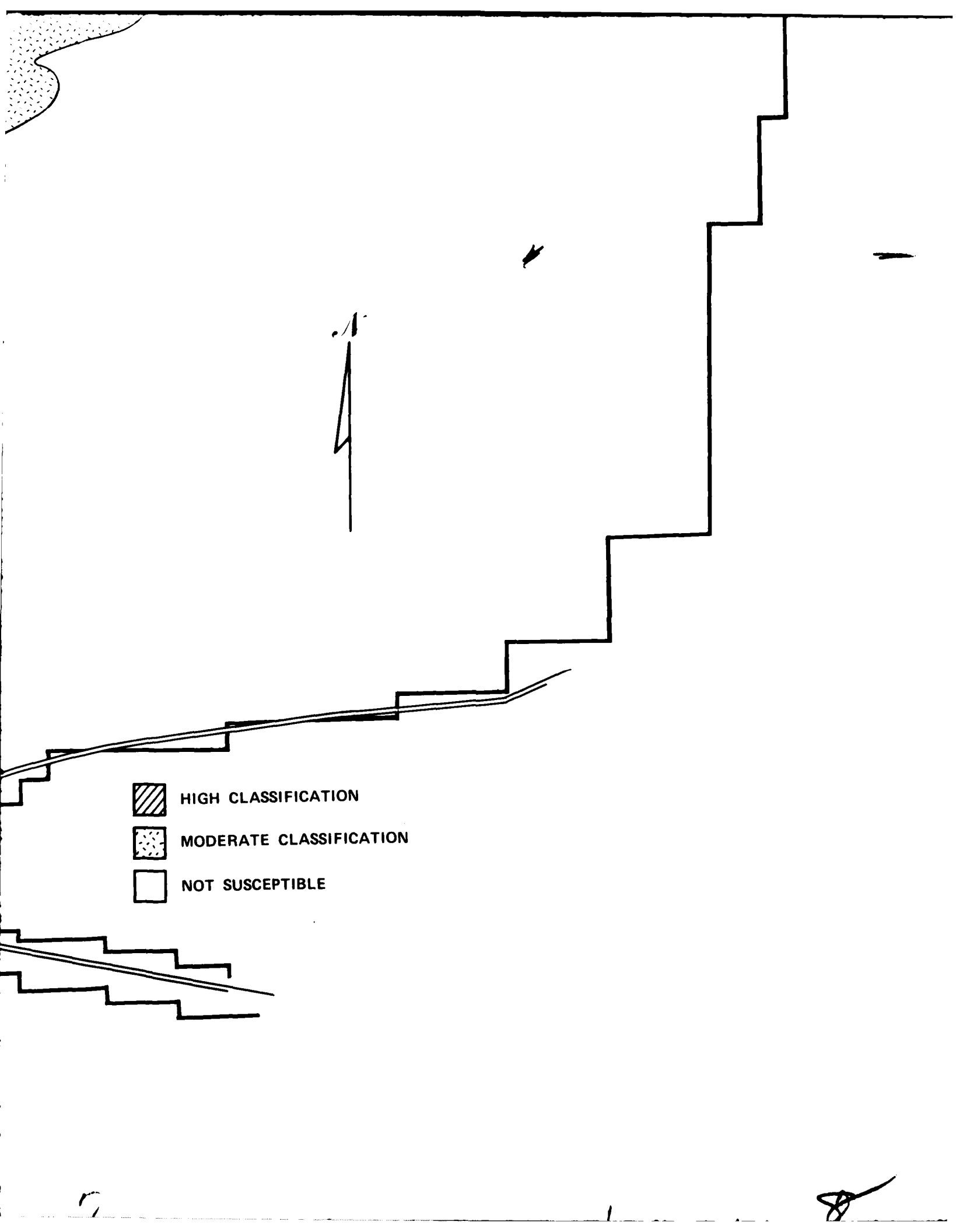
HIGH CLASSIFICATION
MODERATE CLASSIFICATION
NOT SUSCEPTIBLE

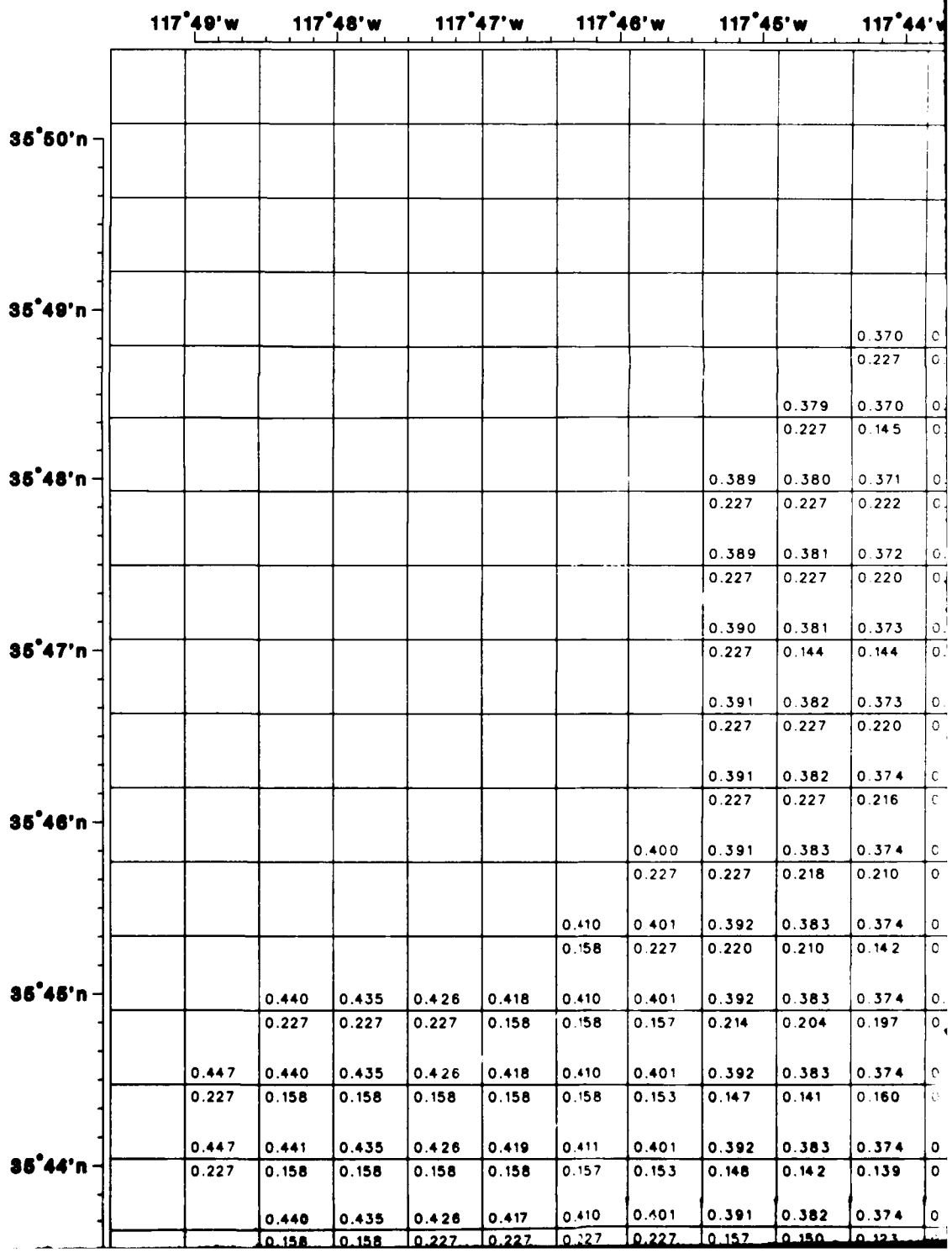
117°49'w
117°48'w
117°47'w
117°46'w
117°45'w
117°44'w
35°50'n
35°49'n
35°48'n
35°47'n
35°46'n
35°45'n
35°44'n
0.370
0.227
0.379
0.370
0.227
0.145
0.389
0.380
0.371
0.227
0.227
0.222
0.389
0.381
0.372
0.227
0.227
0.220
0.390
0.381
0.373
0.227
0.144
0.144
0.391
0.382
0.373
0.227
0.227
0.220
0.391
0.382
0.374
0.227
0.227
0.216
0.400
0.391
0.383
0.374
0.227
0.227
0.218
0.210
0.410
0.401
0.392
0.383
0.374
0.158
0.227
0.220
0.210
0.142
0.440
0.435
0.426
0.418
0.410
0.401
0.392
0.383
0.374
0.227
0.227
0.227
0.158
0.158
0.157
0.214
0.204
0.197
0.447
0.440
0.435
0.426
0.418
0.410
0.401
0.392
0.383
0.374
0.227
0.158
0.158
0.158
0.158
0.158
0.153
0.147
0.141
0.160
0.447
0.441
0.435
0.426
0.419
0.411
0.401
0.392
0.383
0.374
0.227
0.158
0.158
0.158
0.158
0.157
0.153
0.148
0.142
0.139
0.440
0.435
0.426
0.417
0.410
0.401
0.391
0.382
0.374
0.158
0.158
0.227
0.227
0.227
0.227
0.157
0.150
0.123

117°44'w	117°43'w	117°42'w	117°41'w	117°40'w	117°39'w	117°38'w	117°37'w	117°36'w
		0.344	0.342	0.341	0.335	0.329	0.323	0.318	0.313	0.308	0.303			
		0.147	0.141	0.136	0.137	0.116	0.116	0.146	0.148	0.153	0.158			
	0.352	0.345	0.344	0.342	0.335	0.329	0.324	0.318	0.313	0.308	0.303	0.298		
	0.143	0.140	0.133	0.131	0.108	0.106	0.102	0.156	0.169	0.165	0.172	0.151		
0.370	0.353	0.346	0.344	0.342	0.336	0.330	0.324	0.319	0.313	0.308	0.304	0.298	0.293	0.289		
0.227	0.140	0.136	0.128	0.129	0.127	0.099	0.096			0.103	0.107	0.142	0.142	0.131		
0.379 0.370	0.362	0.354	0.346	0.345	0.343	0.336	0.330	0.324	0.319	0.314	0.309	0.304	0.299	0.294	0.289	
0.227	0.145	0.142	0.138	0.134	0.130	0.127	0.125	0.123	0.102	0.102		0.096	0.096	0.096	0.135	0.135	
0.380	0.371	0.363	0.355	0.347	0.345	0.343	0.337	0.331	0.325	0.319	0.314	0.309	0.304	0.299	0.294	0.289	0.285
0.227	0.222	0.141	0.136	0.133	0.129	0.126	0.124	0.122	0.121	0.091	0.091	0.090	0.090	0.090	0.089	0.131	0.137
0.381	0.372	0.364	0.356	0.348	0.345	0.344	0.337	0.331	0.325	0.319	0.319	0.309	0.304	0.299	0.294	0.289	0.285
0.227	0.220	0.140	0.136	0.133	0.129	0.126	0.124	0.122	0.121	0.120	0.120	0.090	0.090	0.089	0.089	0.131	0.131
0.381	0.373	0.364	0.356	0.348	0.346	0.344	0.337	0.331	0.325	0.320	0.314	0.309	0.304	0.299	0.294	0.244	0.285	0.2
0.144	0.144	0.140	0.136	0.133	0.128	0.125	0.124	0.122	0.121	0.120	0.119	0.119	0.090	0.090	0.090	0.131	0.131	0.1
0.382	0.373	0.365	0.357	0.349	0.346	0.344	0.338	0.331	0.325	0.320	0.314	0.309	0.304	0.299	0.294	0.290	0.285	0.2
0.227	0.220	0.139	0.134	0.131	0.127	0.125	0.123	0.122	0.121	0.120	0.119	0.119	0.090	0.091	0.091	0.131	0.131	0.1
0.382	0.374	0.365	0.357	0.349	0.346	0.344	0.338	0.331	0.325	0.320	0.314	0.309	0.305	0.299	0.294	0.290	0.285	0.2
0.227	0.216	0.206	0.133	0.128	0.125	0.124	0.123	0.122	0.121	0.120	0.120	0.120	0.091	0.094	0.094	0.133	0.133	0.1
0.383	0.374	0.366	0.358	0.350	0.347	0.344	0.338	0.332	0.326	0.320	0.314	0.309	0.304	0.299	0.294	0.290	0.285	0.2
0.218	0.210	0.200	0.137	0.125	0.123	0.122	0.122	0.122	0.121	0.121	0.121	0.121	0.094	0.093	0.093	0.134	0.134	0.1
0.383	0.374	0.366	0.357	0.350	0.348	0.345	0.338	0.332	0.326	0.320	0.315	0.309	0.304	0.299	0.290	0.285	0.281	0.2
0.210	0.142	0.139	0.135	0.123	0.121	0.121	0.121	0.121	0.121	0.121	0.121	0.121	0.094	0.093	0.092	0.135	0.101	0.1
0.383	0.374	0.366	0.358	0.350	0.347	0.344	0.338	0.331	0.326	0.320	0.314	0.309	0.304	0.299	0.294	0.290	0.285	0.2
0.204	0.197	0.137	0.135	0.124	0.120	0.120	0.121	0.121	0.127	0.122	0.122	0.122	0.122	0.094	0.094		0.096	0.1
0.383	0.374	0.366	0.358	0.350	0.347	0.344	0.337	0.331	0.325	0.320	0.314	0.309	0.304	0.299	0.294	0.290	0.285	0.2
0.141	0.160	0.159	0.128	0.125	0.122	0.120	0.120	0.121	0.122	0.123	0.123	0.122	0.122	0.122	0.092	0.093	0.095	0.1
0.383	0.374	0.366	0.357	0.350	0.347	0.344	0.337	0.331	0.325	0.319	0.314	0.309	0.304	0.299	0.294	0.289	0.285	0.2
0.142	0.139	0.160	0.128	0.126	0.123	0.121	0.121	0.121	0.122	0.123	0.123	0.122	0.122	0.092	0.092	0.092	0.094	0.1
0.382	0.374	0.365	0.357	0.350	0.347	0.344	0.337	0.331	0.325	0.319	0.314	0.309	0.304	0.298	0.294	0.289	0.284	0.2

Plate 3

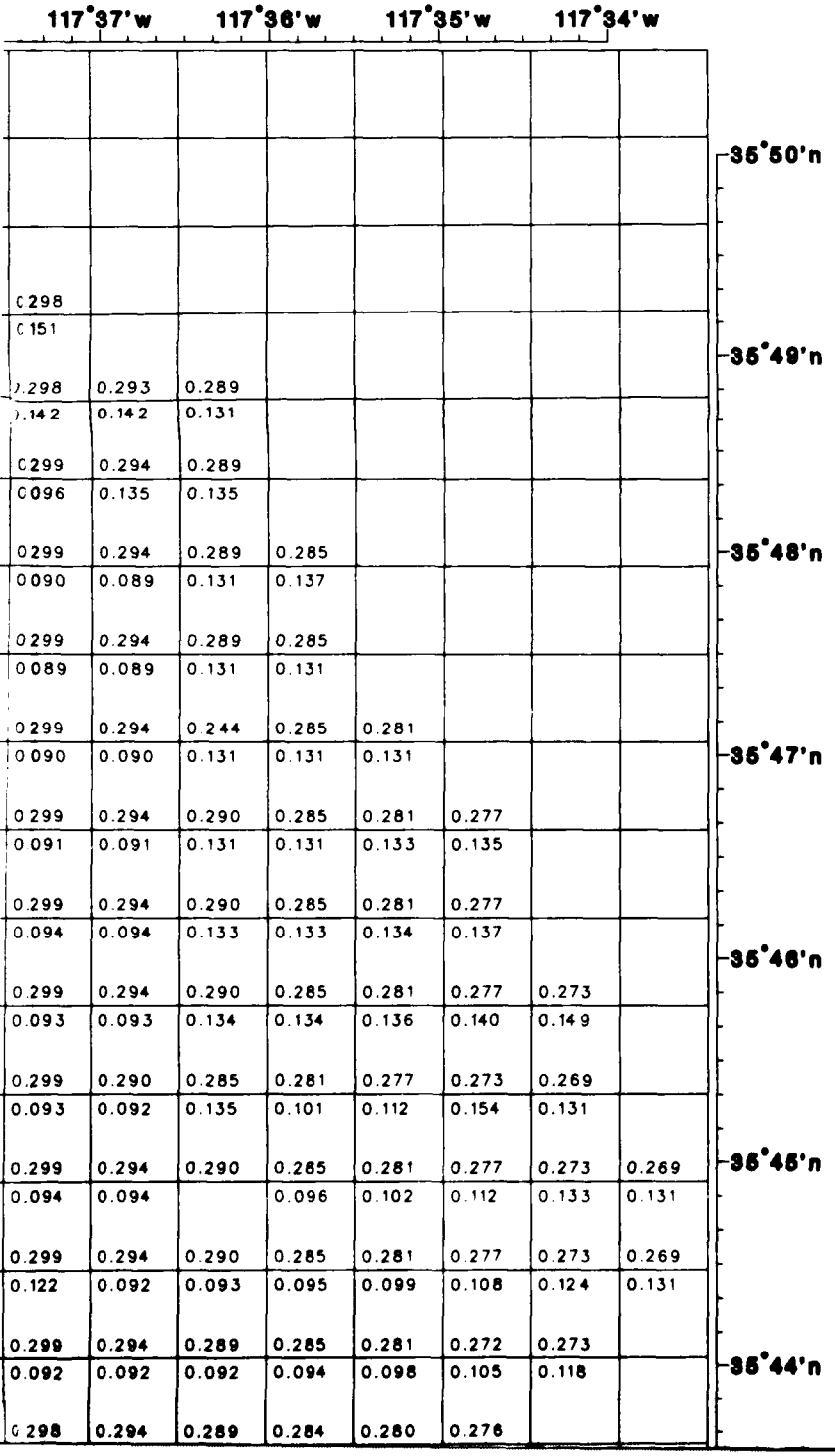
117°37'w
117°36'w
117°35'w
117°34'w
35°50'n
35°49'n
35°48'n
35°47'n
35°46'n
35°45'n
35°44'n
0.298
0.151
0.298 0.293 0.289
0.142 0.142 0.131
0.299 0.294 0.289
0.096 0.135 0.135
0.299 0.294 0.289 0.285
0.090 0.089 0.131 0.137
0.299 0.294 0.289 0.285
0.089 0.089 0.131 0.131
0.299 0.294 0.244 0.285 0.281
0.090 0.090 0.131 0.131 0.131
0.299 0.294 0.290 0.285 0.281 0.277
0.091 0.091 0.131 0.131 0.133 0.135
0.299 0.294 0.290 0.285 0.281 0.277
0.094 0.094 0.133 0.133 0.134 0.137
0.299 0.294 0.290 0.285 0.281 0.277 0.273
0.093 0.093 0.134 0.134 0.136 0.140 0.149
0.299 0.290 0.285 0.281 0.277 0.273 0.269
0.093 0.092 0.135 0.101 0.112 0.154 0.131
0.299 0.294 0.290 0.285 0.281 0.277 0.273 0.269
0.094 0.094 0.096 0.102 0.112 0.133 0.131
0.299 0.294 0.290 0.285 0.281 0.277 0.273 0.269
0.122 0.092 0.093 0.095 0.099 0.108 0.124 0.131
0.299 0.294 0.289 0.285 0.281 0.272 0.273
0.092 0.092 0.092 0.094 0.098 0.105 0.118
0.298 0.294 0.289 0.284 0.280 0.276

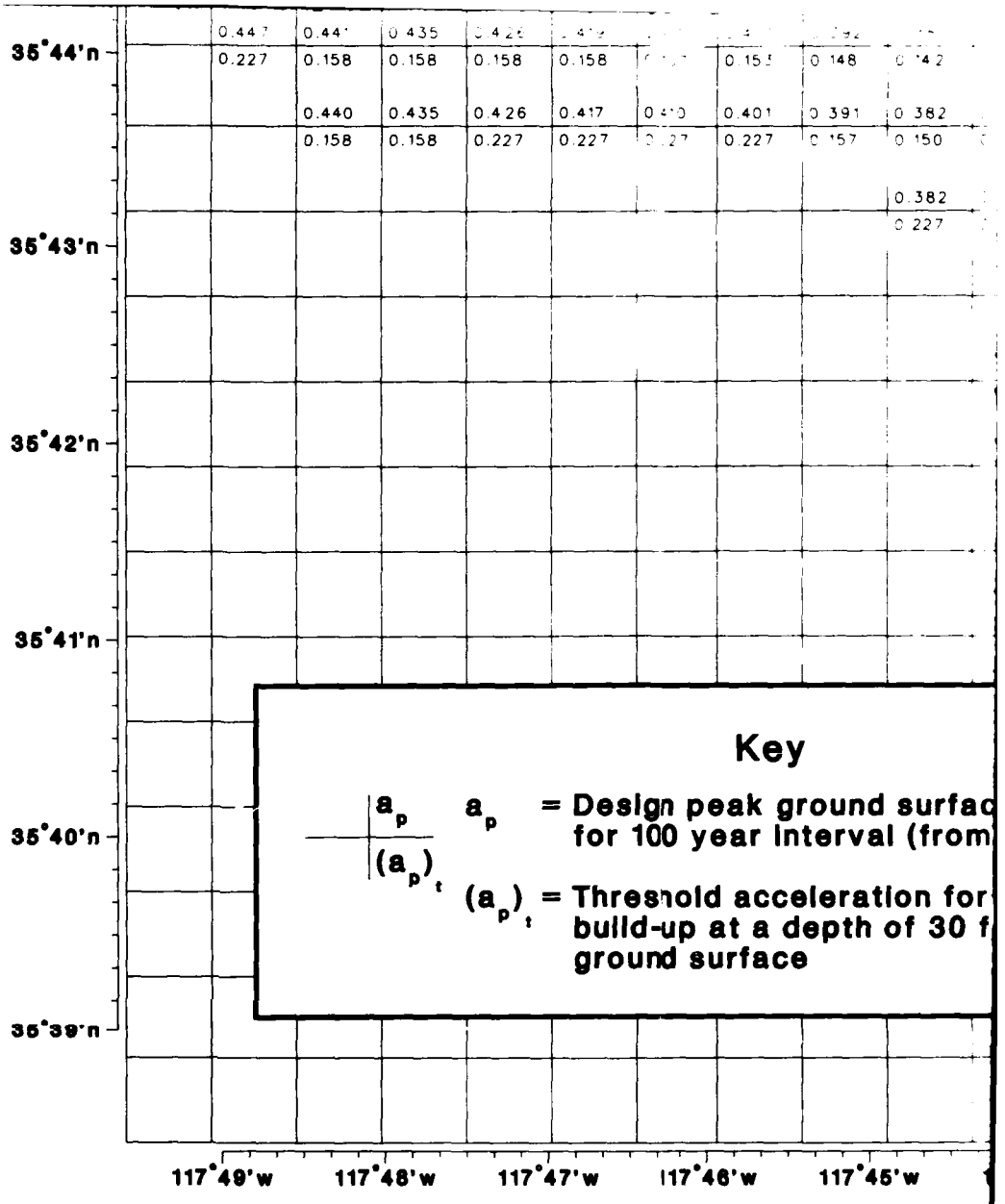
35°44'n
35°43'n
35°42'n
35°41'n
35°40'n
35°39'n
117°49'w
117°48'w
117°47'w
117°46'w
117°45'w
0.447
0.441
0.435
0.426
0.417
0.401
0.391
0.382
0.227
0.158
0.158
0.158
0.158
0.155
0.148
0.142
0.440
0.435
0.426
0.417
0.401
0.391
0.382
0.158
0.158
0.227
0.227
0.227
0.157
0.150
0.382
0.227
Key
$\frac{a_p}{(a_p)_t}$
a_p = Design peak ground surfac for 100 year interval (from
$(a_p)_t$ = Threshold acceleration for build-up at a depth of 30 f ground surface

Thre

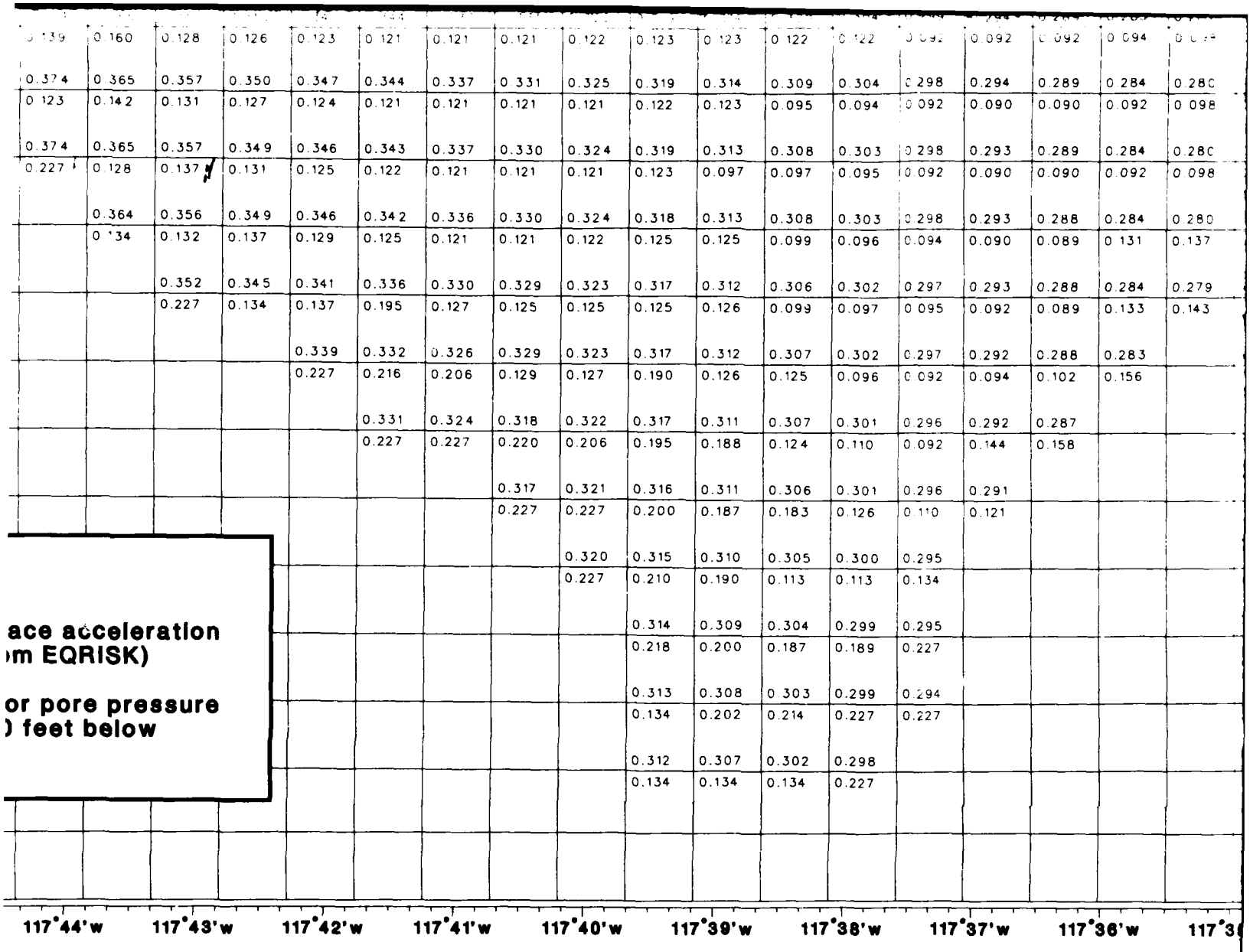

100 Year Design Peak Ground Surface Accelerations with Corresponding Liquefaction reshold Accelerations for the Naval Weapons Center, China Lake, California

Scale 1:62500

1 0.5 0 1 2 3 4

5

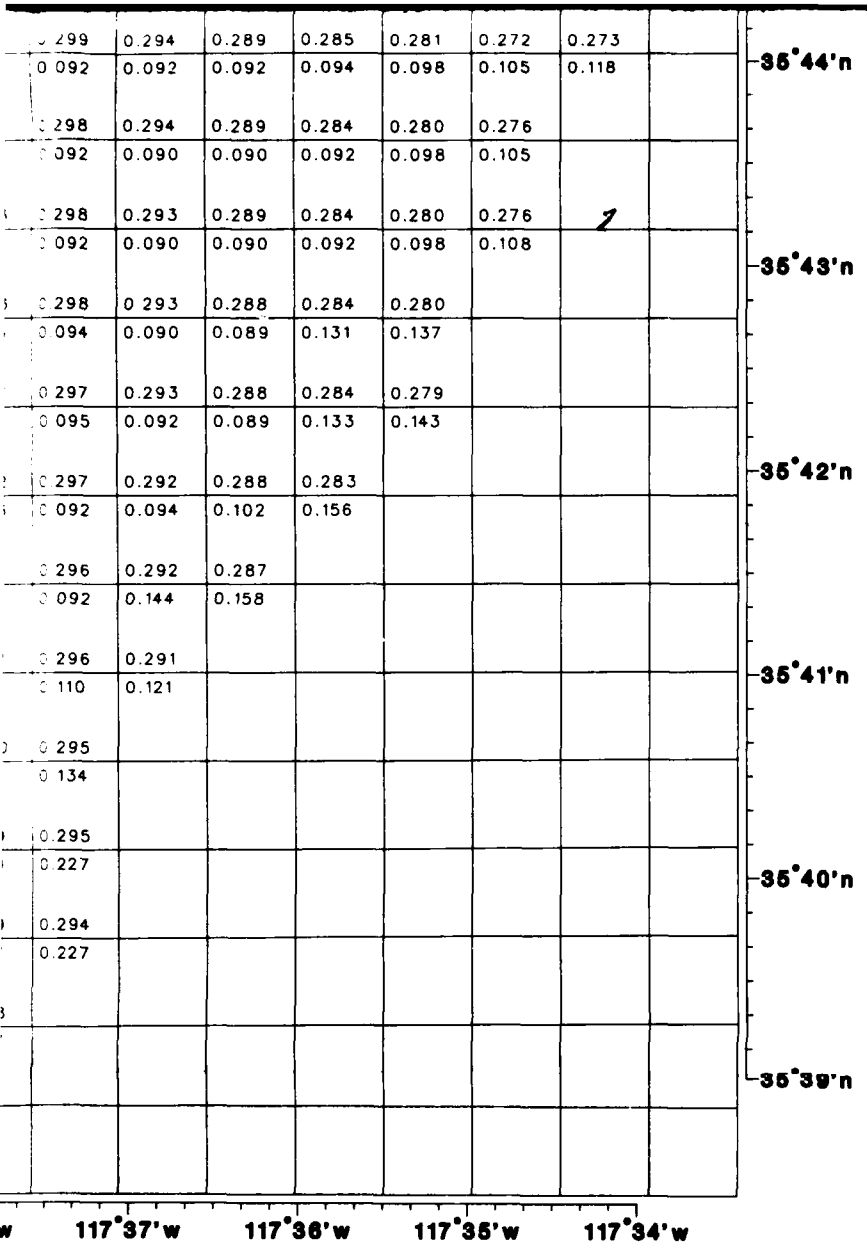
0.299 0.294 0.289 0.285 0.281 0.272 0.273
0.092 0.092 0.092 0.094 0.098 0.105 0.118
0.298 0.294 0.289 0.284 0.280 0.276
0.092 0.090 0.090 0.092 0.098 0.105
0.298 0.293 0.289 0.284 0.280 0.276
0.092 0.090 0.090 0.092 0.098 0.108
0.298 0.293 0.288 0.284 0.280
0.094 0.090 0.089 0.131 0.137
0.297 0.293 0.288 0.284 0.279
0.095 0.092 0.089 0.133 0.143
0.297 0.292 0.288 0.283
0.092 0.094 0.102 0.156
0.296 0.292 0.287
0.092 0.144 0.158
0.296 0.291
0.110 0.121
0.295
0.134
0.295
0.227
0.294
0.227
35°44'n
35°43'n
35°42'n
35°41'n
35°40'n
35°39'n
117°37'w
117°36'w
117°35'w
117°34'w
N

LIQUEFACATION POTENTIAL
NAVAL WEAPONS CENTER, C

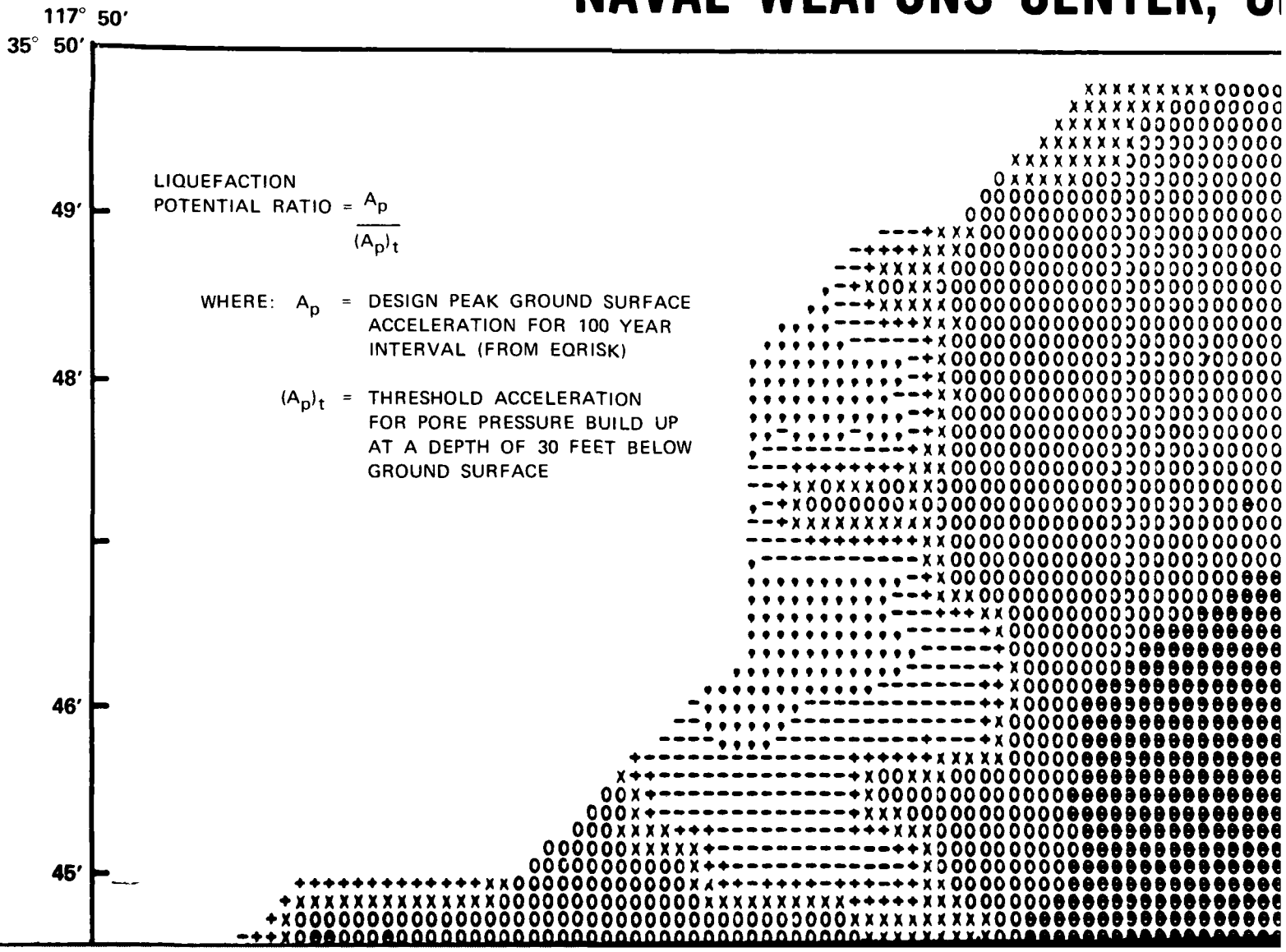

PLATE 4

NTIAL RATIO MAP FOR THE
ER, CHINIA LAKE, CALIFORNIA

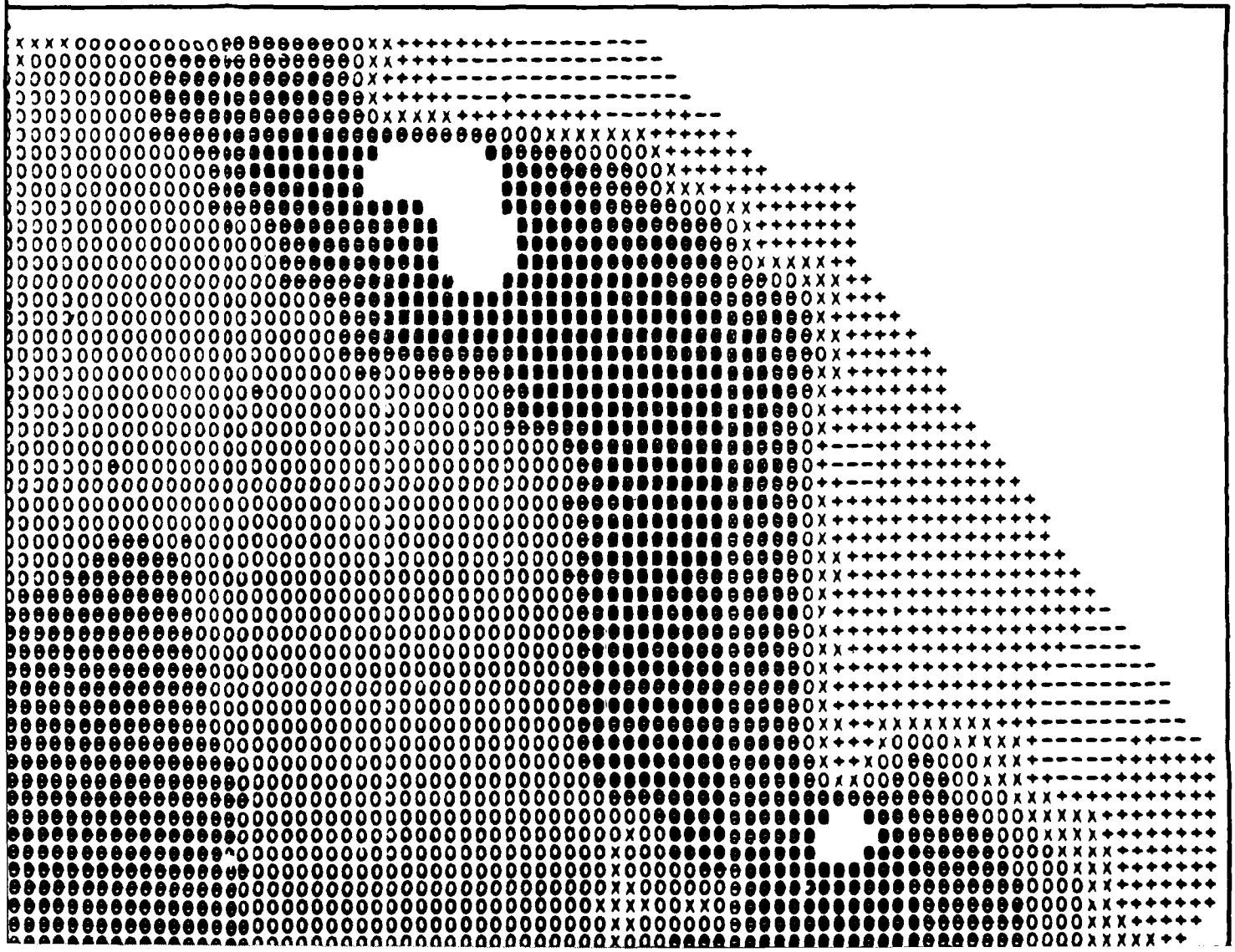

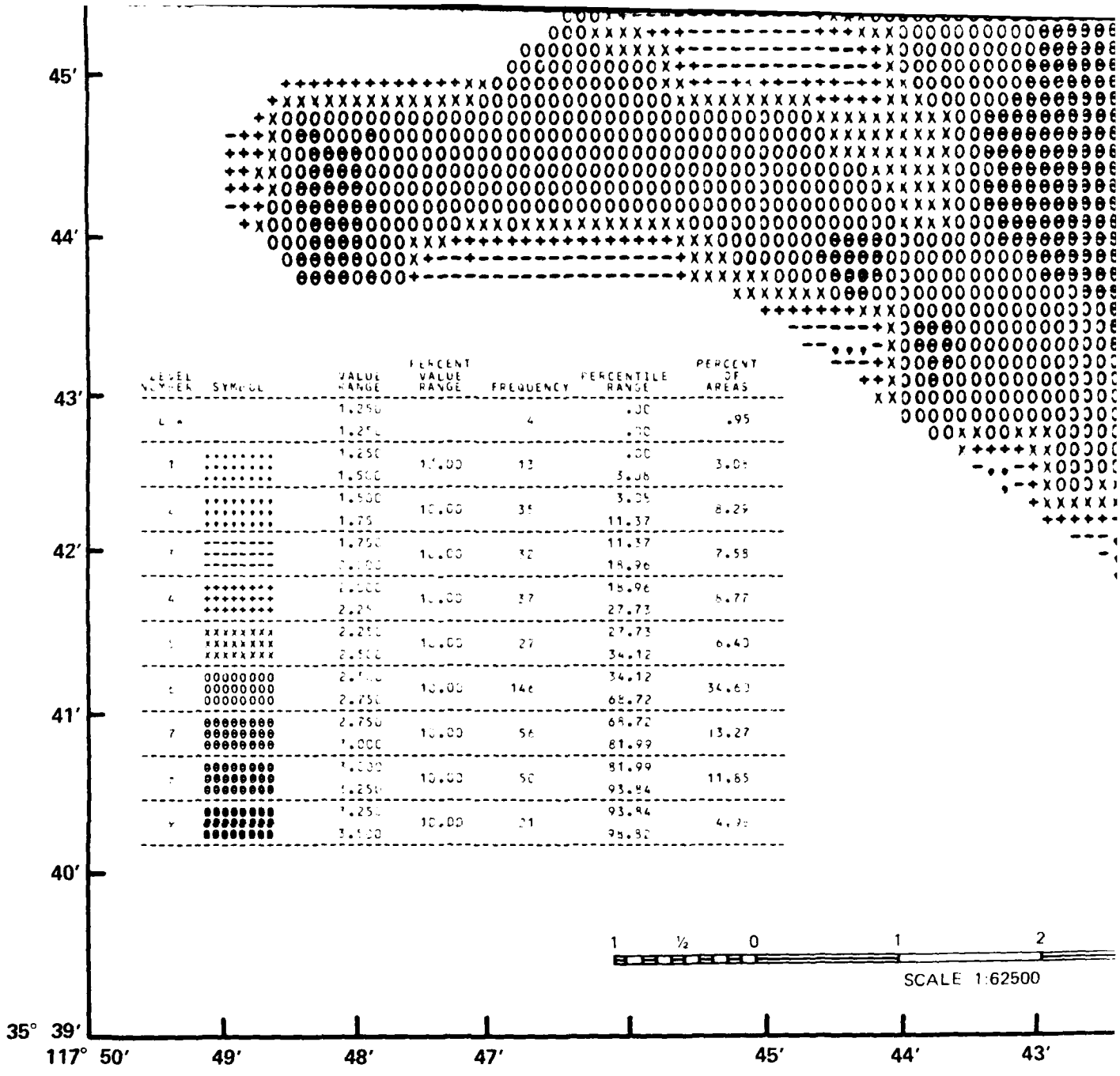

LEVEL NUMBER	SYMBOL	VALUE RANGE	PERCENT VALUE RANGE	FREQUENCY	PERCENTILE RANGE	PERCENT OF AREAS
L *		1.250 1.25[illegible]		4	.00 .00	.95
1	******** ******** ********	1.250 1.500	10.00	13	.00 3.08	3.08
2	******** ******** ********	1.500 1.75	10.00	35	3.08 11.37	8.29
3	--------- --------- ---------	1.750 2.000	10.00	32	11.37 18.96	7.58
4	++++++++ ++++++++ ++++++++	2.000 2.25	10.00	37	18.96 27.73	8.77
5	xxxxxxxx xxxxxxxx xxxxxxxx	2.250 2.500	10.00	27	27.73 34.12	6.40
6	00000000 00000000 00000000	2.500 2.750	10.00	146	34.12 68.72	34.60
7	@@@@@@@@ @@@@@@@@ @@@@@@@@	2.750 3.000	10.00	56	68.72 81.99	13.27
8	@@@@@@@@ @@@@@@@@ @@@@@@@@	3.000 3.250	10.00	50	81.99 93.84	11.85
9	@@@@@@@@ @@@@@@@@ @@@@@@@@	3.25[illegible] 3.500	10.00	21	93.84 98.82	4.98

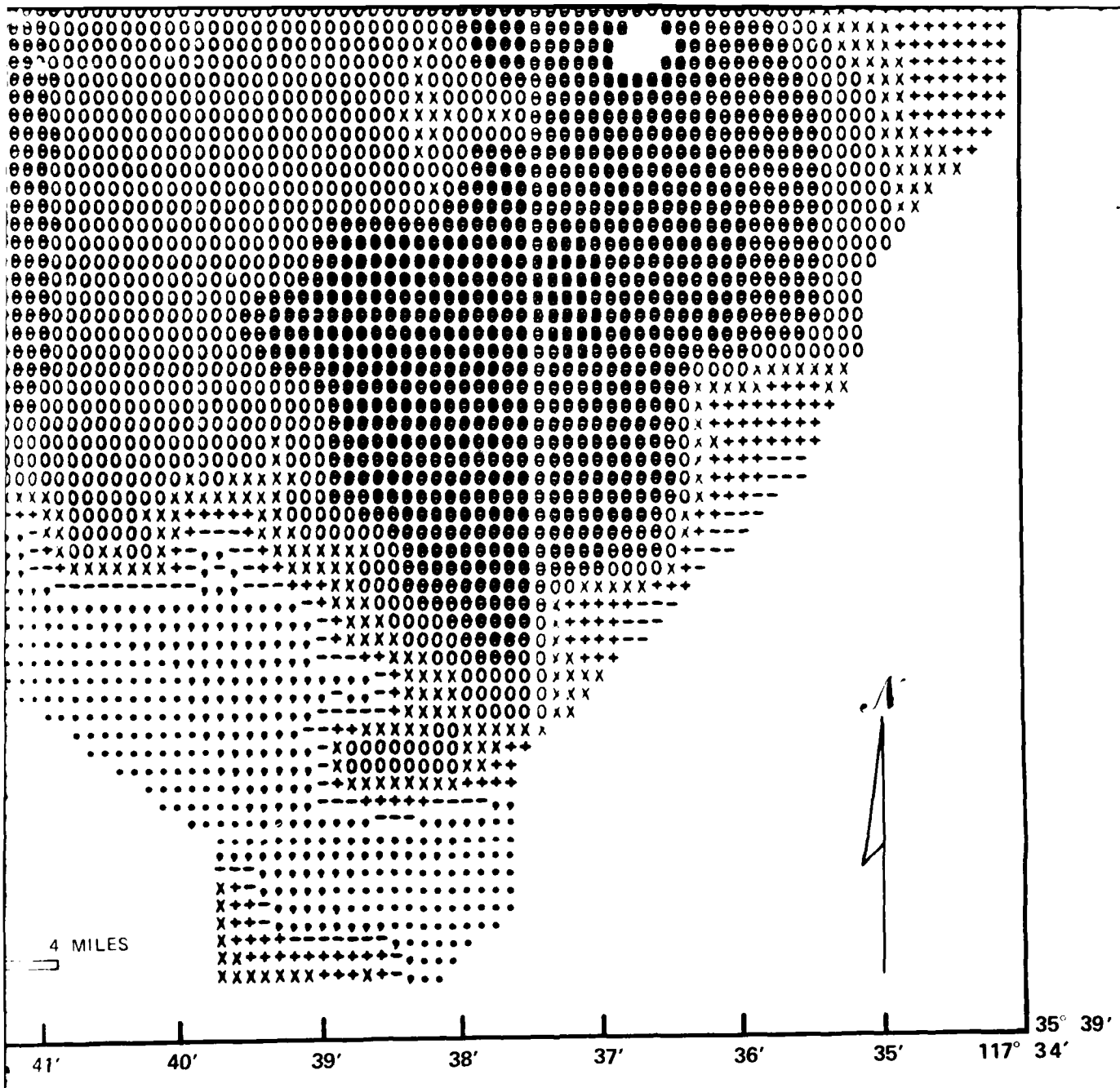
4 MILES
35° 39′
41′
40′
39′
38′
37′
36′
35′
117° 34′